Optical and magnetic resonance studies of doped magnesium oxide

Bluck, Leslie John Charles

OPTICAL AND MAGNETIC RESONANCE STUDIES OF DOPED MAGNESIUM OXIDE

by

LESLIE JOHN CHARLES BLUCK BSc.

A thesis submitted to the Faculty of Science of the University of Durham for the Degree of Master of Science

Department of Applied Physics and Electronics
Science Laboratories
Durham City

March 1979

To My Mother.

To My Late Father.

UNIVERSITY OF OXFORD · DEPARTMENT OF PHYSICS
Clarendon Laboratory · Parks Road · Oxford

Telephone Oxford (0865) 59291

Postal Address Clarendon Laboratory
Oxford
OX1 3PU

I, Leslie John Charles Block, declare that the material contained in the thesis "Optical and Magnetic Resonance Studies of Doped Manganese Oxide", is my own work, and has not been submitted, either wholly or partially for degrees in the University of Durham or elsewhere, before this present time.

LJC Block

9 April 1991.

ACKNOWLEDGEMENTS

I am indebted and shall always remain grateful to Dr. J.S. Thorp for his understanding and constant lively interest in this research work, and the endless time and patience he afforded me during its supervision.

My thanks are due to Professor G.G. Roberts for allowing me to use the facilities of the Department, and to the technical staff led by Mr. F. Spence for their assistance.

I wish to thank the Worshipful Company of Scientific Instrument Makers and the Fenton Trust for partial financial support through the development of this study.

I should like to thank my friends and colleagues in the University who in one way or another have contributed to the success of this research work, especially Messrs. T.G. Bushell, S. Hodgekiss, D. Hossain, N. Rad, B. Shaw, P. Waite, and Dr. S. Gezci.

Last, but by no means least, I would like to thank Mrs. J. Henderson who typed the manuscript of this thesis.

L.J.C. Bluck

March 1979

ABSTRACT

Magnesium Oxide crystals doped with chromium and cobalt have been investigated by optical spectroscopy and electron spin resonance spectroscopy. The optical work has provided information about the oxidation state and lattice site of the dopant ions, whilst the magnetic resonance results have given insight into the exchange interactions between them.

The Optical work on MgO:Cr has confirmed that the majority of dopant enters the lattice substitutionally as Cr^{3+} up to 15100 p.p.m., although at the higher concentration samples show evidence for a small amount of a second phase being formed. This has tentatively been ascribed as the spinel structure $MgCr_2O_4$. A linewidth analysis of the electron spin resonance signal due to the even isotopes of Cr^{3+} in substitutional sites has been made at room temperature. The value of linewidth is found to be considerably less than predicted by Van Vleck's second moment theory, and furthermore is independant of concentration as opposed to the $(\text{concentration})^{\frac{1}{2}}$ dependance expected from this theory. The discrepancy has been explained on the grounds of a strong exchange field between the chromic ions which gives rise to exchange narrowing. This idea is supported by the coefficients of kurtosis for the absorption lines which indicate a substantial trend to the Lorentzian lineshape. The strength of the exchange field has been measured as 4.45×10^{12} Hz from the e.s.r. data at both 9.5155 GHz and 35.5 GHz.

A similar course of study was adopted for MgO:Co. Optical spectroscopy at both room and liquid nitrogen temperatures has shown that when discussing the optical energy levels of Co^{2+} substitutional in MgO considerable attention must be payed to spin-orbit coupling. The linewidth of the e.s.r. spectrum of this Co^{2+} taken at 9.5155 GHz between 4.2 and 65 K showed the linewidth to be a function of both temperature and concentration. The temperature dependance is attributed to a change in relaxation mechanism, and it is postulated that the Orbach

process dominates above about 40K, utilising the first excited state of the spin orbit coupling levels. An attempt to factor off the temperature dependance of the linewidth has been made, and again strong evidence for exchange narrowing, both from linewidth and lineshape arguments is seen. The strength of the exchange field has been calculated as 4.53×10^{12} Hz. Finally some previously published results for iron have been examined. From these the corresponding exchange field for Fe^{3+} in MgO has been evaluated as 1.14×10^{13} Hz.

CONTENTS

CHAPTER ONE

INTRODUCTION

Magnesium Oxide is widely used in industry as a refractory material. Its electrical properties are often exploited, for example it is used as an insulator between outer sheath and conducting filament in cooker and kettle elements. It was an industrial problem arising from this application which drew MgO to the attention of this Department, namely that at rather high temperatures (approximately 1000 K) the insulating behaviour of the MgO may collapse and, consequently, the material conducts leading to the failure of the element. It has been suggested that the diffusion of impurities from the sheath of the element, of which over 80% of the constituents are Iron, Chromium, Cobalt and Manganese, into the MgO lattice could be an explanation of this phenomenon, but this argument has not yet been proved.

Even the most pure commercially available MgO has trace impurities easily detectable by modern physical techniques (1.1). These are mainly elements of the first transition series, chiefly iron, with chromium, manganese and nickel also prominent. Previous workers in this department have been engaged in investigating the effect of these impurities on the physical properties of MgO, and recently it was found that exchange effects occur between iron impurities, even at low concentration, by an electron spin resonance lineshape analysis technique (1.2). The aim of the present work has been to extend these ideas by the investigation of similar effects in MgO containing chromium and cobalt impurities.

1.1 STRUCTURAL COMMENTS

Magnesium Oxide crystallizes with the NaCl, or rocksalt, structure (1.3). The simplest description of this structure is that each Mg^{2+} ion is

surrounded by six Cl^- ions, and each Cl^- by six Mg^{2+} to form a regular three-dimensional array. In more precise crystallographic language the oxygen anions form a cubic close-packed array with magnesium ions occupying all the octahedral interstices (see Figure 1.1). It is conventional to state this in terms of atomic coordinates thus:

Mg^{2+} at ½,0,0 ; 0,½,0 ; 0,0,½ ; ½,½,½ ;

O^{2-} at 0,0,0 ; 0,½,½ ; ½,0,½ ; ½,½,0 .

The atomic coordinates are expressed as fractions of the unit cell edges, along the three axial directions.

Since the systam is one in which the binding is predominantly ionic, the sizes of the ions play a most important part in determining the final structure, as Coulombic forces are undirected. From Figure 1.2 it can be seen that for the NaCl structure the condition for the anions to be in mutual contact as well as in contact with the cations is $r_+ = (\sqrt{2} - 1)r_-$ where r_+ and r_- are respectively the cationic radius and anionic radius. These are quoted as 66 pm. for Mg^{2+} and 132 pm. for O^{2-} (1.4). This gives a radius ratio, r_+/r_-, of 0.5. Hence MgO cannot have the idealised structure of Figure 1.2, but instead it is as shown in Figure 1.3, with the anions not quite touching; this is the rule rather than the exception with crystalline solids, and provided that this distortion is not too large the term "cubic close-packed" is still applied.

Reference to Figure 1.3 shows that the unit cell dimension, a_o, should be given by

$$a_o = 2r_o = 2(r_+ + r_-)$$

which gives a value of a_o = 396 pm., in good agreement with the experimental value of 420.3 pm. (1.5), bearing in mind the empirical

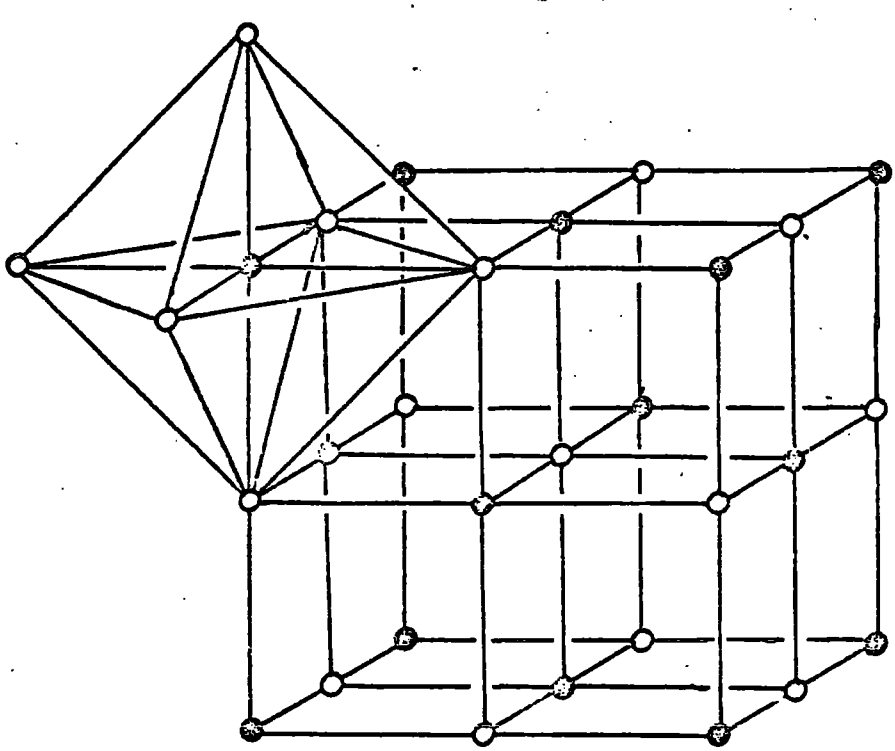

FIGURE 1.1 The structure of MgO
⊙ = magnesium, o = oxygen,
showing octahedral coordination
of the magnesium.

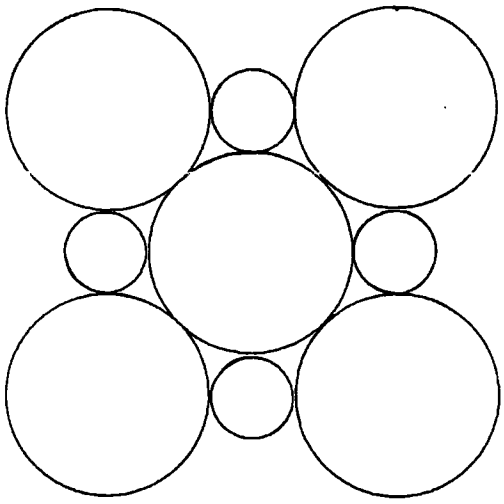

FIG 1·2 Cross section of ideal NaCl unit cell

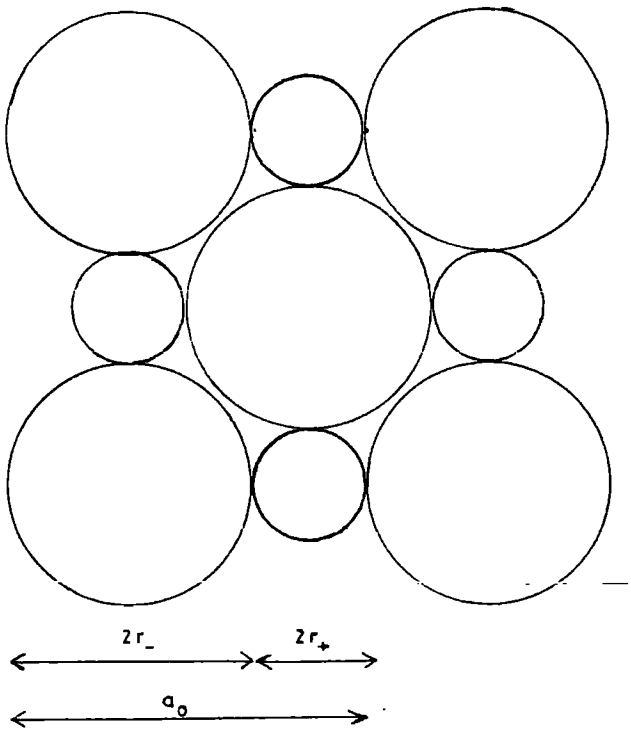

FIG 1·3 Cross-section of unit cell of MgO

nature of the measurement of ionic radii. One of the problems in asigning an ionic radius to a species, and then expecting consistency with experiment in a simple calculation such as the above, lies in the fact that in no solid is it fully satisfied that the bonding resembles complete electron transfer from cation to anion. To illustrate this for MgO it is convenient to adopt an approach due to Pauling (1.6). In this the binding in our crystal is regarded as a resonance between ionic and covalent bonding, giving the resultant time averaged wavefunction for a bonding electron as

$$\psi = \psi_{cov} + \lambda\psi_{ion}$$

where ψ_{cov} and ψ_{ion} are normalised wavefunctions for completely covalent and ionic forms, and λ is a parameter which determines the degree of ionic character in the bond. On this basis the per cent ionciity is $100\ \lambda^2/(1 + \lambda^2)$.

Pauling now suggests that the percentage ionicity can be related to his electronegativity scale by

$$\text{per cent ionicity} = 100\left[1 - \exp\left\{-\left(\frac{x_+ - x_-}{2}\right)^2\right\}\right]$$

where x is the electronegativity of the ion concerned. Pauling gives values of 1.31 and 3.44 respectively for Mg^{2+} and O^{2-}. Using these figures the percentage ionic character in the MgO bond is 68, and that $\lambda \doteq 1.45$. This is, of course, a crude semi-quantitative calculation, but it does show that in treating MgO as a totally ionic solid we make a large approximation in ignoring covalent effects, which account for about one third of the total bonding character.

Having considered the lattice of pure MgO in a little detail the next problem is how to modify the picture when considering the effect of impurities. It is generally agreed that iron in MgO occupies a

substitutional site, and that it is present as Fe^{3+}(1.2), which immediately would seem to pose one problem. This is the fact that the substitution of Fe^{3+} for Mg^{2+} will obviously need some form of charge compensation. Three possibilities have been suggested for the mechanism by which this occurs. There are (1) Li^{+} compensation , (2) Interstitial oxygen anions, (3) cation vacancies.

The first of these is considered unlikely since, although MgO will quite readily accept lithium into its lattice as a dopant, analysis shows that Li is not present in MgO crystals in significant concentration unless deliberately introduced, so it is not the usual source of charge compensation of trivalent ions (1.7).

Interstitial oxygen anions are thought to be unlikely purely on a size basis. As already mentioned, the cationic to anionic radius ratio is about 0.5, and so substitution of an O^{2-} ion even in a cation vacancy would involve heavy distortion of the lattice. As the octahedral site is the biggest interstice in the crystal it is felt to be extremely unlikely that the O^{2-} ion could fit in any other. Also if interstitial oxygen were the main form of compensation pyknometric methods should be able to detect them at high doping levels.

Hence the remaining possibility is charge compensation to be due to cation vacancies. On the face of it this may seem unlikely since it requires one vacancy for every pair of trivalent impurity ions, and one might feel that at high impurity levels the structure might be "full of holes" and consequently collapse.

1.2 THERMODYNAMIC CONSIDERATIONS

The formula for the system may be written as $Mg_{1-3\delta}X_{2\delta}\square_{\delta}O$, where X is any trivalent cation occupying a substitutional position. Thus the doping level in parts per million (ppm) is $2\delta \times 10^{6}$. Incidently this

sort of system is not unknown, e.g. $Mn^{4+}Mg_6^{2+}O_8^{2-}$ which can be written as $Mn^{4+}\square Mg_6^{2+}O_8^{2-}$.

For N oxygen anions there will be $2N_\delta$ X^{3+} ions, N_δ cation vacancies, and $(1-3_\delta)N$ Mg^{2+} ions. Let w be the work required to remove three Mg^{2+} ions and replace them with two X^{3+} ions leaving one site in the crystal vacant. Now the process pure crystal $\longrightarrow$ impure crystal will have

$$\Delta U = N_\delta w \tag{1.1}$$

The Boltzmann relationship states

$$\Delta S = k\mathrm{Ln}\Omega \tag{1.2}$$

where ΔS is the entropy change, Ω is the number of complexions, and k is the Boltzmann constant. If it is assumed that the occupation of the cation sites by the various species is random, (i.e. no clustering effects, or impurity ion/vacancy ordering occurs), the number of complexions is

$$\Omega = \frac{N!}{(1-3_\delta)N\,!\,(N_\delta)!\,(2N_\delta)!} \tag{1.3}$$

This may be appreciated as follows; the total number of ways of putting N different objects on N different sites is N! However in this system there are only three different types of object, Mg^{2+}, X^{3+}, and vacancies. The $(1-3_\delta)N$ sites occupied by the Mg^{2+} ions may be so in $(1-3_\delta)N!$ ways, and similarly for the X^{3+} and the vacancies; this leads to the above expression.

The Helmholtz free energy for the change is thus

$$\Delta A = \Delta U - T\Delta S$$

From equations (1.1), (1.2), (1.3)

$$\Delta A = N_\delta w - kT\mathrm{Ln}\frac{N!}{[(1-3_\delta)N]!\,(N_\delta)!\,(2N_\delta)!}$$

By Stirling's approximation

$$\mathrm{Ln}(x!) = x\mathrm{Ln}x - x$$

Hence

$$\Delta A = N\delta w - kT\left[N\mathrm{Ln}N - \{(1-3\delta)N\}\,\mathrm{Ln}\,\{(1-3\delta)N\} - (N\delta)\mathrm{Ln}(N\delta) - (2N\delta)\mathrm{Ln}(2N\delta)\right]$$

The minimum value of ΔA, which will correspond to the equilibrium system is found by differentiating with respect to δ.

$$\frac{\partial \Delta A}{\partial \delta} = Nw - kT\left[3N\mathrm{Ln}(1-3\delta)N - N\mathrm{Ln}(N\delta) - 2N\mathrm{Ln}(2N\delta)\right]$$

For a turning point

$$\frac{\delta \Delta A}{\partial \delta} = 0$$

Hence

$$Nw = kTN\mathrm{Ln}\left\{\frac{(1-3\delta)N^{3}}{N\delta(2N\delta)^{2}}\right\}$$

With one mole of oxygen anions $N = N_o$ and

$$N_o w = RT\mathrm{Ln}\,\frac{1}{4}\left(\frac{1-3\delta}{\delta}\right)^{3} \qquad (1.4)$$

Consider now the term for the change in internal energy. To a first approximation w = 3 x the coulombic potential energy of an Mg^{2+} ion in the crystal, minus 2 x the coulombic potential energy of an X^{3+} ion in the crystal, minus any crystal field effects which migh occur for the X^{3+} ion. The electeostatic potential energy of an ion of charge Z_1 in a lattice of ions of charge Z_2 at an interionic distance r is given by

$$V = \frac{AZ_1Z_2e^{2}}{(4\pi\varepsilon_o)^{2}r}\left(1 - \frac{\rho}{r}\right)$$

where A and ρ are constants for any given lattice. The only parameter

that changes, assuming that r remains constant, on substitution of a trivalent ion for a divalent ion is Z_1. Hence the coulombic part of w is given by

$$(3 \times 2 - 2 \times 3) \frac{AZ_2}{r} \left(\frac{0}{4\pi\varepsilon_0}\right)^2 \left(1 - \frac{\rho}{r}\right) = 0 \qquad (1.5)$$

Now iron in a triply charged state has outer electron configuration d^5. This is, in a high spin state, a unique configuration for two reasons; firstly it has the highest spin multiplicity of the d-block configurations; having five unpaired electrons, and secondly, apart from d^0 or d^{10}, it is the only high spin configuration to have a crystal field stabilisation energy of zero.

Hence for Fe^{3+} w = 0 to a first approximation. Substitution of this into equation (1.4) gives a value of δ of 0.22. Thus from this calculation the equilibrium state of the crystal is

$$Fe_{0.44}\square_{0.22}Mg_{0.34}O$$

Figure 1.4 shows in graphical form the variation of ΔA with δ. It is seen that the stabilisation attained on adding a few ppm. of iron to pure MgO is quite marked, in fact the curve is at its steepest here. The importance of this calculation, (and its results) is that it may give the reason why it is impossible to prepare MgO free from iron and also gives insight into why Chromium and Cobalt were chosen for the present work. It has already been noted that the crystal field effects for a d^5 ion have no stabilising properties. Reference to equation (1.4) will show that this has the effect of making the equilibrium value of δ independent of temperature. This effect is peculiar to the electron configurations d^0, d^5, and d^{10}. Since the likely oxidation states of Cr and Co in MgO are

$$Cr^{2+}\ (d^4),\quad Cr^{3+}\ (d^3),\quad Co^{2+}\ (d^7),\quad Co^{3+}\ (d^8)\ ,$$

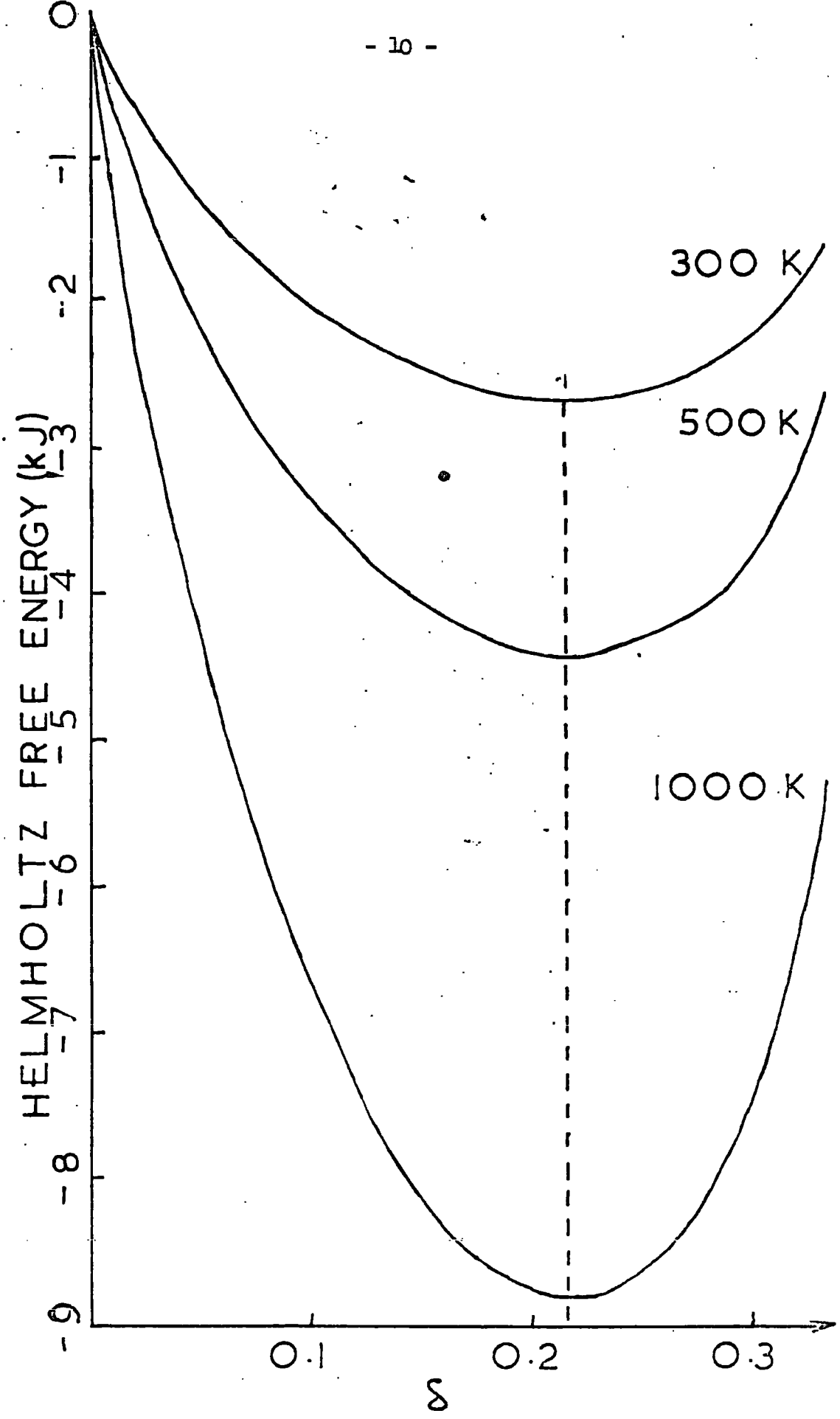

FIGURE 1.4 A plot of Helmholtz free energy for the system $Mg_{1-3\delta}Fe_{\ldots}$ Note the minimum at $\delta = 0.22$

this effect will not pertain. Also, it is well known that d^4 is related to d^6, and d^3 to d^7 via the "hole formalism." Thus these dopants complement each other and contrast with iron in their ground state electron configurations.

1.3 CLUSTERING AND ASSOCIATION

Consider the mean distance between dopant ions in the MgO lattice, and write the formula as $Mg_{1-3\delta}X_{2\delta}\square_{\delta}O$. The molecular weight is given by $(1-3\delta)M_{Mg\delta} + 2M_{X\delta} + M_Q$ where M_Q represents the atomic mass of the element Q. Hence in $40.3 + (2M_X - 120.9)_{\delta}$ grams contain $1.204 \times 10^{24}{}_{\delta} X^{3+}$ ions. The mean distance between the X^{3+} ions may be obtained from the formula

$$\bar{r}_{ij} = \left[\frac{40.3 + (2M_X - 72.9)\delta}{1.203 \times 10^{24}\rho\delta}\right]^{\frac{1}{3}}$$

where δ is the density.

For the dopants of interest at present M_X is about 55, and δ is not far from the density of pure MgO, which is 3.58 g/cm^3. Hence the quantity $\bar{r}_{ij}$ can be evaluated for a number of values of δ.

δ	$\bar{r}_{ij}$
5×10^{-5}	5.72 nm
5×10^{-4}	2.65 nm
1×10^{-3}	2.11 nm
2×10^{-3}	1.67 nm
3×10^{-3}	1.46 nm
4×10^{-3}	1.33 nm
5×10^{-3}	1.23 nm
6×10^{-3}	1.15 nm
7×10^{-3}	1.10 nm
8×10^{-3}	1.05 nm
9×10^{-3}	1.01 nm
1×10^{-2}	0.98 nm

this being the approximate range of samples to be investigated.

However there has been suggestions that ions in the MgO lattice do not occupy sites in a purely random fashion, bur rather tend to cluster. This would reduce the effective value of $\bar{r}_{ij}$, and tend to increase impurity-iimpurity interactions. It has been shown. however, that the tendency to cluster is less for Cr^{3+} than Fe^{3+} in MgO (1.8).

It should be noticed that these mean inter-ionic radii are large compared with the average chemical bond length (typically of the order of pm.), as the purpose of this work is to investigate the interactions of these ions, which will be shown to be quite large, even over a distance as great as has been evaluated here, several times the accepted relevant range of influence of the electronic wavefunctions.

CHAPTER TWO

THE DOPED MAGNESIA CRYSTALS

A seclection of single crystals of doped magnesium oxide were purchased from W.C. Spicers Ltd. (Cheltenham) with the following nominal concentrations in parts per million (ppm); all were grown by electro-fusion techniques.

MgO : Cr			MgO : Co		
	800	A		310	A
	1300	A		1250	A
	3600	X		1900	X
	4200	X		2500	A
	5000	X		3300	X
	6200	X		4800	X
	7400	X		8200	X
	9500	X		9900	X
	15100	X			

A = analysed by absorptiometry

X = analysed by x-ray methods.

To the eye the crystals appeared single and of high quality; the chromium doped crystals ranged in colour from light green to olive green with increasing concentration, and the cobalt containing crystals from pale pink to deep pink. Two different sizes of each crystal were purchased, both cleaved along the <100> crystallographic plane. The first size was obtained for the purpose of e.s.r. spectroscopy and took the form of small cuboids of approximately 3 mm edge. The other form of crystal was intended for optical spectroscopy. These were slices specified to be 10 mm x 10 mm x about 3 mm, the thickness decreasing with

concentration, to fit the spectrophotometer holder. The actual thicknesses required were worked out by first recording the spectrum of a sample of each material, and then evaluating the optimum thickness for absorption spectroscopy by assuming Beer's law to hold.

In order to test the quality of the crystals and also to check on their orientation, x-ray back reflection photographs were taken. These revealed two features. Firstly, all the crystals showed the same pattern, which was exactly as predicted for reflection from a <100> face, confirming the orientation of the specimens. Secondly all the samples gave sharp, well defined spots, indicating good single crystal quality, with no evidence for twinning, mosaic structure, or an abnormally large number of defects.

To characterise the crystals more closely some x-ray powder photography was also performed. Recent publications have commented on the variantion of lattice parameter of doped MgO with dopant concentration. Some work (2.1) on MgO:Cr has shown that the lattice parameter decreases linearly as more and more octahedral sites are occupied by Cr^{3+} to about 13000 ppm, when the lattice parameter remains constant, and if further Cr^{3+} is added the spinel $MgCr_2O_8$ is formed. This decrease in lattice parameter is slight ($\sim$ 0.1%), and it was felt doubtful if it could be observed with the 15 cm diameter powder camera currently available in the Department. Moreover since the lattice parameter of $MgCr_2O_3$ is very nearly twice that of MgO the diffracted lines tend to coincide making observation of each phase independently difficult by an x-ray powder method.

With these reservations in mind it was decided to measure the lattice parameter of both the MgO:Cr and MgO:Co crystals. A small piece was cut from the specimens to be used for optical spectroscopy, ground up,

and used for x-ray diffraction in a Debye-Scherrer camera, with Cu K_α radiation incident. Results for the MgO:Co samples are given below in Table 2.1. As can be seen no significant change in latter parameter was observed. Similar results were obtained for the MgO:Cr samples, again no significant change being noted.

Dopinant Concentration (ppm)	Lattice Parameter, a (pm)
0	421.2
2500	420.9
3300	421.0
4800	421.0
8200	421.1
9900	421.0

Table 2.1: The Lattice Parameter of the MgO:Co samples.

CHAPTER THREE

OPTICAL SPECTROSCOPY : THEORY AND TECHNIQUES

3.1 THE THEORY OF THE CRYSTAL FIELD

It is well known that to evaluate the energy states of a many-electronic atom or ion, solutions are required of the equation

$$\hat{H}\psi = E\psi \tag{3.1}$$

where $\hat{H}$ is the Hamiltonian operator for the system. At the moment, consider only that part of the energy which is directly due to the electrostatic attraction between the nucleus and electrons, and also the repulsion between the like charges of the electrons. In this case the Hamiltonian becomes

$$\hat{H} = \sum_{i}^{\kappa} \left(\frac{\hat{p}_i^2}{2m} - \frac{Ze^2}{r} \right) + \sum_{i<k} \frac{e^2}{r_{i\kappa}} \tag{3.2}$$

One fact becomes obvious immediately, and that is that the energy eigenstates depend on κ the number of electrons in the system. For this reason particular ions must be considered individually.

3.1.1 The Cr^{3+} ion

Chromium in a triply charged state has an outer electron configuration d^3. It is not an unreasonable assumption to say that the inner electrons form a closed shell, and are not involved in the transitions which give rise to the optical spectrum. In other words the energy of the inner electrons may be considered constant and the choice of energy zero is such that they need not be considered. Now, given that angular momentum and linearly, i.e. $\underline{L} = \underline{\iota}_1 + \underline{\iota}_2 + \underline{\iota}_3$, an M_L, M_S table can be

derived where the usual convention of $M_L = L_z/h$ and $M_S = S_z/h$. This is shown below.

	M_S				
	3/2	1/2	-1/2	-3/2	Implied terms
5	0	1	1	0	^2H
4	0	2	2	0	^2G
3	1	4	4	1	^4F ^2F
2	1	6	6	1	^2D ^2D
1	2	8	8	2	^4P ^2P
M_L 0	2	8	8	2	-
-1	2	8	8	2	-
-2	1	6	6	1	-
-3	1	4	4	1	-
-4	0	2	2	0	-
-5	0	1	1	0	-

The energy of each of these terms it to be evaluated. This calculation although straightforward, is long and tedious, and so is merely outlined. The matrix elements of the Hamiltonian are split into two parts, one being made up of one-electron operators only, the other entirely of two electron operators. It is then easy to show that the only part of the expression which varies is that made up of the two electron operators. This can be expanded via exchange and coulombic integrals and Slater-Condon parameters, which are given below

$$E(^4F) = 3A - 15B$$

$$E(^4P) = 3A$$

$$E(^2H) = 3A - 6B + 3C$$

$$E(^2P) = 3A - 6B + 3C$$

$$E(^2G) = 3A - 11B + 6C$$

$$E(^2F) = 3A + 9B + 3C$$

$$E(^2D) = 3A + 5B + 5C \pm (193B^2 - 8BC + 4C^2)^{\frac{1}{2}}$$

So far only the free chromium (III) ion has been considered. However, in a system such as the one envisaged, the Hamiltonian (3.2) is incomplete in that the host crystal in which the chromium atoms are sited was neglected. This provides an electrostatic field of the same symmetry as the site occupied by the chromium ion, and calculations must be made which take this into account. This is the theory of the crystal field. However this is not the only effect that the surrounding ions can have on the central one. In pure MgO the bonding is not totally ionic and this also applies to the bonds formed between the oxygen ions and the substitutional dopant ions. When these covalent effects are taken into account the modified theory is then called ligand field theory, and will be discussed later.

Consider now the case of the external field being of octahedral symmetry. A term describing the effect of this field must be added to the expression (3.2), and hence the Hamiltonian becomes

$$\hat{H} = \hat{H}_1 + \hat{V}_{oct} \qquad (3.3)$$

where H_1 is the Hamiltonian of (3.2). To evaluate the energy levels from this a priori has not yet proved possible, and so an approximation is used.

This is made by either treating the term $\hat{V}_{oct}$ as a small perturbation on $\hat{H}_1$, the weak-field coupling scheme, or by taking $\hat{H}_1$ as the perturbation on $\hat{V}_{oct}$, the strong-field coupling scheme. Ions of the first transition series are better described by the former scheme in general (3.1), so the effects of the perturbation on the energy levels given above may be evaluated.

Since most transitions are to excited states from the ground state, a useful example is the ^4F term. This has components (L,M_L) thus; (3,3), (3,2), (3,1), (3,0), (3,-1), (3,-2), (3,-3). Thus (3,3) component must be $|2^+, 1^+, 0^+>$ using the notation $|m_1^{\pm}, m_2^{\pm}, m_3^{\pm}>$ and taking the $M_S = 3/2$ part. We can obtain the other components via the shift operator $\hat{L}_-$ which is given by

$$\hat{L}_- = \hat{l}_{1-} + \hat{l}_{2-} + \hat{l}_{3-}$$

$$\hat{L}_- F_{LM} = h\left[(l_1+m_1)^{\frac{1}{2}}(l_1 - m_1 + 1)^{\frac{1}{2}}|m_1 - 1, m_2, m_3> + (l_2+m_2)^{\frac{1}{2}}(l_2 - m_2 + 1)^{\frac{1}{2}} x \right.$$

$$\left. |m_1, m_2 - 1, m_3> + (l_3+m_3)^{\frac{1}{2}}(l_3 - m_3 + 1)^{\frac{1}{2}}|m_1, m_2, m_3 - 1>\right]$$

$$= hF_{LM-1}$$

Hence, taking into account the Pauli exclusion principle, and the fact that m_l is always less than l

$$(3,3) = |2^+, 1^+, 0^+>$$

$$(3,2) = |2^+, 1^+, -1^+>$$

$$(3,1) = \sqrt{(3/5)}\,|2^+, 0^+, -1^+> + \sqrt{(2/5)}\,|2^+, 1^+, -2^+>$$

$$(3,0) = (1/5)\,|1^+, 0^+, -1^+> + (2/5)\,|2^+, 0^+, -2^+>$$

$$(3,-1) = \sqrt{(3/5)}\,|1^+, 0^+, -2^+> + \sqrt{(2/5)}\,|2^+, -1^+, -2^+>$$

$$(3,-2) = |1^+, -1^+, -2^+>$$

$$(3,-3) = |0, -1^+, -2^+>$$

The matrix elements of ^4F can now be evaluated. First write the wavefunction in its full determinantal form (3.2). The quantity needed is given by expressions of the form

$$\frac{1}{6}\int \begin{vmatrix} 2^+(1) & 2^+(2) & 2^+(3) \\ 1^+(1) & 1^+(2) & 1^+(3) \\ 0^+(1) & 0^+(1) & 0^+(3) \end{vmatrix} \hat{V}_{oct} \begin{vmatrix} 2^+(1) & 2^+(2) & 2^+(3) \\ 1^+(1) & 1^+(2) & 1^+(3) \\ 0^+(1) & 0^+(2) & 0^+(3) \end{vmatrix} d\tau$$

where the numbers in brackets refer to the electrons, and the specific case of the (3,3) component is taken. Because $\hat{V}_{oct}$ acts on each electron independently,

$$\hat{V}_{oct} = \hat{V}(1) + \hat{V}(2) + \hat{V}(3)$$

This simplifies the problem immensely and the matrix element is now given by

$$V_{33} = \frac{2}{6}\int 2^+(1)\hat{V}(1)2^+(1) + 1^+(1)\hat{V}(1)1^+(1) + 0^+(1)\hat{V}(1)0^+(1) +$$
$$2^+(2)\hat{V}(2)2^+(2) + 1^+(2)\hat{V}(2)1^+(1) + 0^+(2)\hat{V}(2)0^+(2) +$$
$$2^+(3)\hat{V}(3)2^+(3) + 1^+(3)\hat{V}(3)1^+(3) + 0^+(3)\hat{V}(3)0^+(3)\ d\tau$$

and since electrons are indistinguishable

$$V_{33} = \int 2^+\ \hat{V}\ 2^+ + 1^+\ \hat{V}\ 1^+ + 0^+\ \hat{V}\ 0^+\ d\tau\ .$$

The values of these integrals are well known, they are matrix elements of a single d electron under an octahedral field, and they are given below

M_L	2	1	0	-1	-2
2	$\frac{\Delta}{10}$	0	0	0	$\frac{\Delta}{2}$
1	0	$\frac{-2\Delta}{5}$	0	0	0
0	0	0	$\frac{3\Delta}{5}$	0	0
-1	0	0	0	$\frac{-2\Delta}{5}$	0
-2	$\frac{\Delta}{2}$	0	0	0	$\frac{\Delta}{10}$

Hence $V_{33} = -(3/10)\Delta$. All the matrix elements of ^4F can be found in the same way and are given below.

	(3,3)	(3,2)	(3,1)	(3,0)	(3,-1)	(3,-2)	(3,-3)
(3,3)	-0.3Δ	0	0	0	$\sqrt{0.15}\Delta$	0	0
(3,2)	0	0.7Δ	0	0	0	0.5	0
(3,1)	0	0	-0.1Δ	0	0	0	$\sqrt{0.15}\Delta$
(3.0)	0	0	0	-0.6Δ	0	0	0
(3,-1)	$\sqrt{0.15}\Delta$	0	0	0	-0.1Δ	0	0
(3,-2)	0	0.5Δ	0	0	0	0.7Δ	0
(3,-3)	0	0	$\sqrt{0.15}\Delta$	0	0	0	-0.3Δ

To obtain the final eigenvalues solution of the secular equations

$$c_i(V_{ik} - ES_{ik}) = 0 \quad \text{is required.}$$

This gives three levels, as is predicted by group theory, which are

$^4T_{1g}$ energy $= +0.6\,\Delta$

$^4T_{2g}$ energy $= -0.2\,\Delta$

$^4A_{2g}$ energy $= -1.2\,\Delta$

Actually there is one further complication since the matrix elements between the ^4P term and the ^4F term are not always zero. This is shown by the matrix

	$^4T_{1g}(F)$	$^4T_{1g}(P)$
$^4T_{1g}(F)$	$+0.6\,\Delta$	$0.4\,\Delta$
$^4T_{1g}(P)$	$0.4\,\Delta$	15B

and the solutions of the corresponding secular determinant gives the energy of the $^4T_{1g}(F)$ state of $\frac{1}{2}[15B + 0.6\Delta - (225B^2 - 18B + \Delta^2)^{\frac{1}{2}}]$ and that of the $^4T_{1g}(P)$ state of $\frac{1}{2}[15B + 0.6\Delta + (225B^2 - 18B\Delta + \Delta^2)^{\frac{1}{2}}]$. A full set of matrix elements which give rise to secular determinants which enable the energies of all the states of a d^3 ion have been calculated by Finkelstein and Van Vleck (3.3). They are given (Appendix 2) in a slightly adapted form from those in the original literature.

The parameter Δ which appears in these equations is the crystal field splitting energy, and is a measure of the strength of the octahedral potential. It is conventional to plot energy of the terms against Δ, and this is shown for a d^3 ion in Figure 3.1.

3.1.2 The effect of spin-orbit coupling

So far in this discussion spin-orbit coupling has been ignored. This is treated as a further perturbation on the system already described. The theory is well known, and for the sake of brevity, the results only are quoted.

The spin-orbit coupling energies can be obtained from the matrix elements

$$\int \phi^* \lambda \underline{L}.\underline{S} \psi d\tau$$

where the constant λ may be either positive or negative. For the present system the most important consequence of the spin-orbit coupling is that the energy levels just derived are split in some cases into more than one sub-level. If these splittings are large enough, and this depends on the magnitude of the spin-orbit coupling constant λ , then this effect may be observed spectroscopically (3.4).

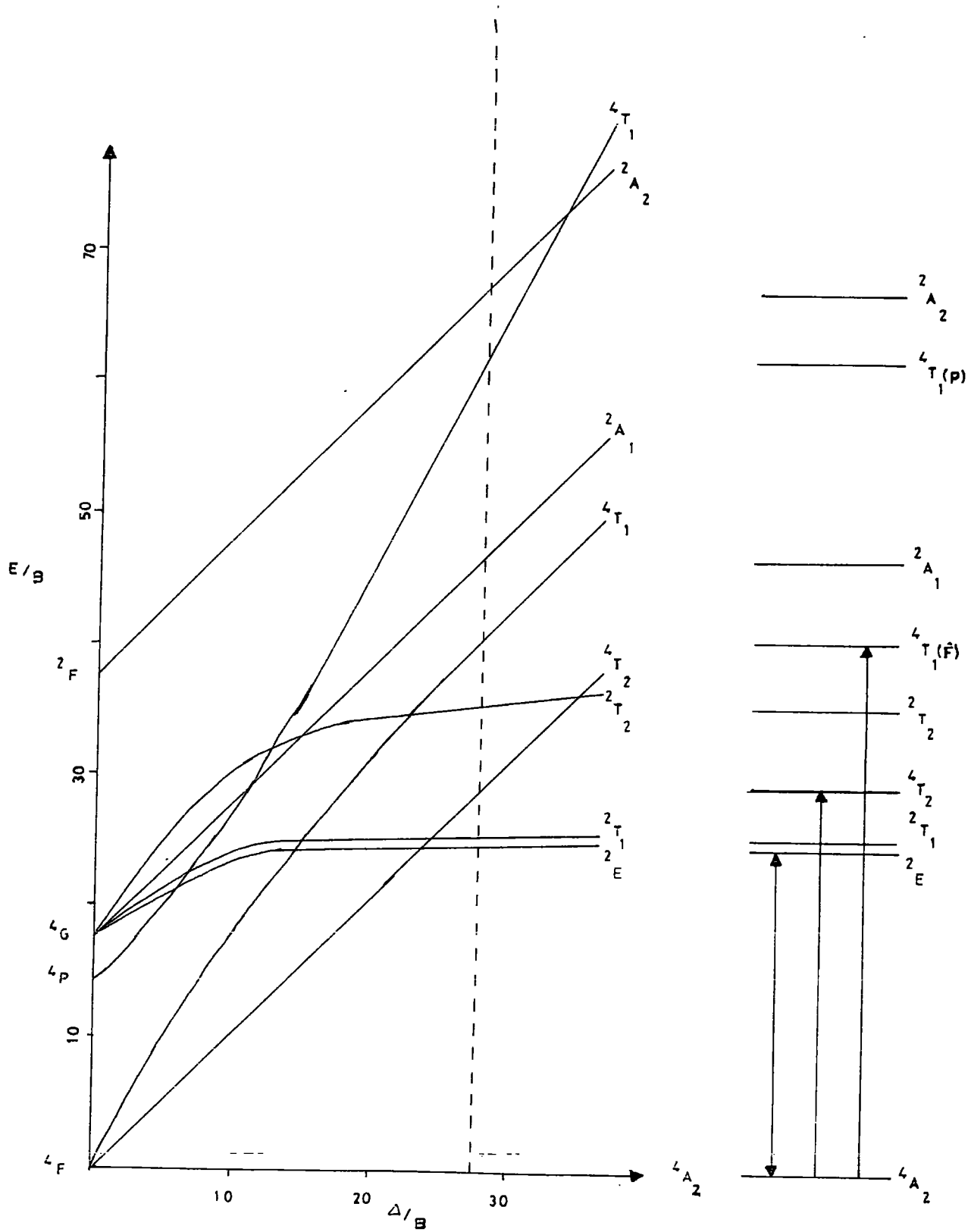

FIGURE 3.1 The optical energy levels for a d^3 ion in an octahedral field and the observed spectral transitions for MgO:Cr

3.1.4 The effect of covalent bonding

As explained in Chapter 1 it is unrealistic to ascribe all the bonding in such systems as doped MgO to a pure ionic mechanism. A calculation such as the one given there indicates that the bonding between oxygen anions and a transition metal cation of the type considered is about 50% ionic, and 50% covalent, and so a totally ionic model is substantially incorrect.

It is found that three factors need to be modified to account for the covalent effects. Firstly the electron repulsion integrals need to be reduced since covalency "spreads out their wavefunctions", and thus reduces their repulsion. Experimentally this results in the reduction of the parameter B for the ion in the lattice compared to that for a free ion. Presumably, although this is not so readily observed, the third Racah parameter C should be reduced by the same factor. Secondly the spin-orbit coupling constant, λ, should also be reduced since the electron now exists in an orbital made up partly by ligand orbitals where coupling between its spin and the (metal) orbital angular momentum will be small. Thirdly, the orbital contribution to the magnetic moment will be reduced for the same reason that the spin-orbit coupling is reduced. These reductions greatly add to the empirical nature of calculations of the energy levels of the system as we cannot calculate the extent of them for the particular system under consideration. However, with these reservations in mind, the aforegoing theory is still highly successful in correlating qualitatively much spectral and magnetic data.

3.1.5 The Co^{2+} ion

Cobalt in a doubly charged state has an outer configuration d^7. This may be regarded in two ways, (a) as seven electrons forming an incomplete electron shell, or (b) as three holes in a complete shell (3.5).

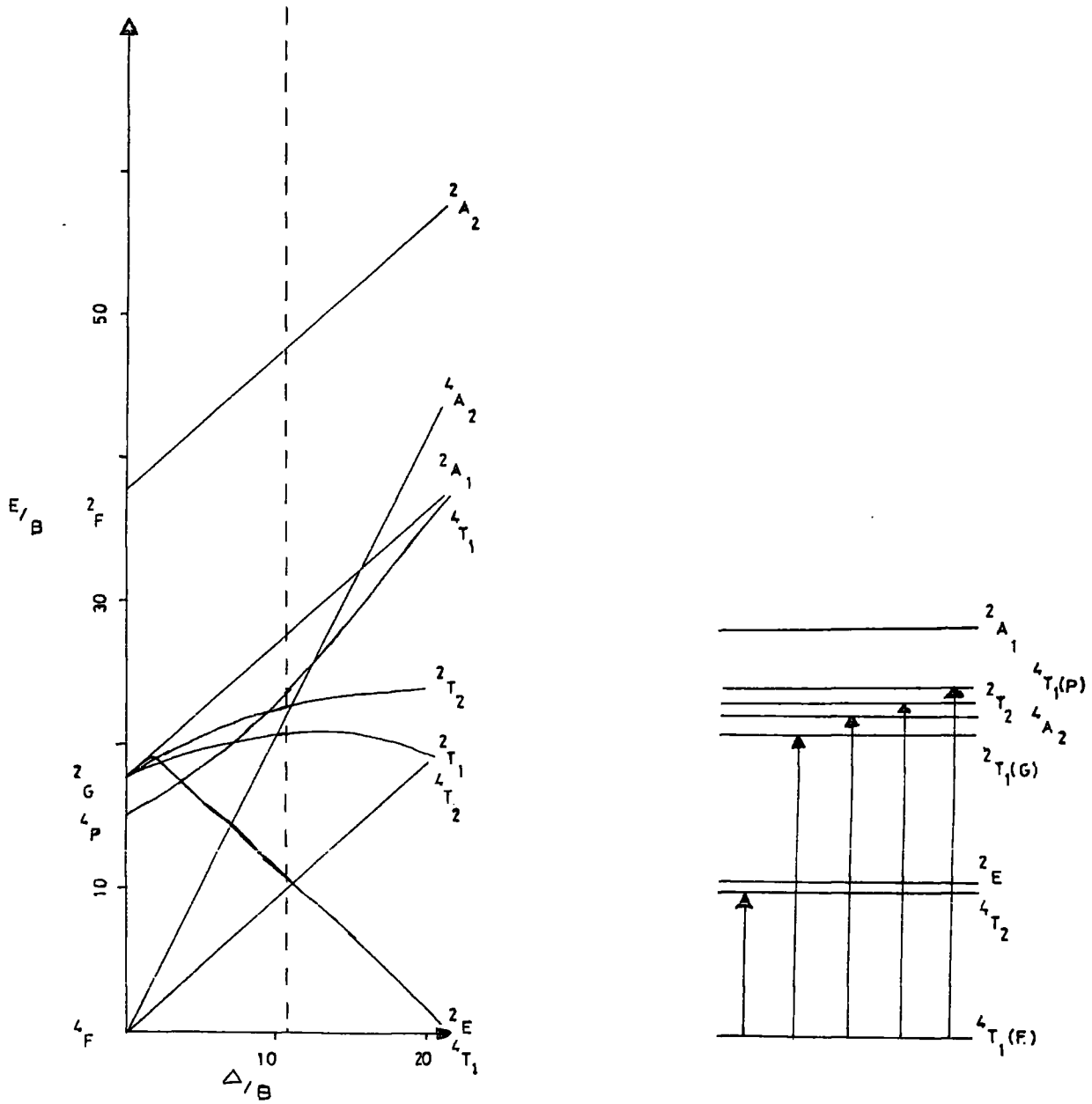

FIGURE 3.2 The optical energy levels for a d^7 ion in an octahedral field and the observed spectral transitions for MgO:Co

It is this so-called hole-formalism which simplifies the problem of evaluating the optical energy levels of Co^{2+} in an octahedral environment, since one of its consequences is that precisely the same theory can be used as has just been obtained for a d^3 ion, provided the substitution of-Δ for Δ is made everywhere. Hence an energy level diagram can be drawn for the Co^{2+} ion in an octahedral crystal field from the same matrix elements as used for the d^3 case (Appendix 2).

3.2 EXPERIMENTAL TECHNIQUES

Optical transmission spectra of the Chromium and Cobalt doped samples were scanned between 185 nm and 1 μm on an Optica CF4 DR recording spectrometer, and between 1 μm and 3 μm on an Optica CF4 DRNI recording spectrophotometer. In addition the optical emission spectra of the Chromium doped crystals were recorded on a home-built rig. Both these systems are described in detail below.

3.2.1 The Transmission Spectrophotometers

Both Optica instruments are basically the same design and a diagram is given in Figure 3.3. Light from the lamp passes through a filter, to remove the second and higher orders of the grating, into a monochromator of the Littrow type. The plane grating used in the CF4 DR instrument is ruled at 600 lines per mm, and the grating used in the CF4 DRNI instrument at 300 lines per mm. The object of the double-beam arrangement of the optical head is to compensate for any non-linearity in the spectral emission of the source and the spectral sensitivity of the detectors. The light emerging from the monochromator is passed alternately through the reference compartment and the sample compartment with a switching frequency of about 18 Hz. The light through either finally impinges on a detector which,

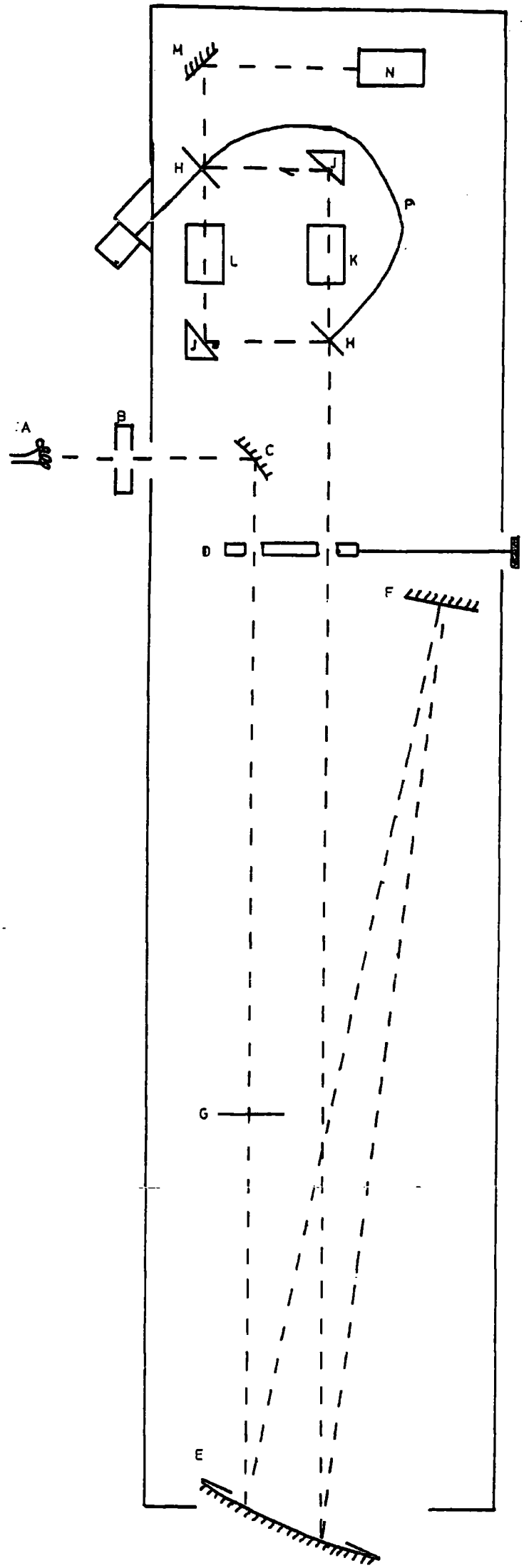

KEY

A	LAMP
B	FILTER
C	MIRROR
D	SLIT
E	MIRROR
F	MIRROR
G	GRATING
H	ROTATING MIRROR
J	PRISM
K	SAMPLE COMPARTMENT
L	REFERENCE COMPARTMEN
M	MIRROR
N	DETECTOR
P	ROTATING MIRROR FLEXIBLE DRIVE

FIGURE 3.3 The Optical system of the Optica spectrophotometers.

during one half cycle received the light transmitted through the reference compartment and during the other that transmitted through the sample compartment.

The switching of the optical beam system is effected by the two rotating mirrors. These have an arc of 180°, and are displaced one against the other by 180°, so that only one is in the beam at any one time, while the other is switched out.

Corresponding to the optical switching of the beams an electrical switching is also required which is exactly synchronised with the optical switching. This is effected by a permanent magnetic which rotates within a coil, both magnet and mirrors driven by the same flexible drive from an external motor. This generator passes a signal to a relay, which causes a switching of the signals to be measured. After amplification the ratio of sample signal to reference signal is plotted as a function of wavelength.

To scan the full range of 200 nm to 3 μm, a number of combinations of lamp mirror and detector are needed; these are tabulated below.

Range	Lamp	Filter	Detector
200 nm - 350 nm	Hydrogen	White	Photomultiplier EMI 6256B
350 nm - 400 nm	Tungsten	Blue	Photomultiplier EMI 6256B
400 nm - 610 nm	Tungsten	White	Photomultiplier EMI 6256B
610 nm - 1 μm	Tungsten	Red	Photomultiplier Dymont 6911
1 μm - 1.2 μm	Tungsten	White	PbS cell
1.2 μm - 1.8 μm	Tungsten	Green	PbS cell
1.8 μm - 3.0 μm	Tungsten	Yellow	PbS cell

3.2.2 Sample preparation

Single crystals of Magnesium Oxide doped with Chromium and Cobalt were obtained from W.C. Spicer (Cheltenham) Ltd.of approximate size

10 mm x 5 mm x 3 mm to fit the sample holder. This was essentially a metal plate which located precisely in the sample compartment of the Optica, with a hole drilled through to allow the light beam to pass. The sample was fixed to this plate with Apiezon grease. Actually when the samples were ordered the thickness was chosen to decrease with increasing concentration so that the peak height stayed within the range of the spectrometer, the required thickness being evaluated by assuming Boer's law held, and testing a sample of each substance already in the Department's possession.

When performing measurements of this nature it is very important that the faces of all the crystals are as exactly similar as possible. With this in mind it was decided to try to etch the samples in H_3PO_4 at 350°C. Unfortunately a trial run on one sample showed problems, since the thermal shock on immersing the specimen caused it to crack. If a lower temperature was used many pits were seen, which ruined the surface as far as any quantitative transmission spectroscopy was concerned. Consequently attempts at etching were abandoned and instead the samples were polished down to ¼μ and washed in propan-2-ol immediately before the spectrum was taken. The effect of polishing did not alter the intensity of absorption by the dopant ions, but did reduce the background absorption of the MgO.

3.2.3 Cryogenic facilities

So that spectra could be taken at low temperature an existing cryostat was converted to fit the Optica. A diagram is given, Figure 3.4. The sample was mounted on the copper cold finger with Apiezon grease, and a thermocouple mounted on the copper cold finger showed that, using liquid nitrogen as a refrigerent, a minimum temperature of 79 K was attainable after a few minutes. The pumping of the jacket was effected by a rotary pump. As no observable frosting of the windows or the sample occurred it

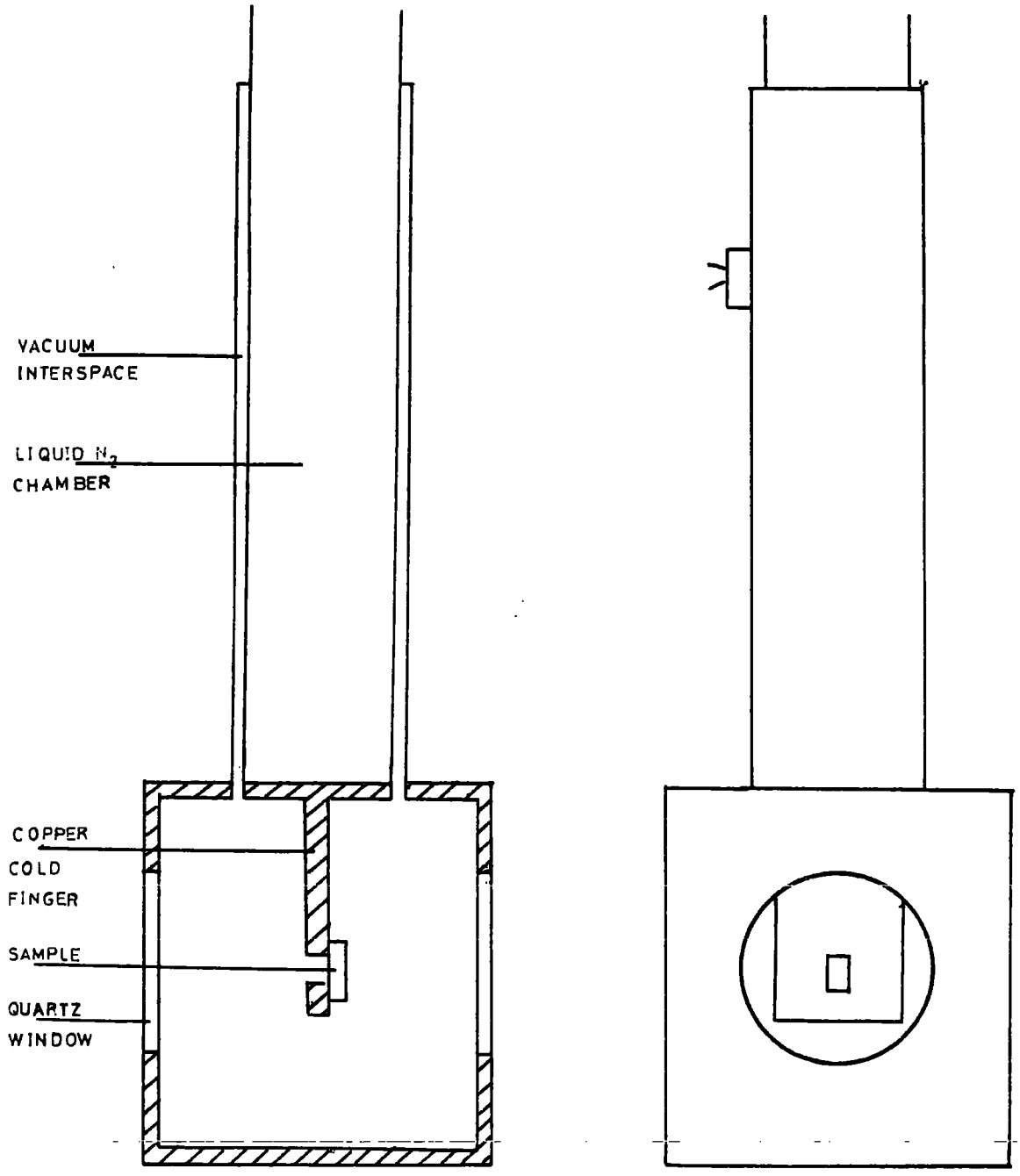

FRONT AND SECTIONAL SIDE VIEW OF OPTICA CRYOSTAT

FIGURE 3.4 The optical cryostat used in transmission work

was not felt necessary to use a diffusion pump, and this corresponding simplification of the vacuum system allowed the cryostat to be easily installed and removed from the instrument.

One of the objections to using this cryostat in a double beam instrument is that the introduction of two quartz windows into the specimen light beam might disturb the optical parallelogram and make the reference beam and sample beam optically non-equivalent. This was tested by comparing room temperature spectra recorded with the cryostat both in and out of position. As no differences were observed it was assumed that the system with the cryostat suffered no effects of the type described above.

3.2.4 The emission spectrometer

Many attempts were made to observe luminescence from the samples using the Optica. This was done by using it in the single-beam mode, i.e. with the rotating mirrors turned off so that all light from the monochromator goes via one path to the detector. The source lamp was removed and instead light emitted from the sample at right angles to the exciting radiation focussed on to the exit slits. This system gave no results at room temperature or at 77 K, and so the apparatus shown in Figure 3.5 was set up, with the aid of Paul Waite.

It will be seen to be a conventional emission spectrometer, with light emitted at 90° to the exciting radiation being monitored. The exciting radiation was from a 260 W high-pressure mercury lamp. It was passed through 2 OX1 filters and a $CuSO_4$ cell to remove all components except the ultra-violet, and was focussed on to the sample. The sample was mounted on a copper cold finger at 45° to the incident beam, in a cryostat similar to the one described in the last section, except that the windows were at 90° to each other. The emitted radiation passed through an

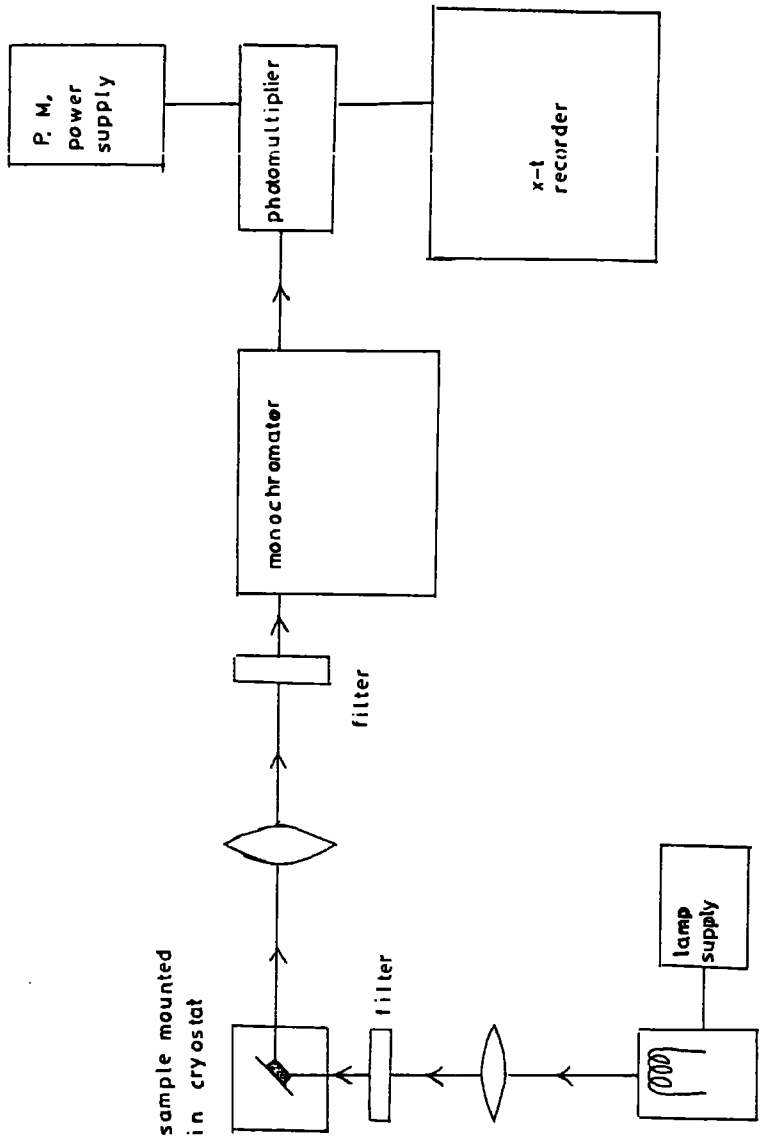

FIGURE 3.5 The photoluminescence spectrometer

LP 63 filter to reduce reflected exciting light, and was focussed on to the slits of a Hilger and Watts grating monochromator. The detector used was a Ga/As photomultiplier.

Samples used in this spectrometer were the same ones as used in the transmission work. They were mounted on the copper cold finger with Edwards silicone high vacuum grease, as the Apiezon grease used in the transmission work was seen to luminesce light blue in the mercury lamp radiation. Before mounting the samples were cleaned with propan-2-ol.

CHAPTER FOUR

OPTICAL SPECTROSCOPY OF MgO:Cr

The optical spectrum of MgO:Cr in both emission and absorption has been studied extensively. The absorption work was first reported by Low (4.1) as part of his systematic investigation of paramagnetic ions in a magnesium oxide host lattice. Much work has been done on studying the emission spectrum, e.g. the series of publications by Schawlaw et al which deal with the photoluminescence of Cr^{3+} in both cubic and non-cubic sites (4.2).

Originally it was decided to obtain the absorption spectra of the samples to be used in the e.s.r. work merely to check their composition, but a number of interesting points arose, which it was felt warranted further investigation. These results and their interpretation are now presented here in the order in which they were obtained, namely the absorption data first, and then the emission work afterwards.

4.1 THE OPTICAL ABSORPTION SPECTRA OF MgO:Cr

It is convenient here to divide the specimens considered into two groups, which will be referred to as samples of low and high concentration. The dividing line is not exactly sharp, but the three samples with dopant levels of 7400, 9500 and 15100 ppm are taken as high concentration.

The low concentration group will be discussed first. These samples give two bands in the visible region of the spectrum, one at 453.6 nm and one at about 620 nm (Figure 4.1). The band at 453.6 nm is present in all samples with a slight shoulder to high wavelength, while the feature at 620 nm consists of one intense line, with a weaker absorption to the high wavelength side at about 709 nm. In addition the 4200 ppm sample shows a weak absorption at 552 nm and a further shoulder on the band at 620 nm.

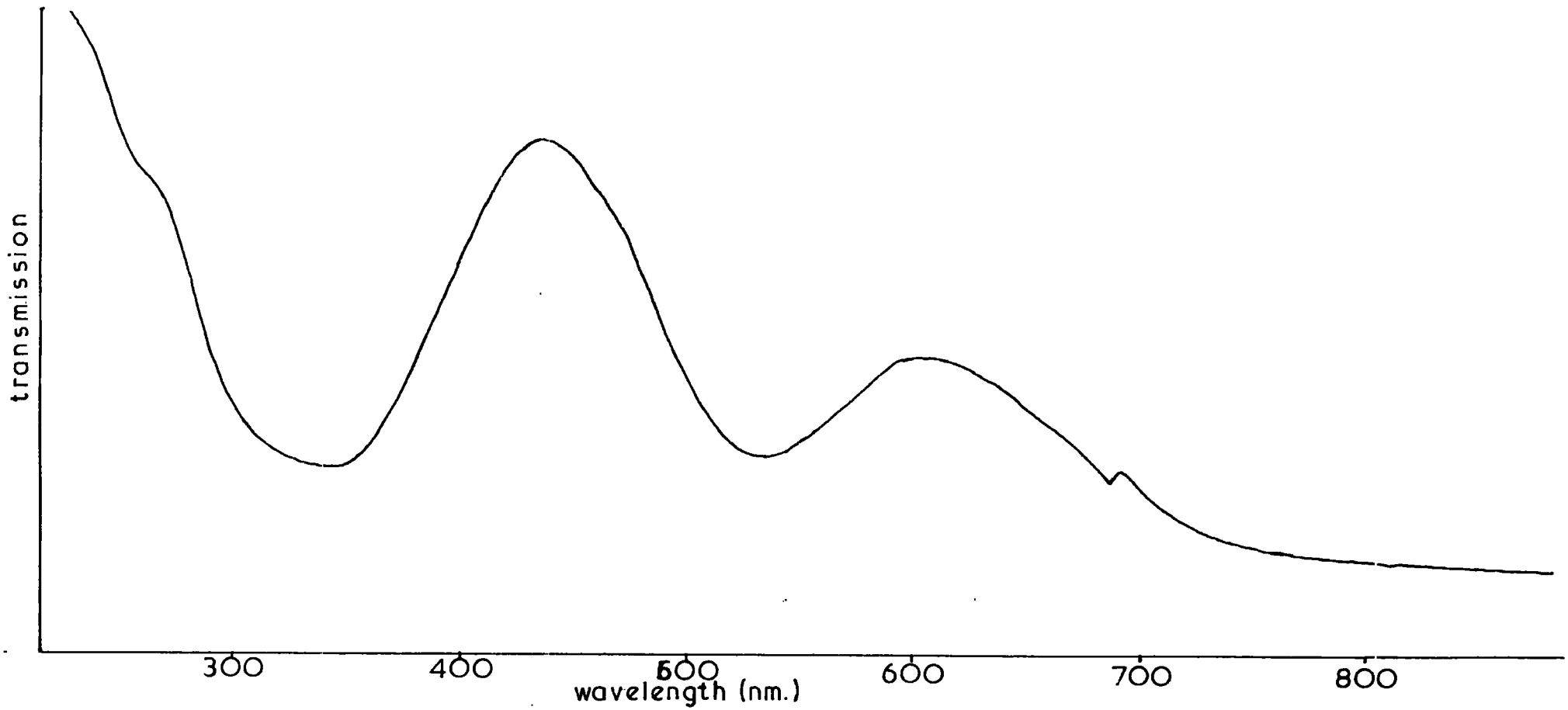

FIGURE 4.1 Optical transmission spectrum of MgO:Cr (1300 ppm)

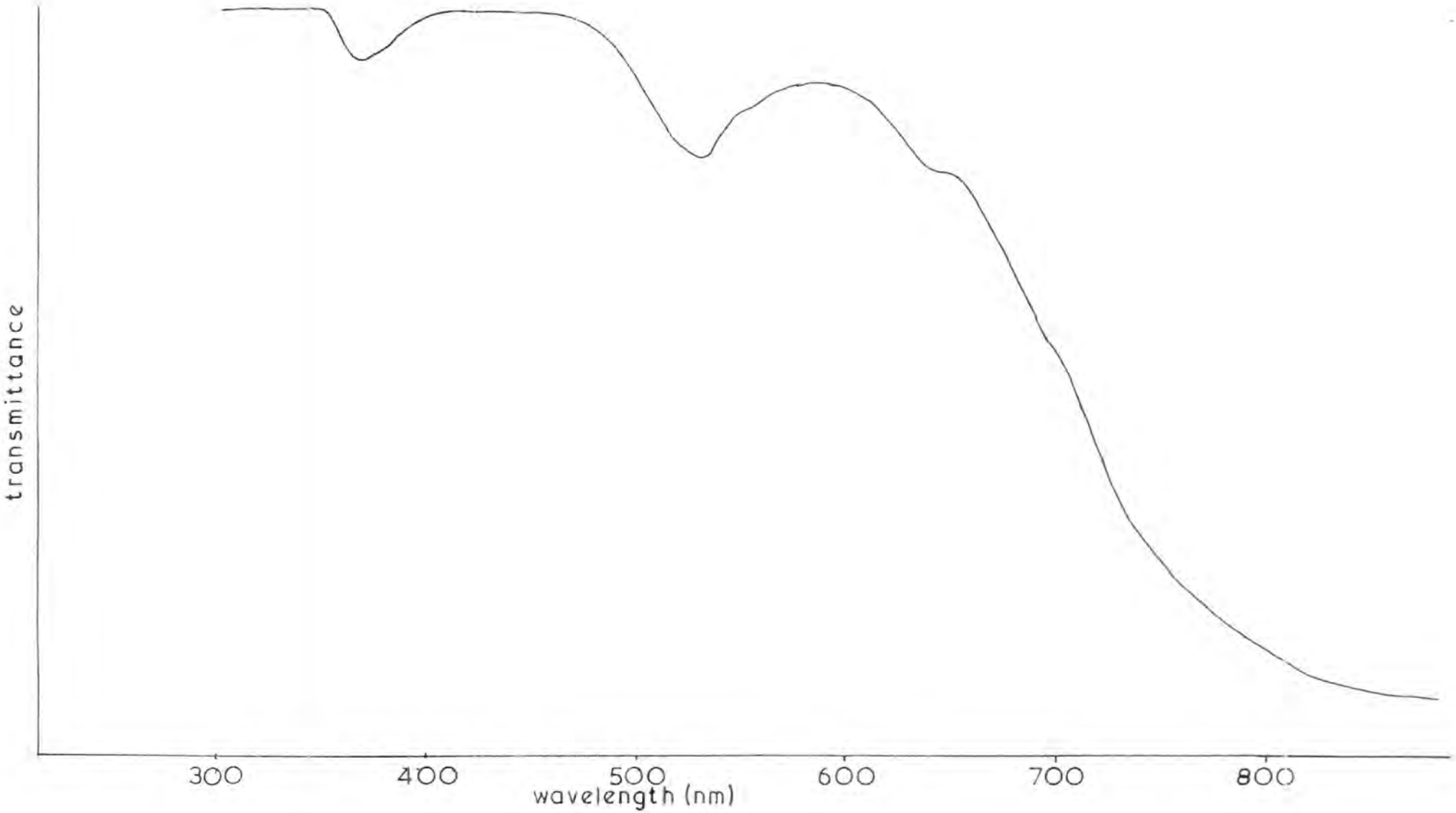

FIGURE 4.2 Optical spectrum of MgO:Cr (15100ppm)

These results are in good agreement with Low (4.1) who reports lines at 445 nm, and 620 nm. He also reports a line at 340 nm, which we do not see. This supports his view that one of his peaks is not due to Cr^{3+}, but rather divalent chromium in the lattice.

The spectra of the high concentration specimens are slightly different to those discussed above (Figure 4.2). The strong absorption at 620 nm is shifted to a lower wavelength, and a new band appears at about 655 nm. The weak absorption at 709 nm is unaltered in position, and the 7400 ppm sample also shows a band at 551.5 nm. Unfortunately it is difficult to obtain any information on the strong band at 453.6 nm as the background absorption of the MgO is much more enhanced and tends to saturate the spectrum, leading to a great uncertainty in the actual position of the absorption.

Recording the spectrum at 77 K produced no new features, apart from the appearance of two small sharp peaks at 485 and 488 nm, and a further doublet at 667 and 669 nm with the low concentration samples.

4.2 INTERPRETATION OF THE ABSORPTION SPECTRA

In low concentration samples it is generally agreed that the lines at 620 nm and 453.6 nm are due to the transitions $^4T_2(F) \leftarrow {}^4A_2(F)$, and $^4T_1(F) \leftarrow {}^4A_2(F)$ respectively (4.3). From this the two parameters B and Δ can be calculated since the energy of the $^4T_2(F) \leftarrow {}^4A_2(F)$ transition is equal to Δ, and that of the $^4T_1(F) \leftarrow {}^4A_2(F)$ to $\frac{1}{2}\left[15B - 0.6\,\Delta - (225B^2 + 18B\,\Delta + \Delta^2)^{\frac{1}{2}}\right] + 1.2\,\Delta$. Hence $\Delta = 16130\ cm^{-1}$ and $B = 576\ cm^{-1}$. These values are different to those given by Low (5.1), (the only author who appears to have given numerical values) since he assigns the bands differently to the scheme propounded above. This requires some explanation, which is given below.

In considering the energy scheme outlined in Chapter 3, Low agreed that the spectrum it would be possible to fit by taking $\Delta \simeq 16200\ cm^{-1}$, and $B \simeq 650\ cm^{-1}$. His objections to this were as follows. Firstly he correctly evaluated the position of the transition $^4T_1(P) \leftarrow {}^4A_2(F)$ as $\frac{1}{2}[15B - 0.6\Delta + (225B^2 + 18B\Delta + \Delta^2)^{\frac{1}{2}}] + 1.2\Delta = 35000\ cm^{-1}$ implying that the transition should be seen at 286 nm. Low observed a line, which we do not, at 340 nm, and subsequently concluded that, since this is far outside experimental error, the original assignment must be wrong. This difficulty does not exist here, however, since this line is not observed; nor has it been reported by other workers. We have been unable to search for the line predicted at 286 nm since the 'anomalous absorption of the MgO' prevents investigation of this region. It is tempting to postulate that the band seen by Low is due to an impurity. Low's comment that this system of assignment gives a value of Δ which is lower than expected, still remains valid.

The weak line at 709 nm is probably the transition $^2E(G) \leftarrow {}^4A_2(F)$. As can be seen from the energy level diagram this transition is largely independent of Δ which explains the sharpness of the line. This transition is discussed in more detail later.

Passing now to the spectra of the high concentration samples, the shift in position of the peak corresponding to the transition $^4T_2(F) \leftarrow {}^4A_2(F)$ indicates a change in Δ. This change is not linear in concentration. The values of Δ implied are $16180\ cm^{-1}$ for the 7400 ppm sample, $17100\ cm^{-1}$ for the 9500 sample, and $16720\ cm^{-1}$ for the 15100 ppm sample. The line at 709 nm remains where it is indicating that its position is almost independent of Δ. There remains now the problem of assigning the new band at 655 nm. It could be due to the Cr^{3+} ion entering a new site in the MgO lattice. This is not entirely unexpected. Considering the thermodynamics of the situation (as was done earlier for iron) shows that

equation (1.4) applies, but now w is the crystal field stabilisation energy. For a d^3 ion this is 1.2Δ, i.e. the amount that the ground state of the complex is stablized over the ground state of the free ion. Hence

$$1.2\Delta N_o = RTLn\left(\frac{1}{4}\left[\frac{1-3\delta}{\delta}\right]^3\right)$$

where the notation of Chapter 1 is still employed.

There now remains the problem of what to take for the temperature T. It has been shown (4.4) that if a crystal is cooled at a faster rate than the rate of a particular reaction then the equilibrium state of the crystal is frozen at that of the higher temperature. This is assumed to be the case here, and T is taken as the temperature at which the crystals were grown, namely the melting point of MgO, 3200 K. This gives $\delta = 0.0314$, where $\Delta = 16139\ cm^{-1}$. If Δ increases then the value of δ decreases. Thus one would not expect such a high maximum doping level with MgO:Cr as with MgO:Fe, implying that to get very high levels another sort of structure might be formed. This has been reported to be the spinel structure (4.5) and so this new band at 655 nm can be tentatively assigned to Cr^{3+} in this structure. This implies a value of Δ for Cr in the octahedral sites of the $MgCr_2O_4$ spinel of about $15300\ cm^{-1}$. Fortunately, as this band is weak, one can assume that there is a small percentage of spinel compared to the straightforward substitutional system, consistent with the x-ray work reported earlier, and it can almost be ignored.

4.3 THE EMISSION SPECTRA OF MgO:Cr

In an attempt to gain more information on the high concentration samples the photoluminescence spectra were recorded. The observed luminescence was weak, about one hundredth of the analogous luminescence of ruby, and furthermore occurs in an inconvenient region of the spectrum, insomuch as it appears as structure superimposed on the second order

diffraction of the exciting mercury radiation. Other exciting lamps were tried, but ones of sufficient power to give observable luminescence were not available, and so various systems of filters were used in conjunction with the Hg lamp to obtain the best possible results. The luminescence was not observed at room temperature, but was apparent at 77 K (see Figure 4.3).

In discussing the results obtained it is convenient again to separate the samples into the high and low concentration sub-divisions as discussed above. The low concentration samples all showed a line at about 699 nm which was sharp, having a half-width of about 6 nm, and also a weaker line, which was also sharp, at about 695 nm. The 5000 ppm sample also showed peaks at 723 nm and at about 715 nm, while the 6200 ppm sample showed an extra line at 705 nm.

The high concentration samples distinguished themselves by showing very little or no spectrum at all. The 7400 ppm sample gave a hint of emission around about 700 nm, but the two higher concentration samples gave an apparently totally featureless spectrum. To check to see if this were so, or if there were peaks which were masked by the second-order mercury line, the cathodoluminescence spectrum of the 15100 ppm sample was kindly taken by Dr. S. Gezci.

The cathodoluminescence of the 15100 ppm sample at 77 K showed four features. Two lines of approximately equal intensity at 697.8 nm and 703.4 nm were observed, with two broader and less intense lines at 725.5 nm, and 719.5 nm also clearly seen. It is possible that these latter lines are superimposed on a broad background emission. This spectrum was fairly noisy since the peaks appeared very close to the end of the range of the photomultiplier used.

4.4 INTERPRETATION OF EMISSION DATA

The photoluminescence of the low concentration crystals will be discussed first, then the high concentration crystals, and finally the cathodoluminescence spectrum. There can be little doubt that the line at 699 nm is due to the magnetic dipole no-phonon transition $^2E(G) \rightarrow {}^4A(F)$ (4.6). Chromium in both cubic and non-cubic sites contribute to this line, and better resolved spectra give a line at 698.1 nm for the cubic sites (the R-line) and 698.9, 699.2, 703.5 and 703.8 nm for non-cubic sites (N-lines) (4.7). It is possible that the line observed at 705 nm from the 6200 ppm sample is due to an enhancement of either the 703.5 or the 703.8 nm lines, or both. The fact that it is seen from the most heavily doped of the samples which gave resolvable spectra supports this suggestion, since Imbush et al (4.8) assign both these lines to a chromium-vacancy-chromium associate in the <100> direction. Such a system will become rapidly more common as the concentration increases.

The lines observed in the spectrum of the 500 ppm sample at 723 and 715 nm are possibly vibrational sidebands of the R- and N-lines. These have been reported at 718 and 725 nm (4.9), and experimentally it was found that the line at 723 nm is the more intense of the two lines, and in the reference just cited this is found to be the case. The 723 nm line is thus tentatively assigned as a phonon assisted transition for a non-cubic site, and the 715 nm line as a phonon assisted transition for a cubic site.

Turning attention to the high concentration samples, the fact that they appear to show very weak photoluminescence is not easy to explain. The first thought is that the position of the line must be shifted to a position where it cannot be seen, as it is masked by the second order diffraction of the exciting radiation. However this is unlikely since the absorption results outlined earlier do not indicate a significant

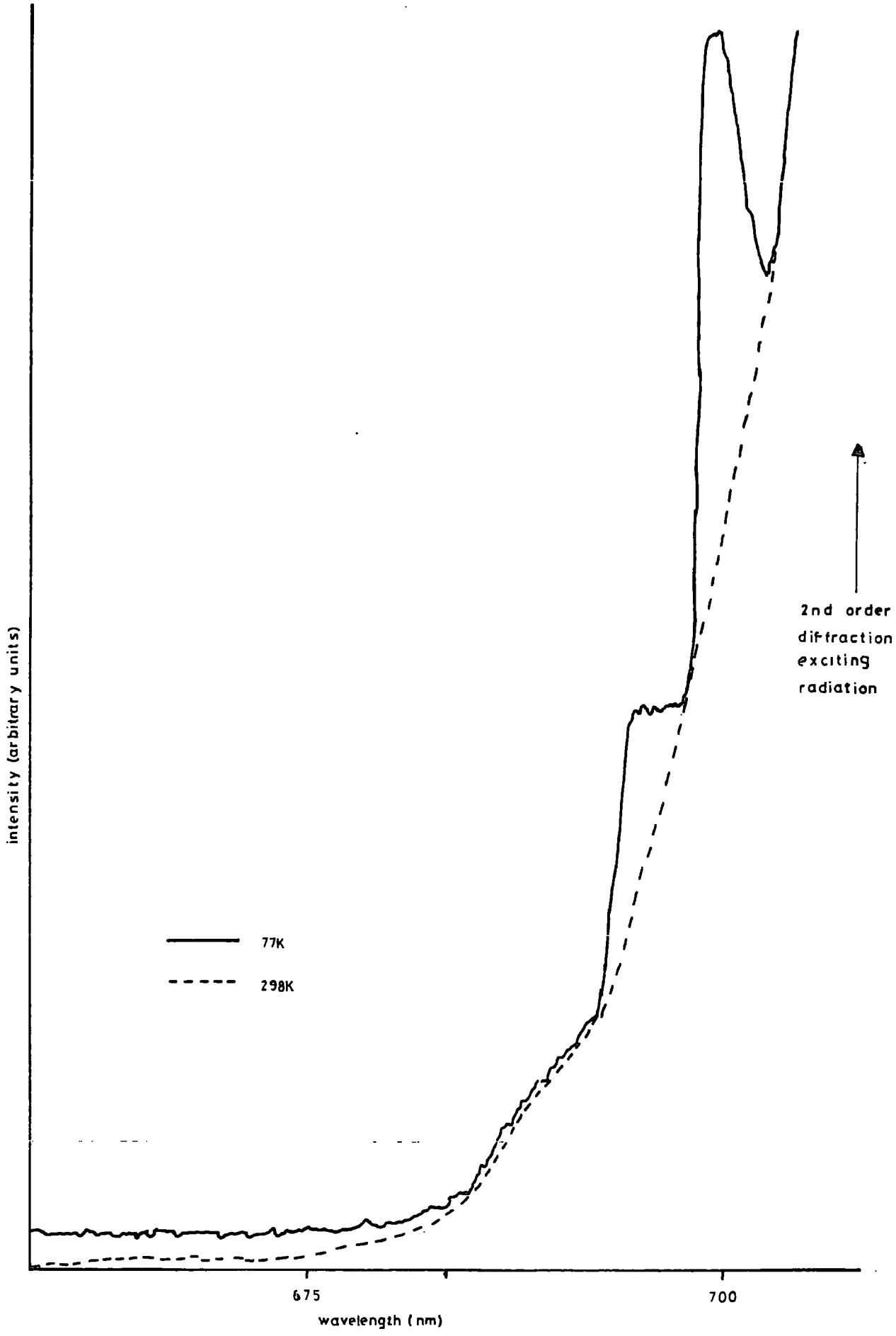

FIGURE 4.3 The photoluminescence spectrum of MgO:Cr (3600ppm)

change in the energy of the transition in question, and indeed one is not expected since the relative energies of the $^2E(G)$ state and the ground state are largely independent of Δ. Another, and preferred, explanation is that the reflectivity of these samples is greater at the wavelength of the exciting radiation than the low concentration samples, causing this line to mask the luminescence. This is born out by the experimental observation that the slits had to be set narrower for these crystals.

In order to check this more fully the cathodoluminescence spectrum was recorded of the 15100 ppm sample. The lines observed agree almost perfectly with previous workers (4.4), and there is no hesitation in assigning the 697.8 nm line to the R-line, as described above, the 703.4 line to the N-lines, and the lines at 719.5 and 725.5 to vibrationally assisted sidebands of the R- and N-lines. Hence there is no difference, within experimental error, between the cathodoluminescence spectrum of the 15100 ppm doped sample and the photoluminescence spectra of the low concentration samples, except perhaps in the relative intensities of the lines, the number of non-cubic sites increasing with concentration, as expected.

CHAPTER FIVE

OPTICAL SPECTROSCOPY OF MgO:Co

The optical spectrum of cobalt in magnesium oxide was first reported by Low, (5.1), in 1958 as part of his systematic investigation of d-block elements in the MgO host lattice. Later it has been discussed by Pappalardo et al (5.2) who were investigating different oxide lattices. More recently Russian workers have reported the spectra (5.3), but the system has received much less attention overall than the MgO:Cr system discussed in the last chapter. One reason for this is that although the absorption spectrum of MgO:Co is easily observable, the corresponding emission spectrum is extremely weak, and occurs in the infra-red region of the spectrum (5.4), which is inconvenient since the sensitivity of detectors is poor in this region.

The optical spectrum of MgO:Co has been examined both at room temperature and liquid nitrogen temperatures, and here the results are presented, along with an attempt to fit them to the theory. The observation of the spectrum at two temperatures provides a convenient way of dividing the data, and the room temperature results will be examined first.

5.1 ROOM TEMPERATURE RESULTS

The present data shows that cobalt in magnesium oxide exhibits absorptions in two regions of the spectrum between 350 nm and 3 μm. There is one band in the visible at about 510 nm, and one in the near infra-red at about 1.15 μm. This is in concordance with previously reported work (5.1).

The structure observed in the visible region consists of a complex envelope of peaks on the tail of the 'anomalous' absorption of MgO, (see

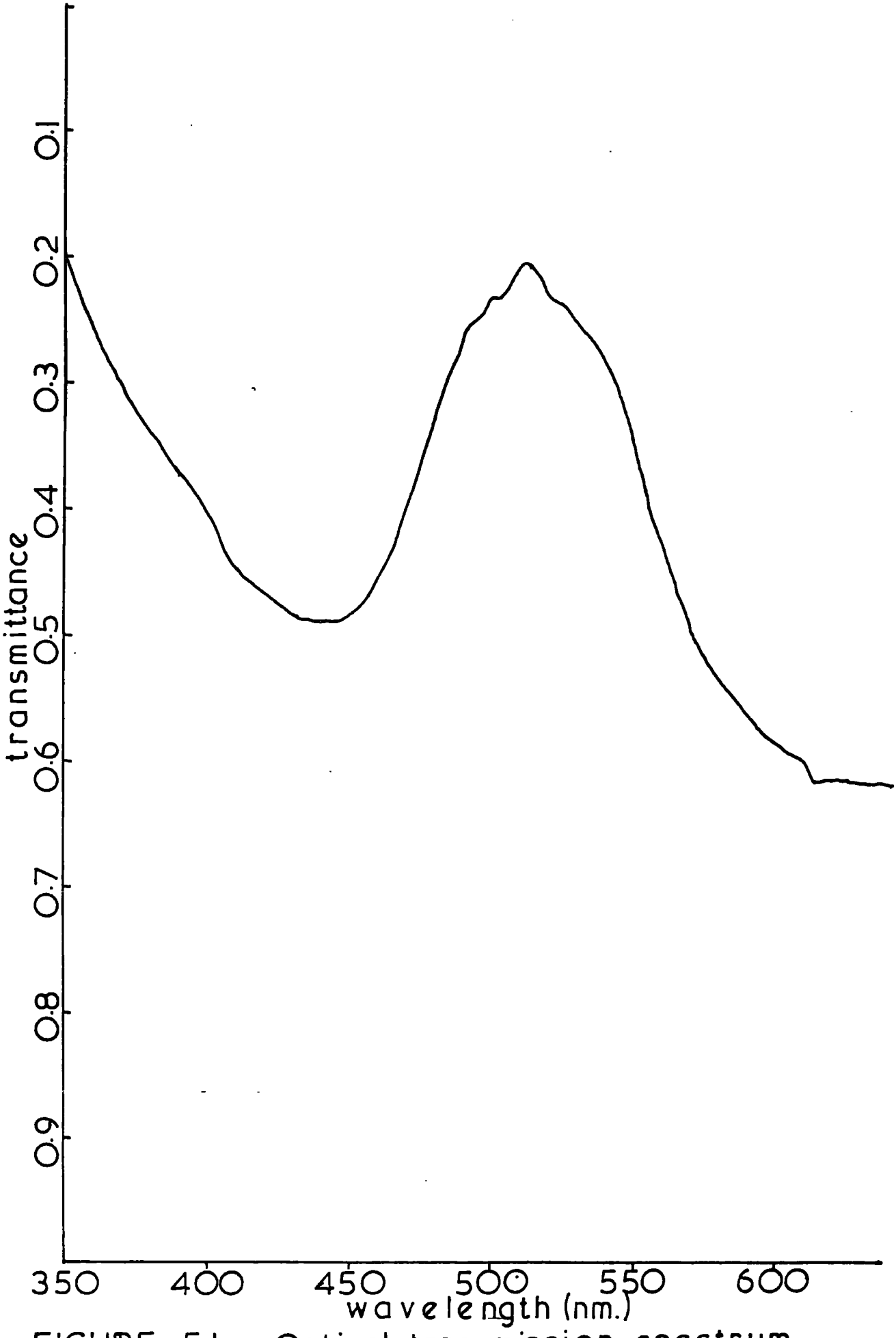

FIGURE 5.1 Optical transmission spectrum of MgO:Co (9900ppm) 298 K

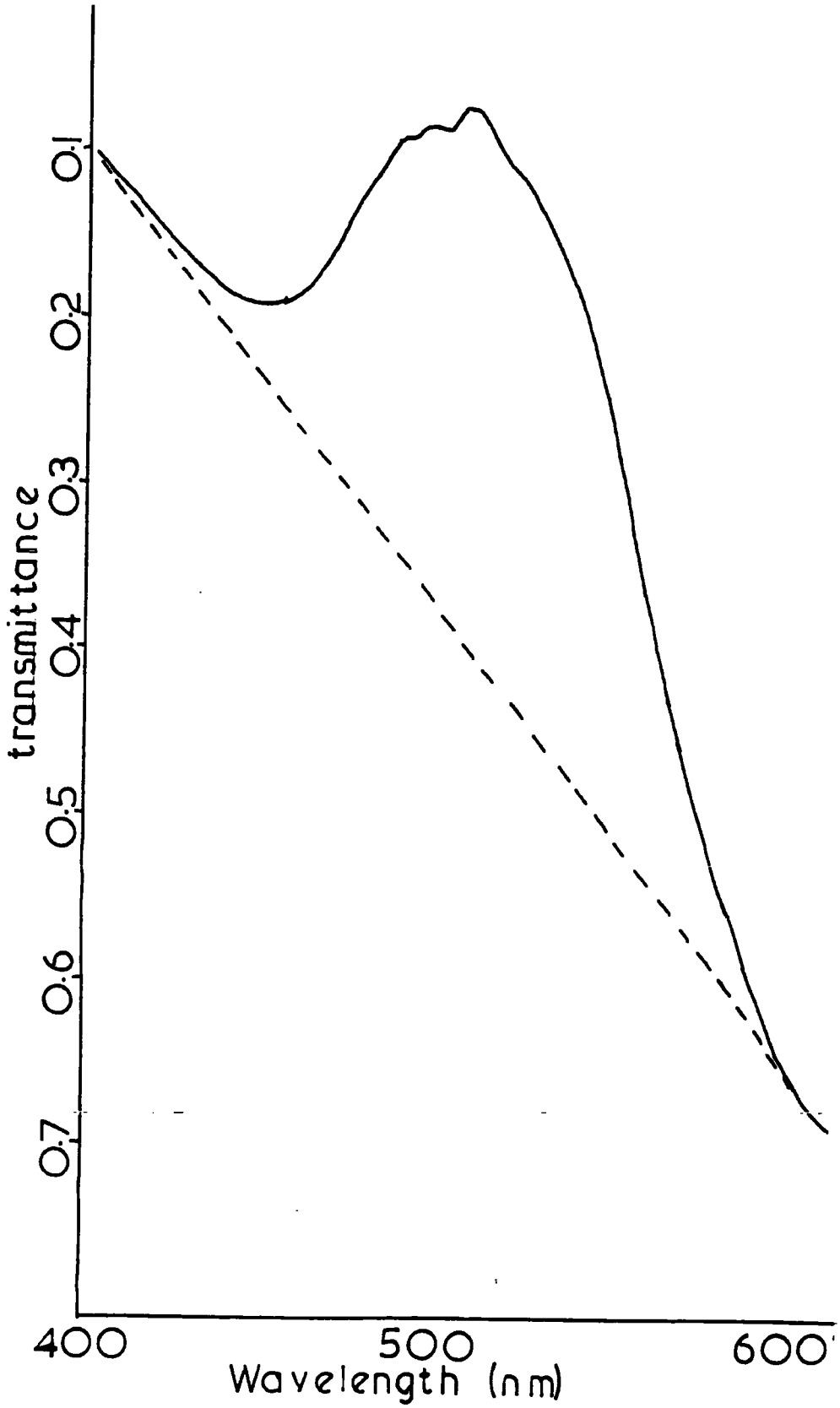

FIGURE 5.2 Optical transmittance spectrum of MgO:Co (3300ppm) 298K

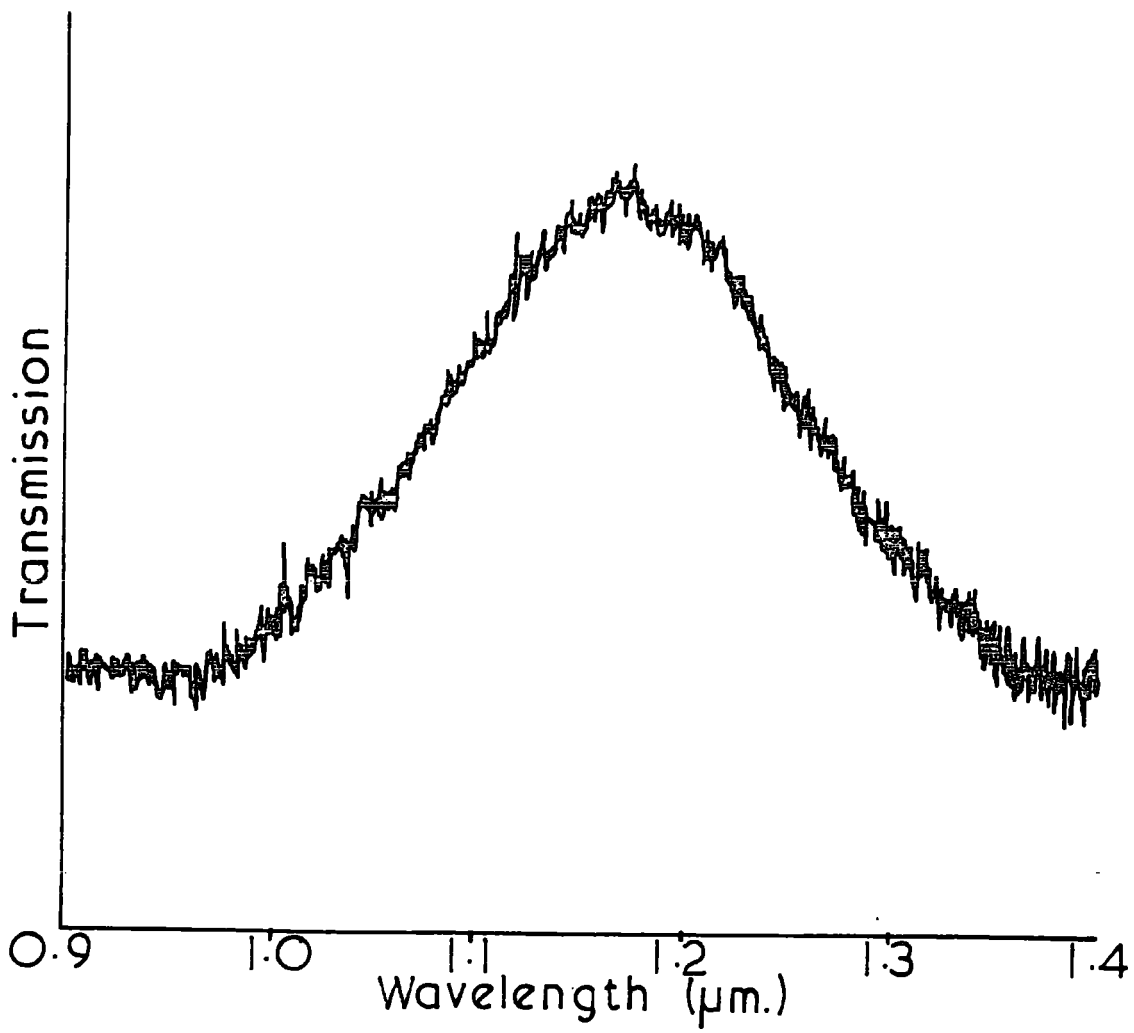

FIGURE 5·3 Infra-red transmission spectrum of MgO:Co (9900 ppm.) 298 K room temperature

Figure 5.1). All samples gave similar spectra, seeming to consist of four peaks at 491, 500, 511 and 526 nm, with possibly some structure at about 400 nm, and a further shoulder on the right hand (long wavelength) side. There is no evidence for a spectral shift as a function of concentration, as recently reported (5.4). This is consistent with the x-ray powder work reported in Chapter 2, which suggested that the lattice parameter of the samples is independent of concentration. The lines observed are in general agreement with the results of Low (5.1), obtained at 77 K. He reported lines at 488, 510, 534 and 581 nm, and also remarked on the band at 406 nm.

The line at about 1.15 μm is shown in Figure 5.3. As can be seen it is a much less complex feature. Again there is general concordance with Low, who gave it a wavelength of 1.181 μm compared with the 1.174 μm observed here. A similar situation pertains to the visible spectrum insomuch as it was found that the position of the line was independent of concentration, in contrast to a recent publication, (5.5).

5.2 INTERPRETATION OF THE ROOM TEMPERATURE DATA

A study of the energy level diagram for a d^7 ion in an octahedral environment shows that there are three spin-allowed transitions from the ground state, and these may be expected to dominate the spectrum. The transitions are:-

$$\left.\begin{aligned} &\text{(a)} \quad {}^4T_2(F) \leftarrow {}^4T_1(F) \\ &h\nu_1 = 0.2\Delta - \tfrac{1}{2}\left[15B - 0.6\Delta - (225B^2 + 18B\Delta + \Delta^2)^{\frac{1}{2}}\right] \end{aligned}\right\} \quad (5.1)$$

$$\left.\begin{aligned} &\text{(b)} \quad {}^4A_2(F) \leftarrow {}^4T_1(F) \\ &h\nu_2 = 1.2\Delta - \tfrac{1}{2}\left[15B - 0.6\Delta - (225B^2 + 18B\Delta + \Delta^2)^{\frac{1}{2}}\right] \end{aligned}\right\} \quad (5.2)$$

$$(c) \qquad {}^4T_1(P) \leftarrow {}^4T_1(P) \qquad (5.3)$$

$$h\nu_3 = (225B^2 + 18B\Delta + \Delta^2)^{\frac{1}{2}}$$

There can be little doubt that the line seen at 1.174 μm is due to the transition

$${}^4T_2(F) \leftarrow {}^4T_1(F)$$

This transition is commonly observed in the infra red for Co^{2+}. Hence we can write

$$0.2\Delta - \frac{1}{2}\left[15B - 0.6\Delta - (225B^2 + 18B\Delta + \Delta^2)^{\frac{1}{2}}\right] = 8518 \text{ cm}^{-1}$$

Assignment of the remaining bands is a much more complex problem. As can be seen the absorption in the visible region of the spectrum is the superposition of many lines, and it is not an easy matter to separate these out into individual components. However, this has been attempted using an analogue curve fitter; by courtesy of Dr. D.T. Clark, Department of Chemistry, University of Durham. This instrument project on to the curve to be fitted the sum of a series of Gaussians. The operator can control ths position, width, and height of each individual Gaussian, until a satisfactory fit to the experimental data is obtained; each Gaussian can then be projected individually in order to see the individual components of the whole. At the same time an estimate of the percentage area of the total is given for each Gaussian.

Fitting was attempted repeatedly for each of the room temperature spectra, until the scheme considered most feasibly was found. This is shown in Figure 5.4. Previously Low also attempted to reconstruct the visible spectrum of MgO:Co,(5.1), but it has been impossible to reconcile either of the construction schemes proposed by Low with the new experimental

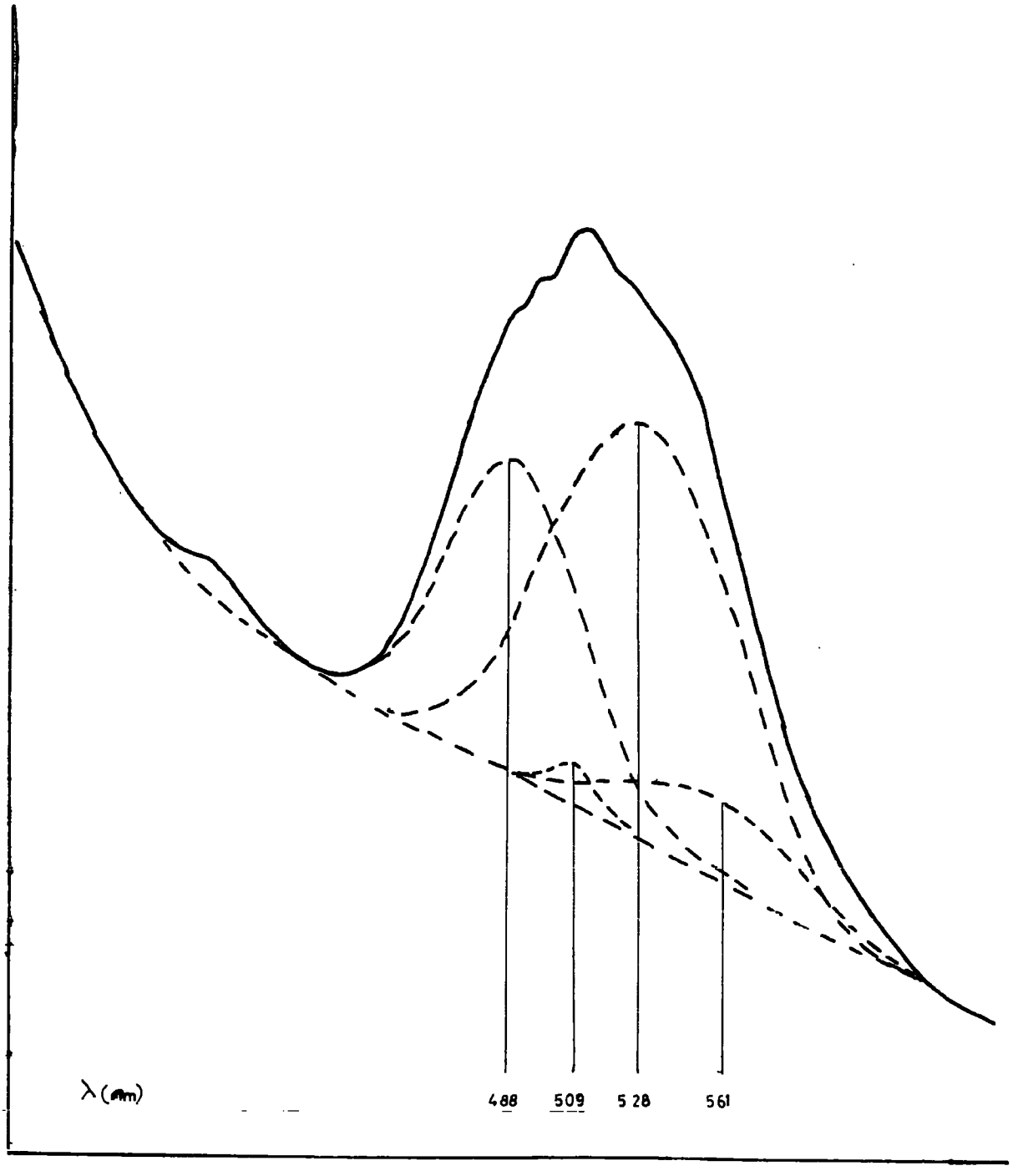

FIGURE 5.4 One reconstruction of the visible region

data. Figure 5.4 shows the proposed reconstruction of the spectrum from four main peaks. Two are of roughly equal intensity ($\sim$ 45%) at 488 nm, and 528 nm; there is a less intense ($\sim$ 11%) and broad peak at 561 nm, and finally a weak line ($\sim$ 1%) at 509 nm.

The best way that this can be fitted to the energy level diagram is to take Δ = 9700 cm^{-1} and B = 880 cm^{-1}. This predicts the transitions

$$^4T_2(F) \leftarrow {}^4T_1(F) \qquad \bar{\nu}_1 = 8520\ cm^{-1}$$

$$^4A_2(F) \leftarrow {}^4T_1(F) \qquad \bar{\nu}_2 = 18220\ cm^{-1}$$

$$^4T_1(P) \leftarrow {}^4T_1(F) \qquad \bar{\nu}_3 = 20540\ cm^{-1}$$

which compares with the observed lines at 8517, 18939 and 20491 cm^{-1}. It will be appreciated that the position of the transition at 8517 cm^{-1} is known to greater accuracy than the reconstructed peaks.

In this construction the weaker lines would be assigned to spin-forbidden transitions. The band at 561 nm is probably due to

$$^2T_1(G) \leftarrow {}^4T_1(F) \qquad \bar{\nu}_4 = 17830\ cm^{-1}$$

and that at 510 nm

$$^2T_2(G) \leftarrow {}^4T_1(F) \qquad \bar{\nu}_5 = 19608\ cm^{-1}\ .$$

These results differ slightly from those obtained by Low, who used a different scheme of reconstruction. For convenience a comparison of the two sets of data is given in Table 5.1.

The fact that there are four transitions of much the same energy makes it apparent that a situation exists where, at this particular set of Δ,B, and C, the optical levels are extremely bunched together, and must be very close to crossing one another. In this situation spin-orbit coupling becomes much more significant than in the case where the levels

Transition	Present data (cm^{-1})		Low's data (cm^{-1})	
	$\bar{\nu}_{obs}$	$\bar{\nu}_{calc}$	$\bar{\nu}_{obs}$	$\bar{\nu}_{calc}$
$^4T_2(F) \leftarrow {}^4T_1(F)$	8517	8520	8470	8470
$^4A_2(F) \leftarrow {}^4T_1(F)$	18939	18220	18700	18000
$^4T_1(P) \leftarrow {}^4T_1(F)$	20491	20540	19600	19800
$^2T_1(G) \leftarrow {}^4T_1(F)$	17830	-	17200	-
$^2T_2(G) \leftarrow {}^4T_1(F)$	19608	-	-	-
Δ	9700		9600	
B	880		833	

Table 5.1: Comparison of this data with that of Low.

are well separated, and calculation of the matrix elements should, more properly, be made in the spin-orbit manifold. Further evidence for this large spin-orbit interaction is provided by the fact that the intensities of the spin-forbidden bands are enhanced, due to the break down of the Laporte selection rule. The effect of this interaction would be to perturb the energy levels by up to a few hundred cm^{-1}, which could account for the discrepancies between the calculated energies and the observed energies for the transitions. It might be interesting to perform this calculation, and re-examine the results above, with a view to testing the accuracy of the assignments. However, even without working to such a degree of sophistication, the fairly close fit of the energy level diagram (to within 5%), gives some confidence in the scheme proposed above.

5.3 LIQUID NITROGEN RESULTS

In order to gain more information on the spectrum of MgO:Co in the visible region it was decided to record it at 77 K. Overall it was hoped that the reduction in temperature might reduce the linewidth of the individual lines sufficiently to allow the use of the more highly resolved spectrum to confirm the conclusions devised in the previous section. A typical absorption spectrum at 77 K is shown in Figure 5.5 . All the samples gave similar results, there being no observable shift in wavelength with concentration, or any apparent change in the relative intensities of the lines. As can be seen at 77 K, many more lines are resolved between 350 and 610 nm. The structure at about 400 nm appears as two sharp peaks superimposed on a broad band, three small peaks appear to high wavelength, and all in all there is evidence for at least six peaks in the body of the main envelope. These spectra are, so far as is known, the best resolved to date, and show the high degree of complexity of the spectrum in this region.

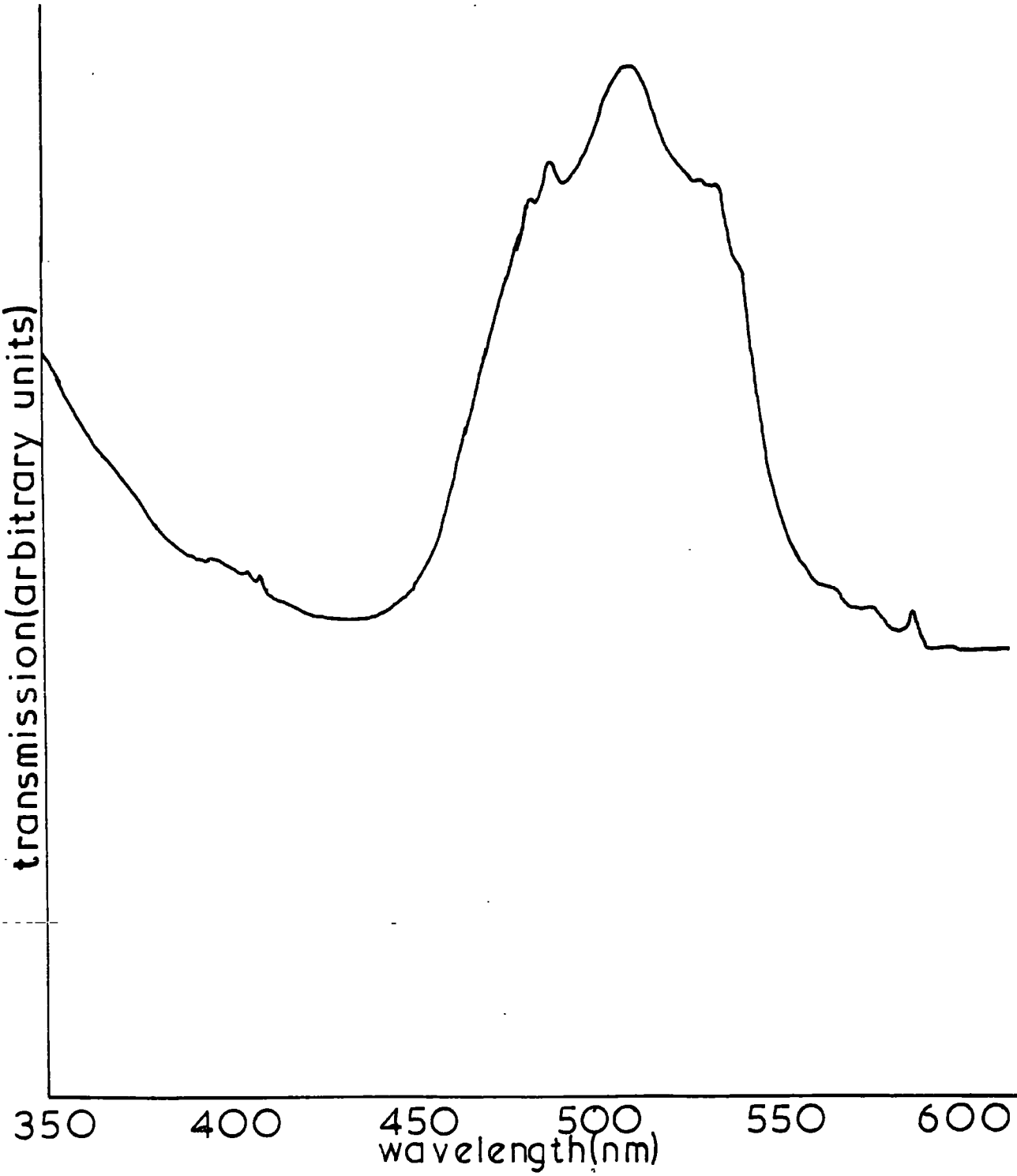

FIGURE 5.6 Optical transmission spectrum of MgO:Co (1250ppm) 77K

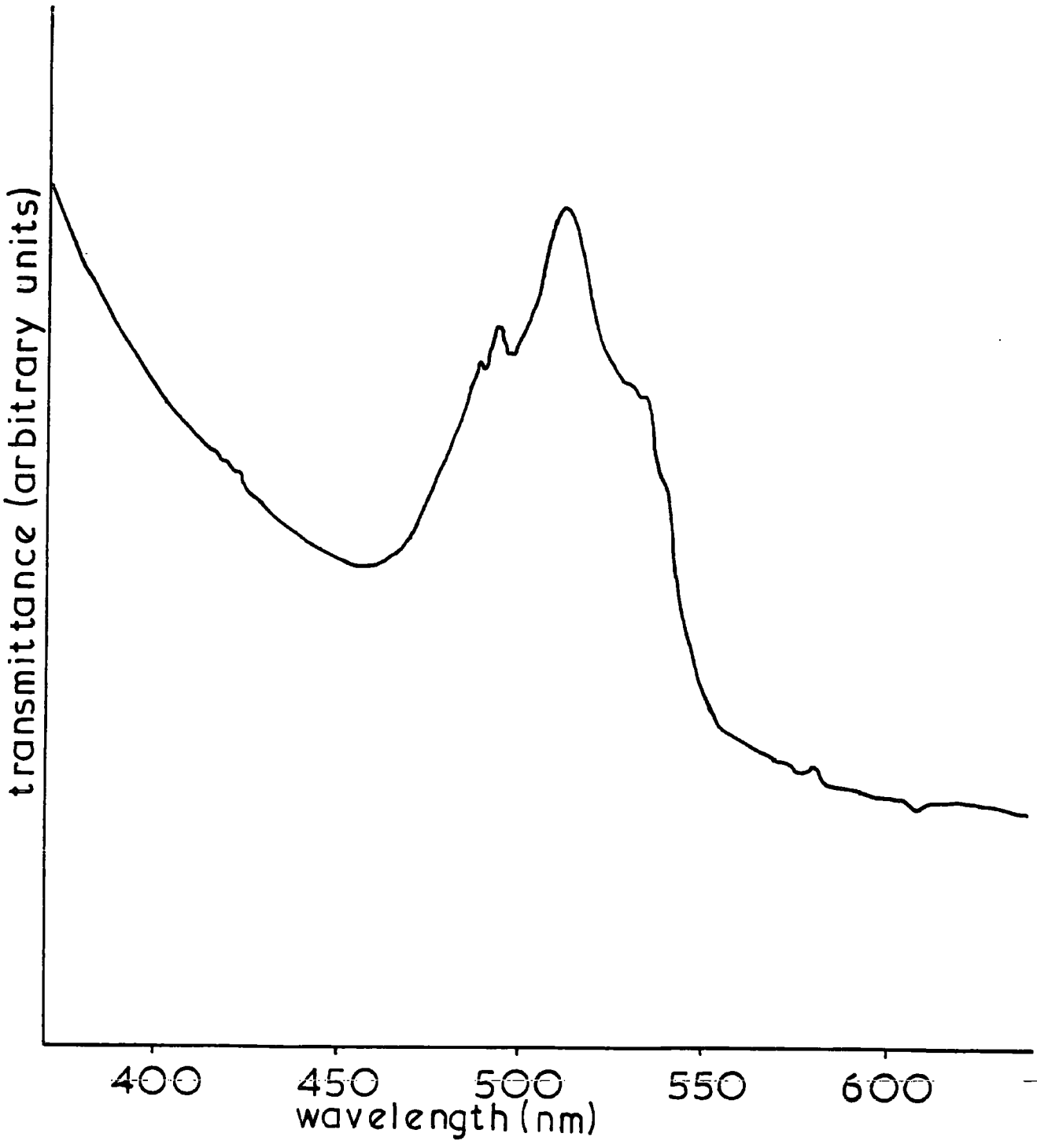

FIGURE 5.5 Optical transmittance spectrum of MgO:Co(9900ppm) 77K

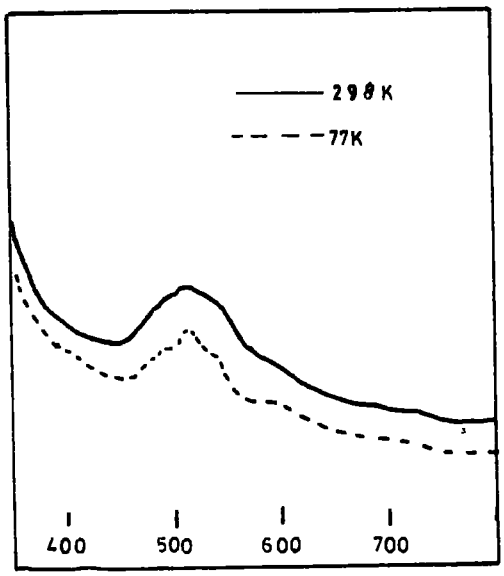

FIGURE 5.7 Low's data for MgO:Co for comparison

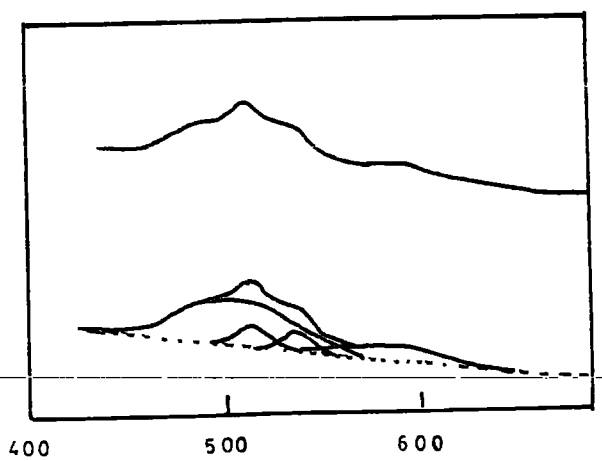

FIGURE 5.8 Low's suggestion for a possible reconstruction [see reference 5.1]

5.4 INTERPRETATION OF THE 77 K RESULTS

The spectrum at 77 K is extremely difficult to interpret, since the fitting of such a complex envelope which, by inspection, must consist of at least thirteen individual transitions, is by no means a trivial matter. However an attempt to do this for one of the spectra has been made and is presented below. In this analysis the intensities of the lines have been divided into three categories. Strong implies a line which accounts for 10-50% of the total intensity; Medium, one accounting for 1-10% and Weak less than 1%. Where more quantitative intensities were measurable they have been added in brackets. A similar comment applies to the widths of the lines which have been divided into two categories, sharp and broad, and have the half-widths, in brackets, added where possible.

The only comment to be made here is that the data is totally consistent with the assignments and comments made in the previous section. The situation must correspond to a region of the energy level diagram in which the optical levels are severely bunched together, and the spectrum is highly complex. There is, of course, no guarantee that all these lines are due to the same species; some may be due to $Co^{2+} - Co^{2+}$ pairs in various orientations, or to Co^{2+} adjacent to some other crystalline defect. A great deal of work would be needed to assign each of the observed bands, and possibly some could still not be unambiguously defined by pure absorption spectroscopy. A more sophisticated technique, such as magnetic circular diachroism, may be required for the final analysis.

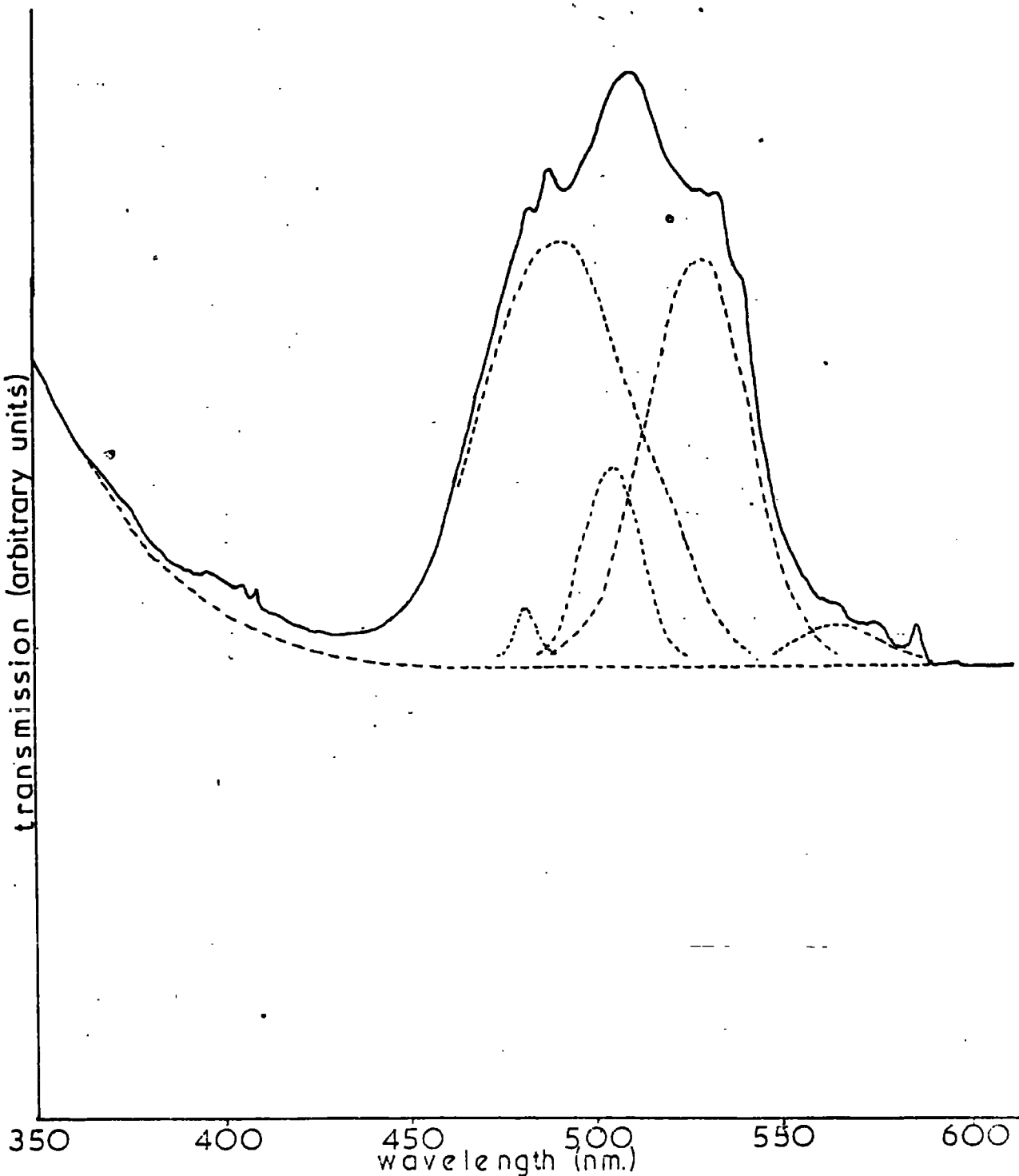

FIGURE 5.9 Optical transmittance spectrum of MgO:Co (1250 ppm.) 77 K showing one possible construction

Line No.	Wavelength (nm)	Energy (cm^{-1})	Intensity	Width
1	374	26710	weak	broad
2	392	25530	weak	broad
3	405	24710	weak	sharp
4	409	24470	weak	sharp
5	482	20730	weak	sharp
6	488	20500	medium (1%)	sharp
7	489	20450	strong (40%)	sharp ($33\ cm^{-1}$)
8	509	19650	medium (4%)	sharp ($20\ cm^{-1}$)
9	528	18940	weak	sharp
10	529	18910	strong (30%)	sharp ($24\ cm^{-1}$)
11	532	18800	weak	sharp
12	538	18600	weak	sharp
13	564	17730	weak	broad
14	564	17730	medium (6%)	broad ($\sim 20\ cm^{-1}$)
15	572	17490	weak	broad
16	584	17130	weak	sharp

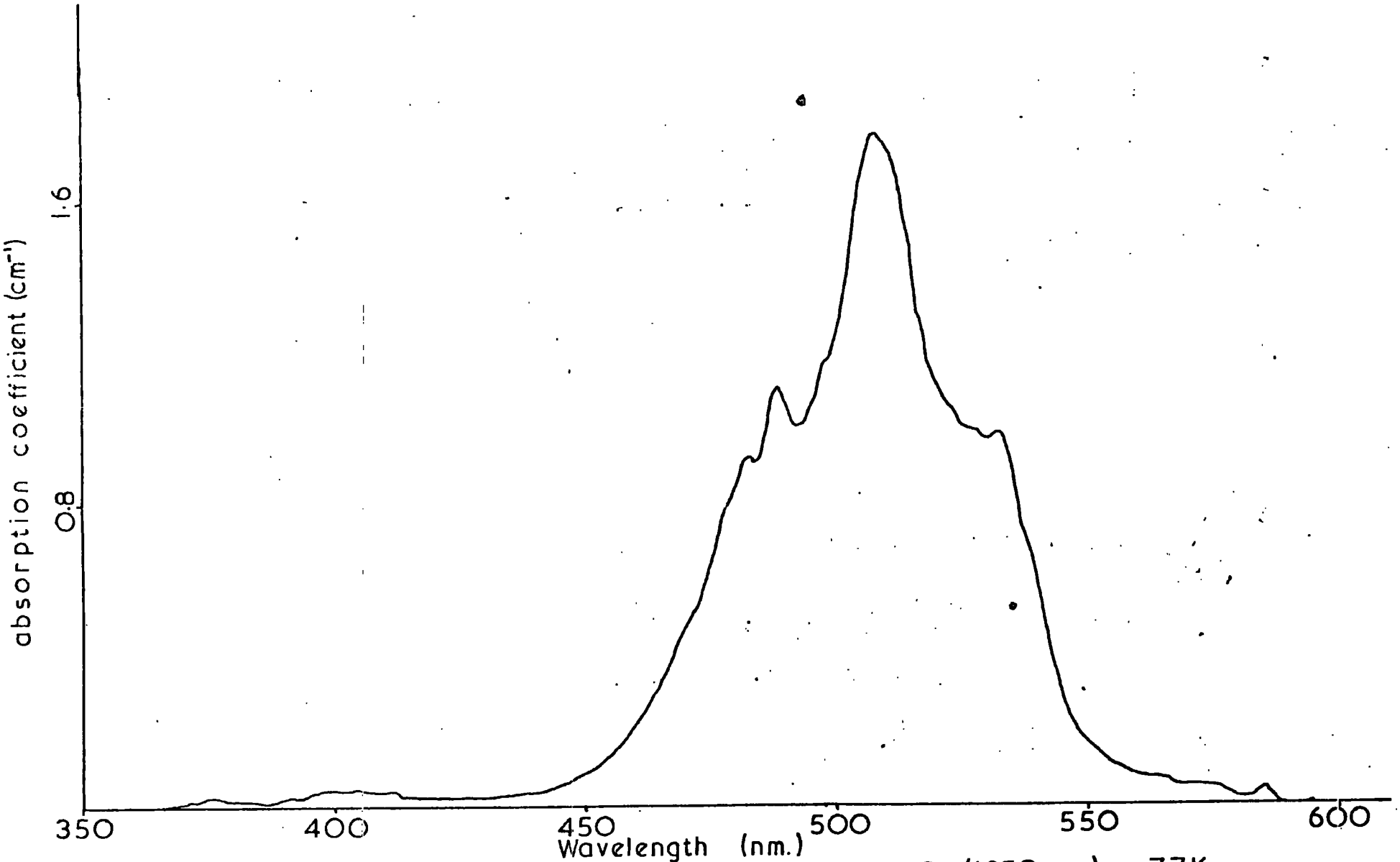

FIGURE 5.10 The optical absorption spectrum of MgO:Co (1250ppm) 77K

CHAPTER SIX

ELECTRON SPIN RESONANCE THEORY

6.1 THE SPIN HAMILTONIAN

Consider an ion in a crystal lattice. Quantum mechanics states that the allowed energies of the ion are eigenvalues of the equation

$$\hat{H}\psi = E\psi \tag{6.1}$$

where $\hat{H}$ is the Hamiltonian operator for the system. The Hamiltonian can be written as the sum of the following terms:-

(1) $\hat{H}_1$ represents the kinetic energy and the energy arising from the Coulombic forces between the electrons and between the electrons and the nucleus. For a κ-electronic system it is written thus (6.1),

$$\hat{H}_1 = \sum_i^{\kappa} \left(\frac{p_i^2}{2m_o} - \frac{ze^2}{r_i} \right) + \sum_{i \neq \kappa} \frac{e^2}{r_{i\kappa}} \tag{6.2}$$

This is usually by far the most dominant term in the Hamiltonian.

(2) $\hat{H}_2$ is born from the electrostatic field of neighbouring atoms. It has already been discussed as the crystal field term, and its importance noted in determining the energy levels between which optical transitions take place.

(3) $\hat{H}_3$ refers to spin-orbit coupling and may be represented by

$$\hat{H}_3 = \lambda \underline{L}.\underline{S} \tag{6.3}$$

where $\hat{\underline{L}}$ is the orbital angular momentum operator, and $\hat{\underline{S}}$ the spin angular momentum operator. The constant λ may be either positive or negative.

(4) $\hat{H}_4$ is the term responsible for paramagnetism, the Zeeman term which may be expressed as

$$\hat{H}_4 = \underline{H}.(\hat{\underline{L}} + g\hat{\underline{S}}) \tag{6.4}$$

where g is the spectroscopic splitting factor.

(5) $\hat{H}_5$ represents magnetic interactions between electrons. It may be written as

$$\hat{H}_5 = \sum_{i<j} \hat{\underline{S}}_i \, \underline{\underline{J}}_{ij} \, \hat{\underline{S}}_j \tag{6.5}$$

where $\underline{\underline{J}}$'s are tensors, and the summation is over all ions.

(6) $\hat{H}_6$ represents interaction between the electron and nuclear spins, and may be thought of as arising from two sources.

(a) The magnetic interaction between the magnetic moments of electron and nucleus.

$$\hat{H}_6' = g g_n \beta \beta_n \left\{ \frac{\hat{\underline{S}}.\hat{\underline{I}}}{r^3} - \frac{3(\hat{\underline{S}}.\underline{r})(\hat{\underline{I}}.\underline{r})}{r^5} - \frac{8\pi \hat{\underline{S}}.\hat{\underline{I}}\delta(r)}{3} \right\} \tag{6.6}$$

and

(b) the electrostatic interaction between the electric quadropole moment of the nucleus.

$$\hat{H}_6'' = \frac{e^2 \hat{Q}}{2\hat{\underline{I}}(\hat{\underline{I}} - 1)} \left\{ \frac{\hat{\underline{I}}(\hat{\underline{I}} + 1)}{r^3} - \frac{3(\underline{r}.\hat{\underline{I}})^2}{r^5} \right\} \tag{6.7}$$

(7) $\hat{H}_7$ is the nuclear contribution and is written

$$\hat{H}_7 = g_n \beta_n \underline{H}.\underline{I} \tag{6.8}$$

(8) $\hat{H}_8$ is the term which mainly gives rise to diamagnetic effefts

$$\hat{H}_8 = \frac{e^2}{8m_o c^2} \sum_i (\underline{H} \wedge \underline{r}_i)^2$$

Thus the total Hamiltonian is

$$\hat{H} = \hat{H}_1 + \hat{H}_2 + \hat{H}_3 + \hat{H}_4 + \hat{H}_5 + \hat{H}_6 + \hat{H}_7 + \hat{H}_8$$

In 1951, however, Abraham and Pryce [6.2] proposed that to evaluate the energy levels involved in electron spin resonance transitions only those parts of the Hamiltonian that are spin dependent need be used. This is because of the relative sizes of these terms. The spin dependdent ones are sufficiently small to be regarded as perturbations of the spin independent ones, and hence the incident energy of the photons used in a present-day experiment ($\sim 1 cm^{-1}$) is nowhere near large enough to promote electrons through the optical type of transitions discussed earlier. Accordingly the spin Hamiltonian becomes

$$\hat{H}_s = \hat{H}_2 + \hat{H}_3 + \hat{H}_4 + \hat{H}_5 + \hat{H}_6 + \hat{H}_7 \qquad (6.9)$$

and use this to discuss the energy levels.

6.2 SPIN-SPIN INTERACTIONS

One immediately notices that one of the terms in the above spin Hamiltonian is intrinsically different from all the rest. $\hat{H}_5$ is caused by interactions between two different paramgnetic ions, whilst all the others are present for an isolated paramagnetic ion in a diamagnetic lattice. Consider this term, $\hat{H}_5$, for a while.

Obviously the tensor $\underline{\underline{J}}_{ij}$ will depend on the relative positions of the ith and jth ions, giving a large interaction for ions close together, and a smaller one for ions further apart. Hence the energies of various

ions of the same species will be slightly different as they occupy lattice sites in a random (or at least quasi-random) fashion. To assess the effect that this will have on the spectrum consider the linewidth. For an isolated ion, in the absence of any spin-spin interaction, the linewidth is governed by the lifetime of the upper state to which the transition occurs. For this transition, occurring when $h\nu = g\beta H$, the linewidth is given by

$$\Delta\nu = h\Delta E$$

Now by the Uncertainty Principle

$$\Delta E \Delta t \sim \hbar/2\pi$$

If the relaxation time is denoted τ_2

$$\Delta\nu\tau_2 = 1/2\pi$$

Hence

$$\Delta\nu = \frac{1}{2\pi\tau_2} \qquad (6.11)$$

But now suppose that, as postulated above, some of the ions have slightly different energies due to the magnetic interactions between their electrons. This would tend to give a range of g values of resonance and so, one would imagine, also contribute to the width of the line. Attempts to quantify the argument are not easy since very many interactions are involved. For a given ion in the lattice there are are a number of other paramagnetic ions at varying distances. The interaction between each pair is a function of the distance between them, the direction cosines of the line joining them, and in some cases of the arrangement of diamagnetic ions between them. The complete spin

Hamiltonian for a set of interacting ions was given in the last section, viz:-

$$\hat{H}_s = \hat{H}_2 + \hat{H}_3 + \hat{H}_4 + \hat{H}_5 + \hat{H}_6 + \hat{H}_7 \tag{6.9}$$

It is convenient now to introduce the following notation

$$\hat{H}_s = \hat{H}_s' - \hat{H}_5 \tag{6.12}$$

Exact diagonalisation of such a complex Hamiltonian as (6.9) to obtain the eigenvalues is impossible, and so an alternative approach due to Waller (6.3) is used.

The nth moment of an absorption line is defined as

$$M_n = \frac{\int (\nu - \nu_o)^n \, f(\nu) \, d\nu}{\int f(\nu) \, d\nu} \tag{6.13}$$

where ν_o is the centre of the line. If $f(\nu)$ is symmetrical about ν_o then all odd moments will be equal to zero, and so attention is concentrated only on the even ones. An extensive treatment of the following theory has been given by Van Vleck (6.4). In view of this merely a sketch of his work will be given following the approach of Abragam and Bleaney.

Firstly, restrict discussion to a system of identical spins, with no fine or hyperfine structure, subjected to an external field $\underline{H}$ whose direction is taken as the z-direction of a Cartesian coordinate system. The general Hamiltonian of (6.9) will then have the form,

$$\hat{H}_s' = \hat{H}_s + \sum_{i<j} \hat{\underline{S}}_i \underline{J}_{ij} \hat{\underline{S}}_j \tag{6.14}$$

Expanding the spin-spin interaction term gives

$$\begin{aligned} \hat{\underline{S}}_i \underline{J}_{ij} \hat{\underline{S}}_j = {} & \hat{S}_{ix} J_{ijxx} \hat{S}_{jx} + \hat{S}_{iy} J_{ijyy} \hat{S}_{jy} + \hat{S}_{iz} J_{ijzz} \hat{S}_{jz} \\ & + \hat{S}_{ix} J_{ijxy} \hat{S}_{jy} + \hat{S}_{ix} J_{ijxz} \hat{S}_{jz} + \hat{S}_{iy} J_{ijyx} \hat{S}_{jx} \\ & + \hat{S}_{iy} J_{ijyz} \hat{S}_{jz} + \hat{S}_{iz} J_{ijzx} \hat{S}_{jx} + \hat{S}_{iz} J_{ijzy} \hat{S}_{jy} \end{aligned} \tag{6.15}$$

The term J_{ijpq} is now separated into two parts, i.e.

$$J_{ijpq} = J'_{ijpq} + J''_{ijpq} = J'_{ijpq} + J''_{ij}\delta_{pp} \tag{6.16}$$

where $J''_{ij} = \frac{1}{3}\mathrm{Tr}(\underline{\underline{J}}_{ij})$, which makes the tensor $\underline{\underline{J}}'_{ij}$ traceless. Hence

$$\begin{aligned}\hat{\underline{S}}_i \underline{\underline{J}}_{ij} \hat{\underline{S}}_j = {} & J''_{ij}\hat{\underline{S}}_i.\hat{\underline{S}}_j + \hat{S}_{ix}J_{ijxx}\hat{S}_{jx} + \hat{S}_{iy}J'_{ijyy}\hat{S}_{jy} + \\ & \hat{S}_{iz}J'_{ijzz}\hat{S}_{jz} + \hat{S}_{ix}J'_{ijxy}\hat{S}_{jy} + \hat{S}_{ix}J_{ijxz}\hat{S}_{jz} + \\ & \hat{S}_{iy}J'_{ijyx}\hat{S}_{jx} + \hat{S}_{ij}J'_{ijyz}\hat{S}_{jz} + \hat{S}_{iz}J'_{ijzx}\hat{S}_{jx} + \\ & \hat{S}_{iz}J'_{ijzy}\hat{S}_{jy}\end{aligned} \tag{6.17}$$

The first term here, i.e. the one involving J''_{ij}, represents an isotropic exchange interaction, whilst the rest represents an anisotropic exchange interaction.

Consider those terms in (6.17) which are diagonal for the total z-component of spin. For a given pair of ions these are

$$J''_{ij}\hat{\underline{S}}_i.\hat{\underline{S}}_j + J'_{ijxx}\hat{S}_{ix}\hat{S}_{jx} + J'_{ijyy}\hat{S}_{iy}\hat{S}_{jy} + J'_{ijzz}\hat{S}_{iz}\hat{S}_{jz} \tag{6.18}$$

Since these terms do not have any directional properties along the x and y axes $\hat{S}_{ix}\hat{S}_{jx} = \hat{S}_{iy}\hat{S}_{jy}$ (6.5). Hence equation (6.18) can be written as

$$J''_{ij}\hat{\underline{S}}_i.\hat{\underline{S}}_j + J'_{ijzz}\hat{S}_{iz}\hat{S}_{jz} + \tfrac{1}{2}(J'_{ijxx} + J'_{ijyy})(\hat{S}_{ix}\hat{S}_{jx} + \hat{S}_{iy}\hat{S}_{jy})$$

and since $\underline{\underline{J}}'_{ij}$ is traceless, i.e. $J'_{ijxx} + J'_{ijyy} + J'_{ijzz} = 0$ this becomes

$$J''_{ij}\hat{\underline{S}}_i.\hat{\underline{S}}_j + \tfrac{3}{2}J'_{ijzz}\hat{S}_{iz}\hat{S}_{jz} - \tfrac{1}{2}J'_{ijzz}\hat{\underline{S}}_i.\hat{\underline{S}}_j \tag{6.19}$$

Hence the spin Hamiltonian (6.12) may now be written as

$$\hat{H}_s = \hat{H}'_s + \sum_{i<j}(J''_{ij} - \tfrac{1}{2}J'_{ijzz})\hat{\underline{S}}_i.\hat{\underline{S}}_j + \tfrac{3}{2}J'_{ijzz}\hat{S}_{iz}\hat{S}_{jz} \tag{6.20}$$

This enables the energy levels for the system to be evaluated, and the nature of the spin Hamiltonian indicates that the energy matrix will be diagonal. It is found that allowed transitions correspond to the selection rule

$$(\Delta \Sigma_i S_{iz}) = 1 \tag{6.21}$$

occurring near $h\nu_o = g\beta H$.

Consider now the problem of calculating the second moment of an absorption line centered on frequency ν_o and write

$$\nu = \nu_o + (\nu - \nu_o)$$

Squareing gives

$$\nu^2 = \nu_o^2 + 2\nu_o(\nu - \nu_o) + (\nu - \nu_o)^2$$

and thus

$$\int \nu^2 f(\nu)\,d\nu = \int \nu_o^2 f(\nu)\,d\nu + \int 2\nu_o(\nu - \nu_o) f(\nu)\,d + \int (\nu - \nu_o)^2 f(\nu)\,d\nu \tag{6.22}$$

If the lineshape is symmetrical then the term

$$\int 2\nu_o(\nu - \nu_o)^2 f(\nu)\,d\nu = 0$$

and since ν_o is a constant and $\int f(\nu)\,d\nu = 1$ by definition

$$\langle \nu^2 \rangle = \nu_o^2 + \int (\nu - \nu_o)^2 f(\nu)\,d\nu$$

By the definition of (6.13)

$$\langle \nu^2 \rangle = \nu_o^2 + M_2 \tag{6.23}$$

where

$$\langle \nu^2 \rangle = \int \nu^2 f(\nu)\,d\nu \tag{6.24}$$

Now suppose transitions are induced by an oscillatory magnetic field polarized along the x-axis. Then, if there is no anisotropy in g, the transition probabilities are found by the matrix elements of the operator $S_x = \sum_i S_{ix}$. Let $\langle n|S_x|n'\rangle$ be the matrix element between two eigenstates of (6.20) denoted by n and n' for which the corresponding frequency is $\nu_{nn'}$, which is

$$\nu_{nn'} = \frac{\langle n|\hat{H}_s|n\rangle - \langle n'|\hat{H}_s|n'\rangle}{h}$$

Then the mean square absorption frequency (in which each frequency is weighted with the squate of the appropriate amplitude) is

$$\langle\nu^2\rangle = \frac{\sum_{nn'} \left\{ \nu_{nn'}^2 |\langle n|\hat{S}_x|n'\rangle| \right\}^2}{\sum_{nn'} |\langle n\, \hat{S}_x|n'\rangle|^2} \qquad (6.25)$$

Both numerator and denominator may be expressed as diagonal sums (6.6) .

$$h^2\langle\nu^2\rangle = \frac{-\mathrm{Tr}\left[\langle n|\hat{H}_s\hat{S}_x - \hat{S}_x\hat{H}_s|n'\rangle\right]^2}{\mathrm{Tr}\left[\langle n|S_x|n'\rangle\right]^2} \qquad (6.26)$$

which has the advantage that the trace is invariant, and can be computed without need to diagonalise the Hamiltonian (6.20) in order to find the individual eigenvalues. Van Vleck has evaluated these traces and found that

$$h^2 M_2 = \tfrac{1}{3}S(S+1)\sum_{i<j}\left[\tfrac{3}{2}J'_{ijzz}\right]^2 \qquad (6.27)$$

Note that this result contains only the anisotropic exchange interaction.

6.3 FURTHER LINE-SHAPE CONSIDERATIONS

Computations of linewidths and moments can be carried out only if the interaction constants are known for all pairs of ions in the crystal.

In general, this limits the computation of these parameters to cases where the interaction is entirely due to magnetic dipole interaction between the spins, which is rare with electronic magnetic moments, but common with nuclear magnetic moments.

However, consider two spins, with isotropic g factors, which interact purely by a dipolar mechanism. From classical theory the energy of two point magnetic dipoles, $\underline{m}_i$ abd $\underline{m}_j$ a distance r apart is

$$W = (\mu_o/4\pi)\left\{r^{-3}\underline{m}_i.\underline{m}_j - 3r^{-2}(\underline{m}_i.\underline{r})(\underline{m}_j.\underline{r})\right\} \qquad (6.28)$$

For a pair of isotropic electron dipoles

$$\underline{m}_i = -g_i\beta\underline{S}_i \; ; \qquad \underline{m}_j = -g_j\beta\underline{S}_j$$

so that (6.28) becomes in operator form

$$\hat{H}_5 = (\mu_o/4\pi)g_ig_j\beta^2\left\{r^{-3}\hat{\underline{S}}_i.\hat{\underline{S}}_j - 3r^{-2}(\hat{\underline{S}}_i.\underline{r})(\hat{\underline{S}}_j.\underline{r})\right\} \qquad (6.29)$$

If the direction cosines of $\underline{r}$ are $(l\,m\,n)$ this can be expanded, giving

$$\hat{H}_5 = (\mu_o/4\pi)g_ig_j\beta^2r^{-3}\left\{\hat{S}_{ix}\hat{S}_{jx}(1-3l^2) + \hat{S}_{iy}\hat{S}_{jy}(1-3m^2) + \hat{S}_{iz}\hat{S}_{jz}(1-3n^2)\right.$$
$$-(\hat{S}_{ix}\hat{S}_{jy} + \hat{S}_{iy}\hat{S}_{jx})3lm - (\hat{S}_{iy}\hat{S}_{jz} + \hat{S}_{iz}\hat{S}_{jy})3mn$$
$$\left.-(\hat{S}_{iz}\hat{S}_{jx} + \hat{S}_{ix}\hat{S}_{jz})3nl\right\} \qquad (6.30)$$

Again selecting those terms diagonal to the z-component of spin which are

$$(\mu_o/4\pi)g_i g_j r^{-3}\left\{\hat{S}_{ix}\hat{S}_{jx}(1-3l^2) + \hat{S}_{iy}\hat{S}_{jy}(1-3m^2) + \hat{S}_{iz}\hat{S}_{jz}(1-3n^2)\right\}\beta^2$$

$$= g_i g_j \beta^2 r^{-3}\left\{\tfrac{1}{2}(\hat{S}_{ix}\hat{S}_{jx} + \hat{S}_{iy}\hat{S}_{jy})(2-3[l^2+m^2]) + \hat{S}_{iz}\hat{S}_{jz}(1-3n^2)\right\}(\mu_o/4\pi)$$

$$= (\mu_o/4\pi)\, g_i g_j \beta^2 r^{-3}\left\{-\tfrac{1}{2}(\hat{\underline{S}}_i.\hat{\underline{S}}_j - \hat{S}_{iz}\hat{S}_{jz})(1-3n^2) + \hat{S}_{iz}\hat{S}_{jz}(1-3n^2)\right\}$$

$$= (\mu_o/4\pi)\left\{-\tfrac{1}{2}(\hat{\underline{S}}_i.\hat{\underline{S}}_j) g_i g_j \beta^2 r^{-3}(1-3n^2) + -\hat{S}_{iz}\hat{S}_{jz} g_i g_j \beta^2 r^{-3}(1-3n^2)\right\}$$

comparison with equation (6.19) will show that for a purely dipolar interaction

$$J''_{ij} = 0 \quad ; \quad J'_{ijzz} = (\mu_o/4\pi) g_i g_j \beta^2 r^{-3}(1 - 3n^2_{ij}) \tag{6.31}$$

Hence combining (6.31), and (6.27) gives a formula for deriving the second moment of a dipolar line; however, there is still no equation for line shape. A common assumption is that the shape factor is that of a Gaussian error function. This is chosen as it seems the logical consequence of the statistics of an aggregate of ions influencing each other in the way described above. Hence the lineshape is given by

$$f(\nu) = \frac{1}{(2\ M_2)^{\frac{1}{2}}} \exp\left\{\frac{-(\nu-\nu_o)^2}{2M_2}\right\} \tag{6.32}$$

From this the linewidth can be calculated, taking $\Delta\nu$ as the width of the line at half maximum height. The values of ν when $f(\nu) = \frac{1}{2}f(\nu_o)$ are given by

$$\exp\left\{\frac{-(\nu-\nu_o)^2}{2M_2}\right\} = \tfrac{1}{2}$$

From this

$$\nu - \nu_o = 1.77 M_2^{\frac{1}{2}}, \quad \text{or } \Delta\nu = 2.35 M_2^{\frac{1}{2}} \tag{6.33}$$

Equation (6.32) also allows determination of the ratio M_4/M_2^2 , the coefficient of kurtosis. For a pure Gaussian this is equal to 3. Van Vleck has explicitly calculated this coefficient by the rigorous method of moments (6.4) and has found that it varies from 2.44 to 2.9, depending on orientation of the sample.

6.4 EFFECT OF EXCHANGE INTERACTION ON LINE SHAPE

As already stated the formulae just derived in the last section apply only to systems where spin-spin interactions are purely dipolar in origin. This tends to be the case when dealing with nuclear magnetic dipoles, but is seldom with electronic ones, since there tends to be an appreciable isotropic part to the spin-spin interaction as well as the anisotropic dipolar part.

Initially, again consider the simple case of a set of identical spins with isotropic g factors and no fine or hyperfine splittings, coupled together by dipolar interaction and isotropic exchange interaction. As already seen the second moment of an absorption line is unaltered by an isotropic exchange term. Van Vleck (6.4) however has shown that the formula for the fourth moment contains the isotropic exchange energy, so that the fourth moment is larger than it would be in the absence of such exchange interaction. Although this is insufficient to determine the line shape, it is easy to see that this implies that the line is narrowed in the middle, and extended in the wings. This is the phenomenon of exchange narrowing, first predicted by Gorter and Van Vleck (6.6). It may be physically interpreted as rapid fluctuations in the local dipolar field of the ions caused by mutual spin flips, such that the local dipolar field tends to be averaged out. For this to be the case the requirement is that $|(J''/h| \gg M_2^{\frac{1}{2}}$, where M_2 is the second moment due to the dipolar interaction.

The problem of the exact shape of an exchange narrowed line has been considered by Anderson and Weiss (6.7), who used a mathematical model to obtain the shape factor. They predict that if the above inequality holds the line should have wings which fall away exponentially, as for a Gaussian shape, but near the centre the line should be Lorentzian in shape, with half-width

$$\Delta\nu \approx M_2/(J''/h) \qquad (6.36)$$

where M_2 is the second moment due to dipolar broadening, and (J''/h) is the exchange energy in frequency units. However when this frequency exceeds the resonance frequence it is not permissable to consider only those terms which are diagonal with respect to z-component of spin in equations (6.17) and (6.30), and all the terms must be used.

Throughout all this theory only lines with no fine or hyperfine structure have been considered. If an ion with a nuclear spin greater than $\frac{1}{2}$, so that the e.s.r. line is a multiplet rather than a singlet, this theory can be used as it stands on each component, provided that they are resolved, for in this case the difference in nuclear spin is a sufficient criterion to regard each line as being due to a different species.

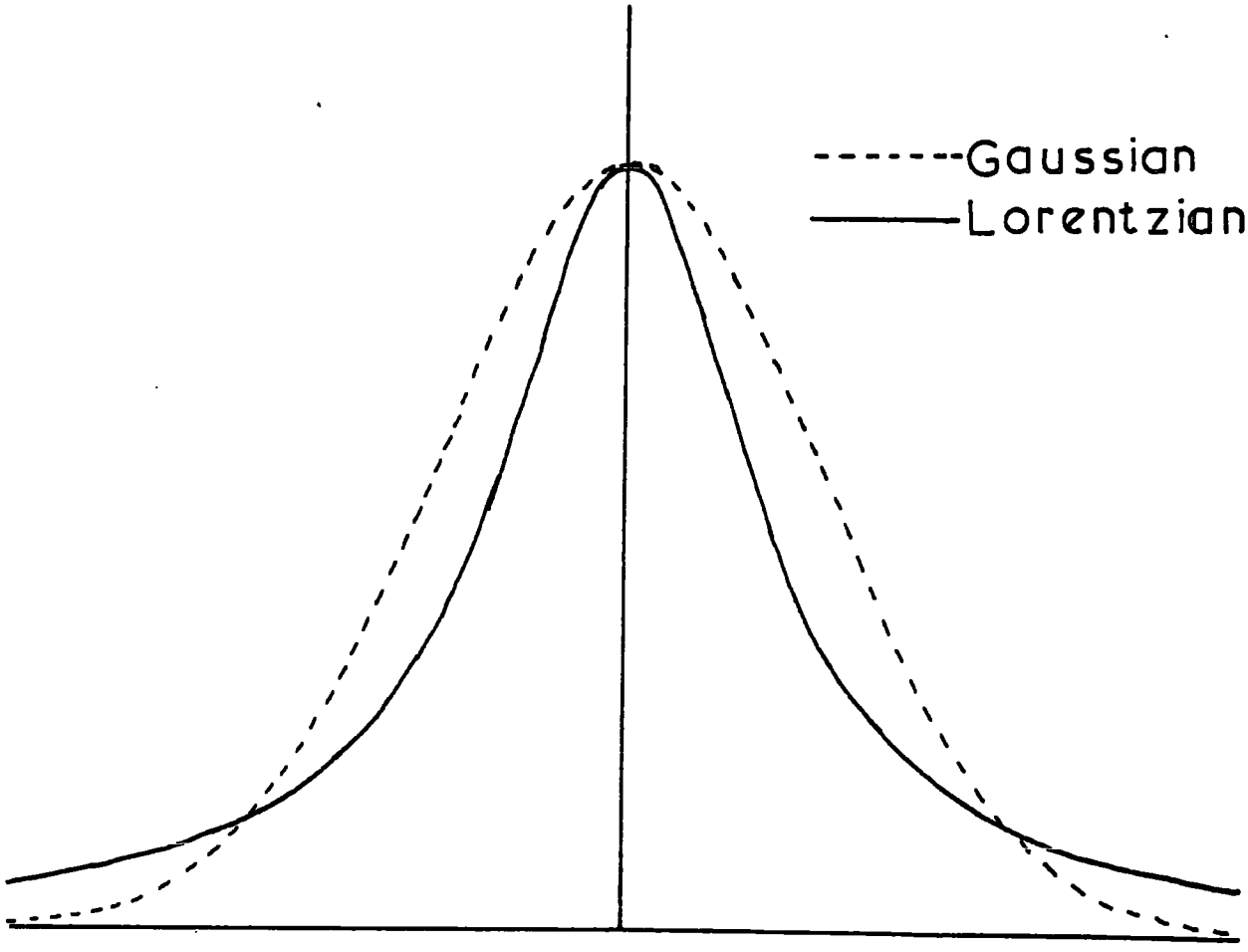

FIGURE 6.1 Comparison of Gaussian and Lorentzian lineshapes

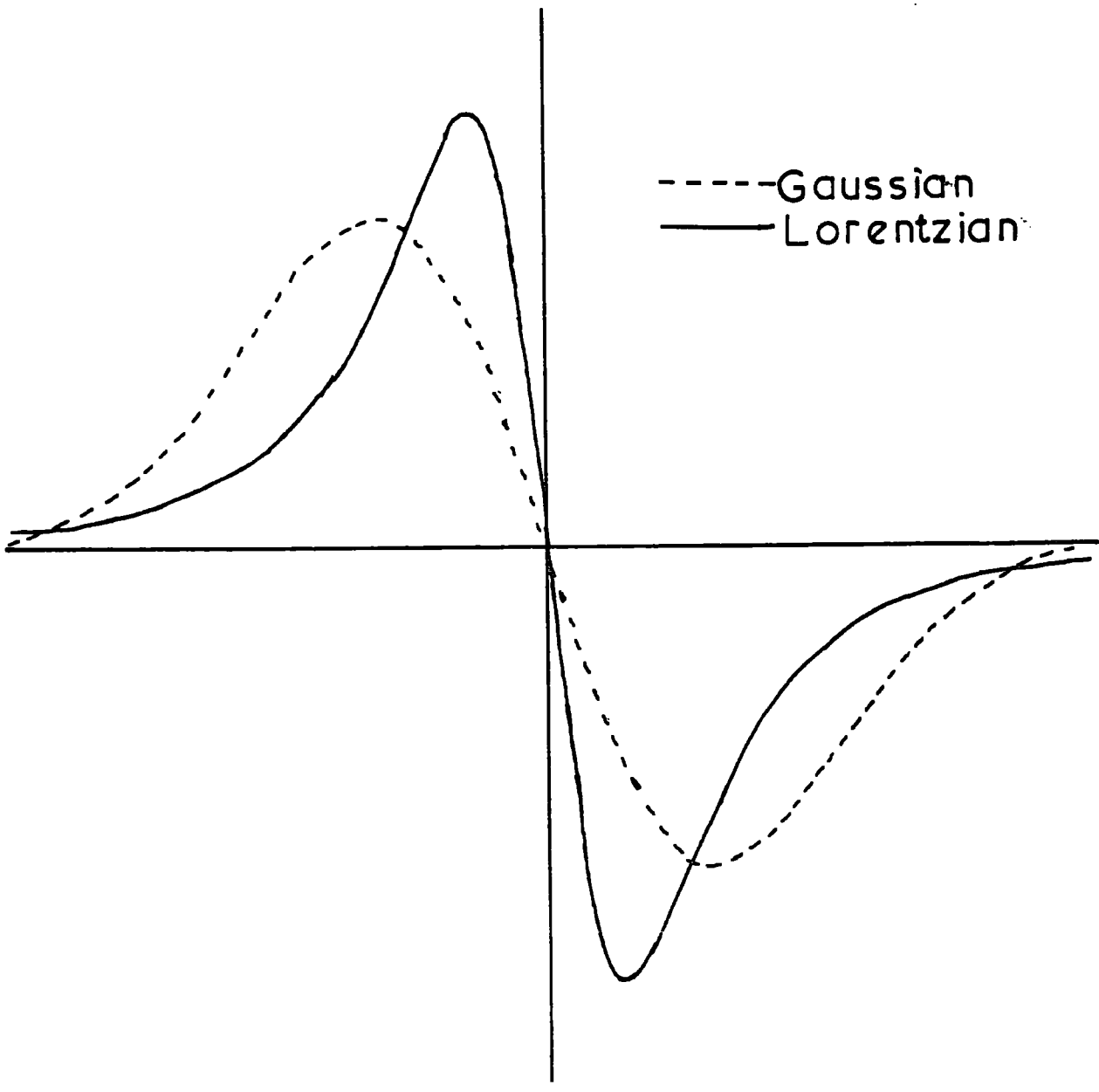

FIGURE 6.2 Comparison of first derivatives of Gaussian and Lorentzian lineshapes

CHAPTER SEVEN

ELECTRON SPIN RESONANCE EXPERIMENTAL TECHNIQUES

7.1 THE X-BAND SPECTROMETER

The X-band Electron Spin Resonance Spectrometer used in this study was a commercial Varian Machine, operating at about 9.5 GHz. It used a rectangular TE 102 cavity, the sample being mounted on a P.T.F.E. rod inserted through the cavity base for room temperature work.

The Magnet was a Varian 12" electromagnetic controlled by a VFR 5203 Field regulated power supply, incorporating the Fieldial system, which is capable of setting the desired field to 1 G with one part in 10^5 repeatability, at 0.02 G resolution. To check this measurements of field were also made using a proton magnetometer.

For work below room temperature an Oxford instruments continuous flow cryostat was used. This has a low helium consumption rate, and will provide temperatures from about 2 K up to room temperature at a resolution of 0.1 K. When the cryostat was used it was found necessary to flood the waveguide with dry nitrogen to prevent water condensing in the microwave cavity.

7.2.1 Construction of the Q-band Spectrometer

A Q-band spectrometer which had fallen into disuse was refurbished. Calibration of the magnet was carried out first, using a Hall Effect Tesla meter, and it was found to be quite capable of producing 1.6 Tesla across a 4.5 cm gap. An estimate of the field homogeneity was obtained at low fields by observing the "rings" on the output of a proton magnetometer; this was found to be better than 1 part in 10^4 at 0.3 T.

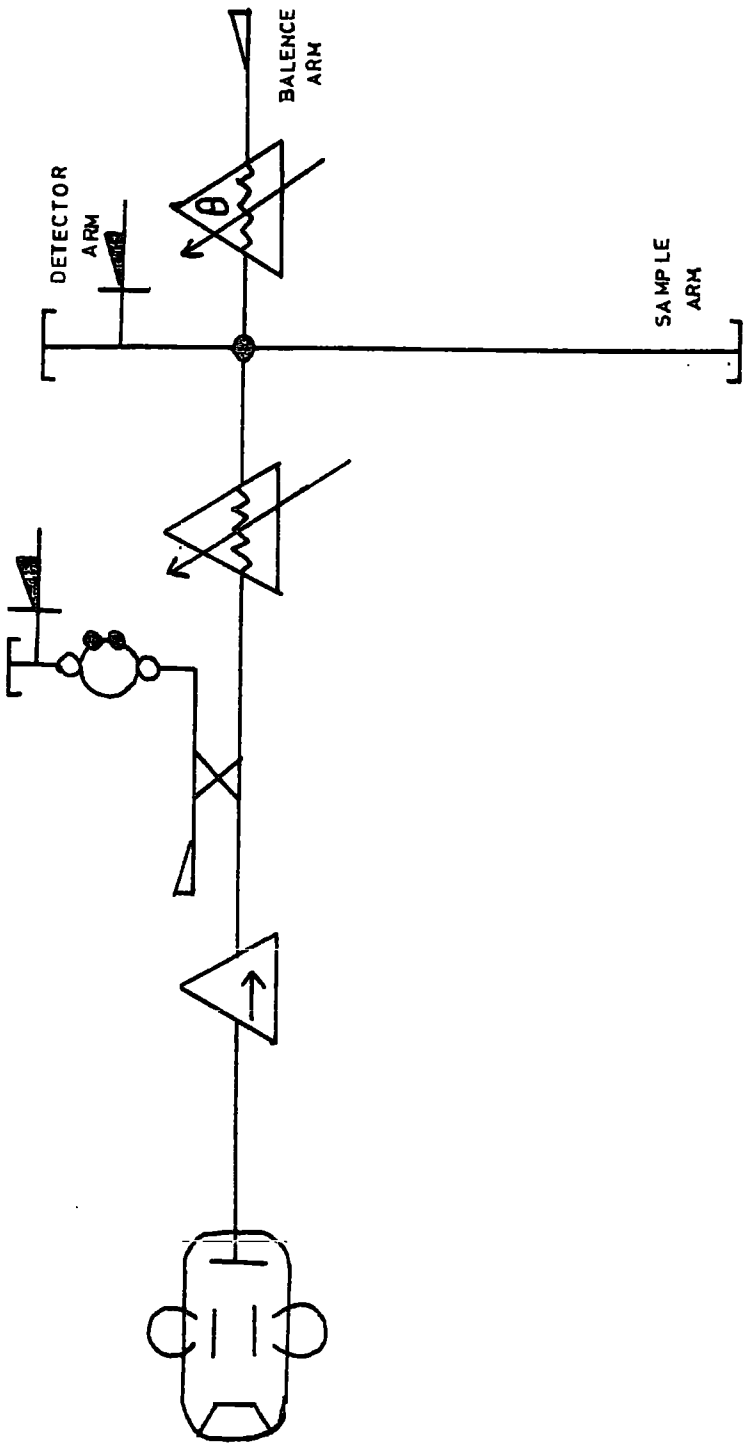

FIGURE 7.1 The microwave circuit for the Q-band spectrometer

Previously the system had used a superheterodyne detection system, but due to lack of time the microwave circuit was redesigned to be as simple as possible. Accordingly a conventional waveguide circuit was constructed, which is shown in Figure 7.1.

Microwaves pass from a klystron through an isolater to a directional coupler which splits the radiation into two parts. One arm leads to a cavity wavemeter which was used in the transmission mode for determining the microwave frequency, whilst the other arm leads, via a precision variable attenuator, to a hybrid tee, which is used as the central component of a microwave bridge. At this hybrid tee the microwave power is divided equally, half passing down to the "cavity" (located between the poles of the magnet), whilst the other half passes to the balancing arm, which consisted of an E-H tuner, and a short circuit. The principle of the microwave bridge is as follows. When the bridge is balanced perfectly by the microwave tuner no radiation falls on the detector diode in arm 2. The bridge is then unbalanced slightly so that, when the sample absorbs microwave energy the output signal impinging on the detector is proportional to the amount of microwave energy absorbed by the sample, i.e. to χ''.

One unusual feature of this microwave circuit was the absence of a cavity containing the sample. A cavity is normally used as it concentrates the microwave energy over the sample, and so a much bigger absorption is achieved. However in T_1 measurements on similar systems it had been found adequate to neglect a cavity, instead terminating a piece of rectangular cupro-nickel waveguide with a short circuiting plunger, and this was the system used here.

The final part of the spectrometer to be constructed was the detection system. In order to improve the signal to noise ratio it is

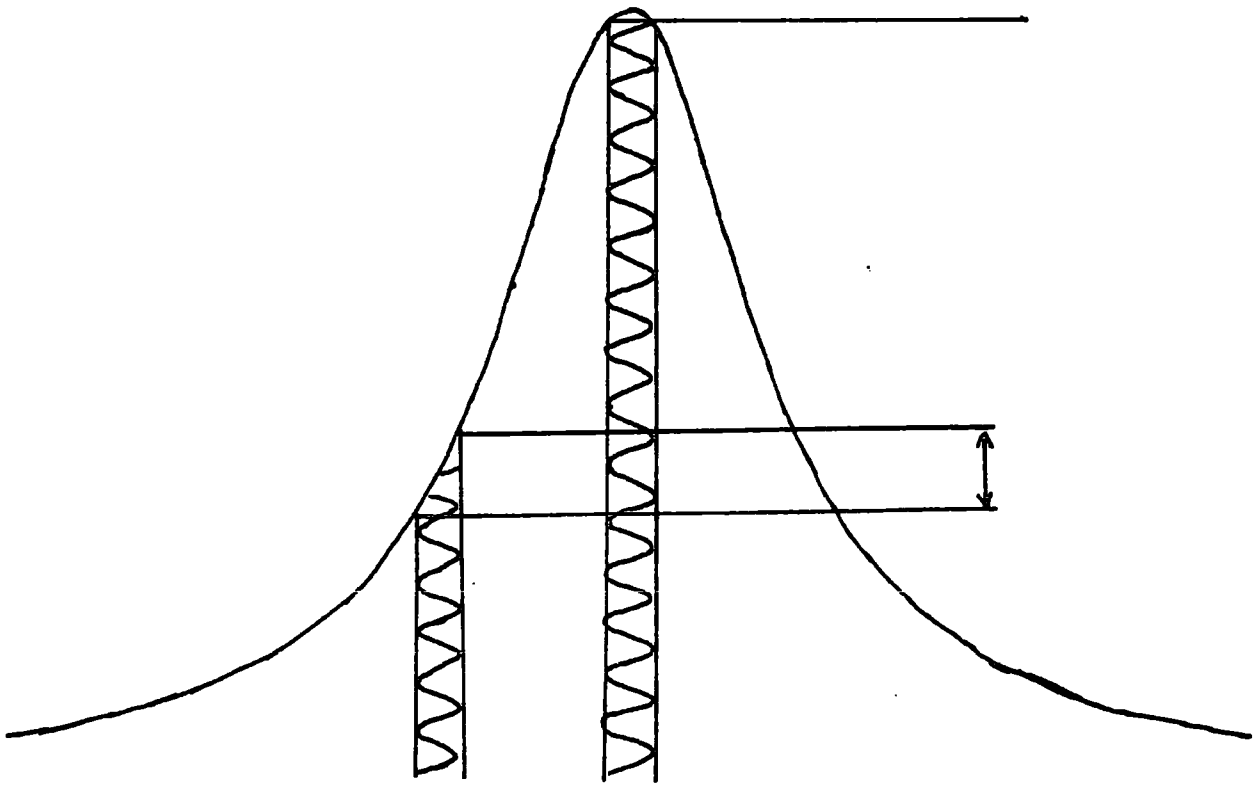

FIGURE 7.2 FIELD MODULATION ACTING ON ABSORPTION LINE GIVING RISE TO FIRST DERIVATIVE OUTPUT

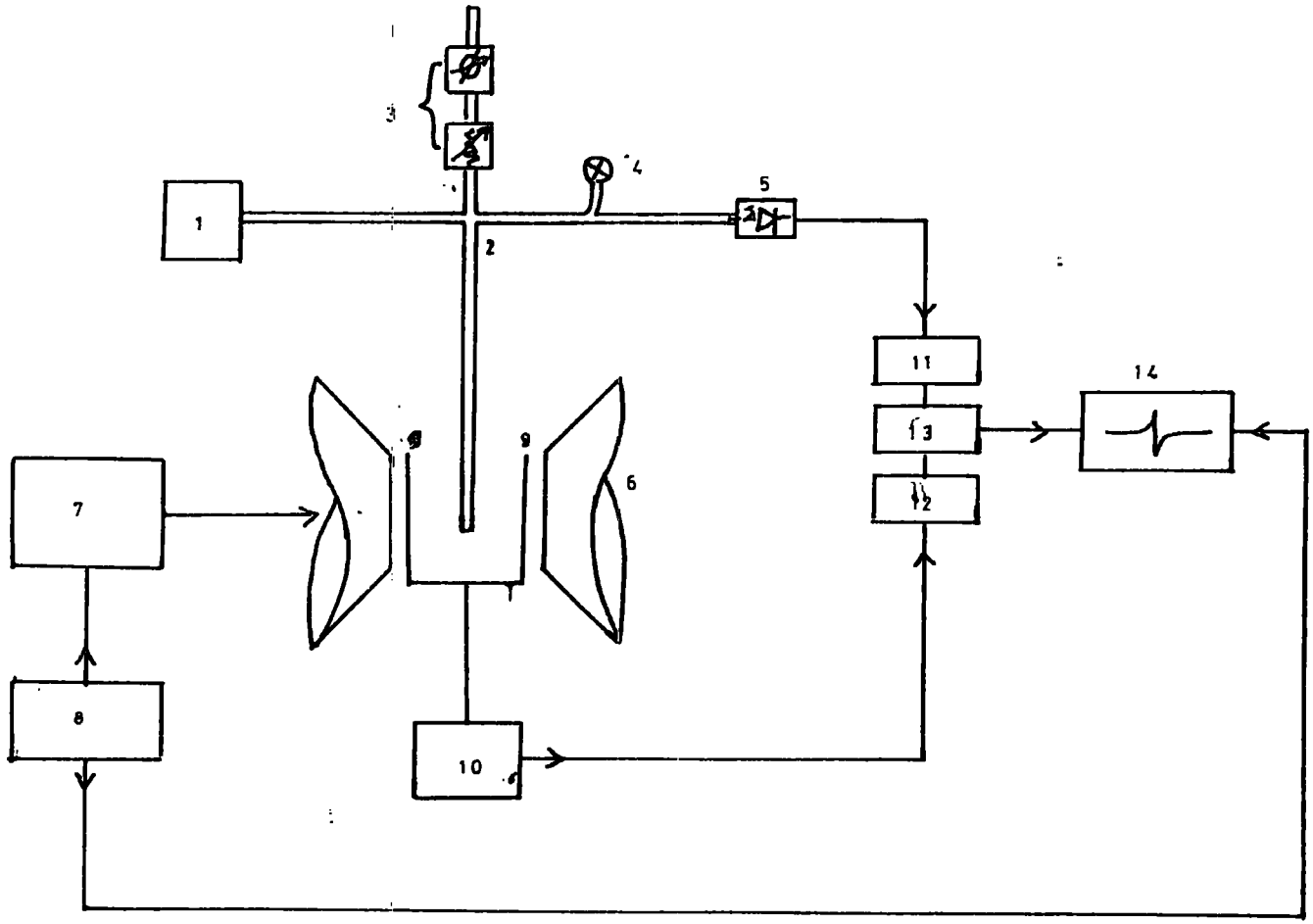

1 KLYSTRON
2 MAGIC T
3 E-H TUNER
4 WAVEMETER
5 DETECTOR
6 MAGNET
7 D.C. POWER SUPPLY
8 SWEEP UNIT
9 MODULATION COILS
10 165 kHz OSCILLATOR
11 LOW NOISE AMPLIFIER
12 PHASE SHIFTER
13 PHASE SENSITIVE DETECTOR
14 RECORDER

FIGURE 7.3 Block diagram of the Q-band spectrometer

general practice to incorporate a Lock-in system as follows. The magnetic field is modulated by an a.c. signal of small amplitude. After amplification, the component of the output of the bridge in phase with the modulation, is filtered off. This is accomplished by a phase sensitive detector and phase shifter combination, the use of which has two effects. firstly the signal to noise ratio is greatly improved, and secondly the output from the phase-sensitive detector is the first derivative of the signal received from the crystal. (Figure 7.2). A complete diagram of the overall system is given in Figure 7.3.

7.2.1 Operation of the Q-band Spectrometer

Several trial runs with D.P.P.H. (Diphenyl, Picryl Hydrazyl) as a sample were performed in order to test that the spectrometer was operating correctly, and the following points were noted:

(a) Bridge Balance:- The E-H tuner was adjusted very carefully so that the trace recorded was the pure absorption spectrum.

(b) Instrumental distortion of the signal:- This arises chiefly from two sources, saturation broadening and modulation broadening. Saturation broadening occurs when too high an incident microwave power is used. This causes excitation of the paramagnetic species to such an extent that the upper states can become as heavily populated as the lower states, which prevents further microwave absorption from taking place. This was prevented by scanning through the line, then reducing the incident microwave power by means of the variable attenuator in the microwave circuit, and scanning through the line again, looking for any difference in line width, or lineshape. This, of course, causes the intensity of the line to drop, and in the interests of obtaining the best signal-to-noise ratio, it is advisable to use the highest incident

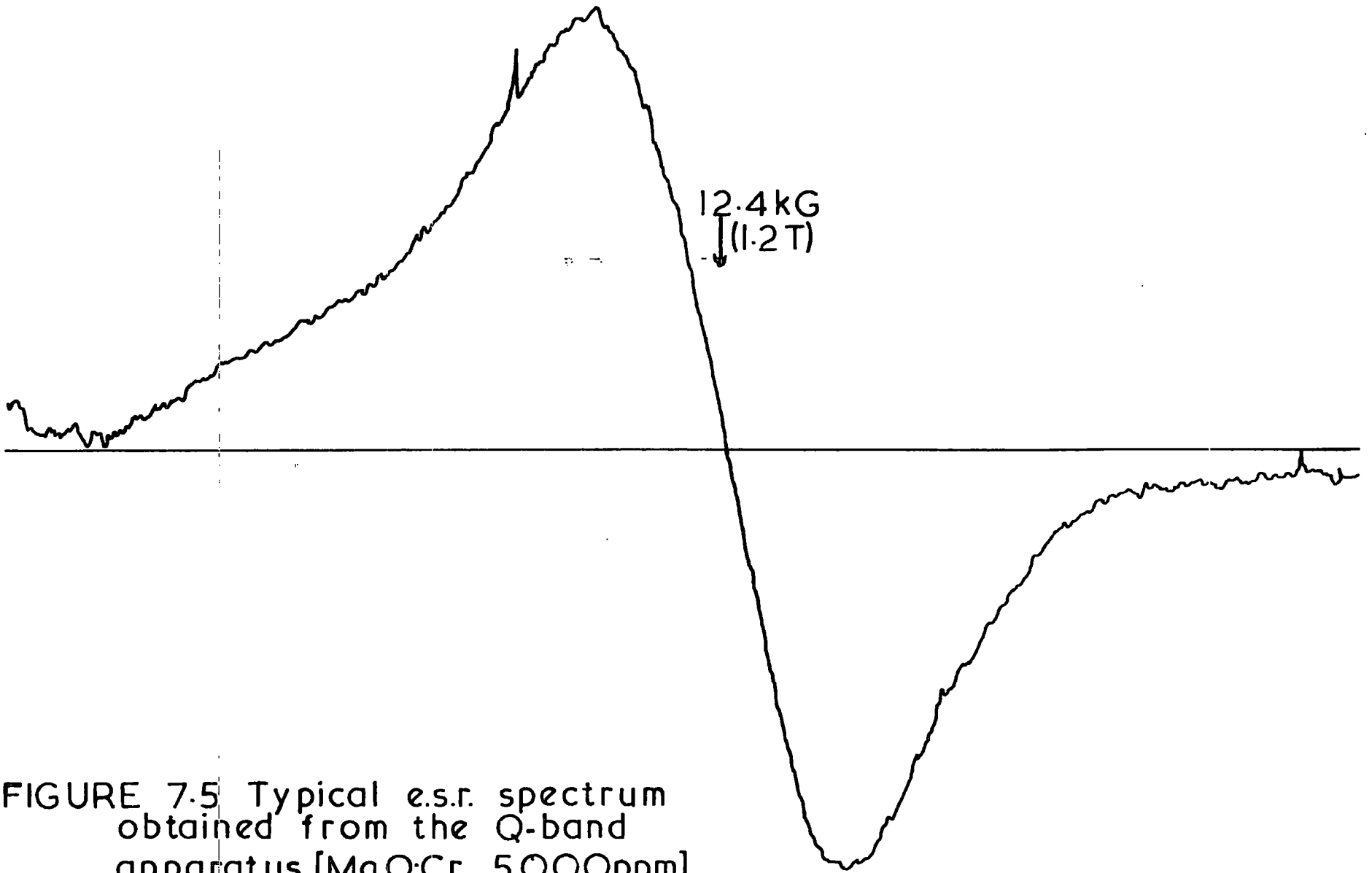

FIGURE 7.5 Typical e.s.r. spectrum obtained from the Q-band apparatus [MgO:Cr 5000ppm]

microwave power possible. This is generally taken to be the highest possible level that introduces no measurable distortion. A similar policy was adopted to prevent modulation distortion. The modulating field was set at roughly half that which gave modulation distortion. In fact the very method of detecting the signal by this system means that the trace obtained is not a true first derivative of the absorption line, but it is generally accepted that using modulation levels of this size causes an effect that is negligible.

7.2.3 Cryogenic Facilities

It was realised that in order to observe signals from MgO:Co it would be necessary to record spectra at low temperatures. With this in mind a helium cryostat and accessories were fitted to the system. A complete diagram of this system is given in Figure 7.5.

Unfortunately the system was only used to cool samples down to 77 K, as the helium cryostat ruptured after about a week of operation, and before any helium temperature data could be obtained.

7.3 TYPICAL RESULTS

The examples of spectra recorded on the re-furbished equipment discussed in this section are of particular relevance to the present work. It may be recalled that one of the reasons that the present series of experiments was commenced, was the industrial problem concerned with the use of magnesium oxide as an insulator in electric heating elements. To recapitulate the problem, it is found that in operation at temperatures of about 1000 K the insulating properties of the MgO sometimes collapse. Since the band gap of MgO is about 8.7 eV (7·1) the collapse of insulating behaviour by thermal excitation of valence-band electrons into

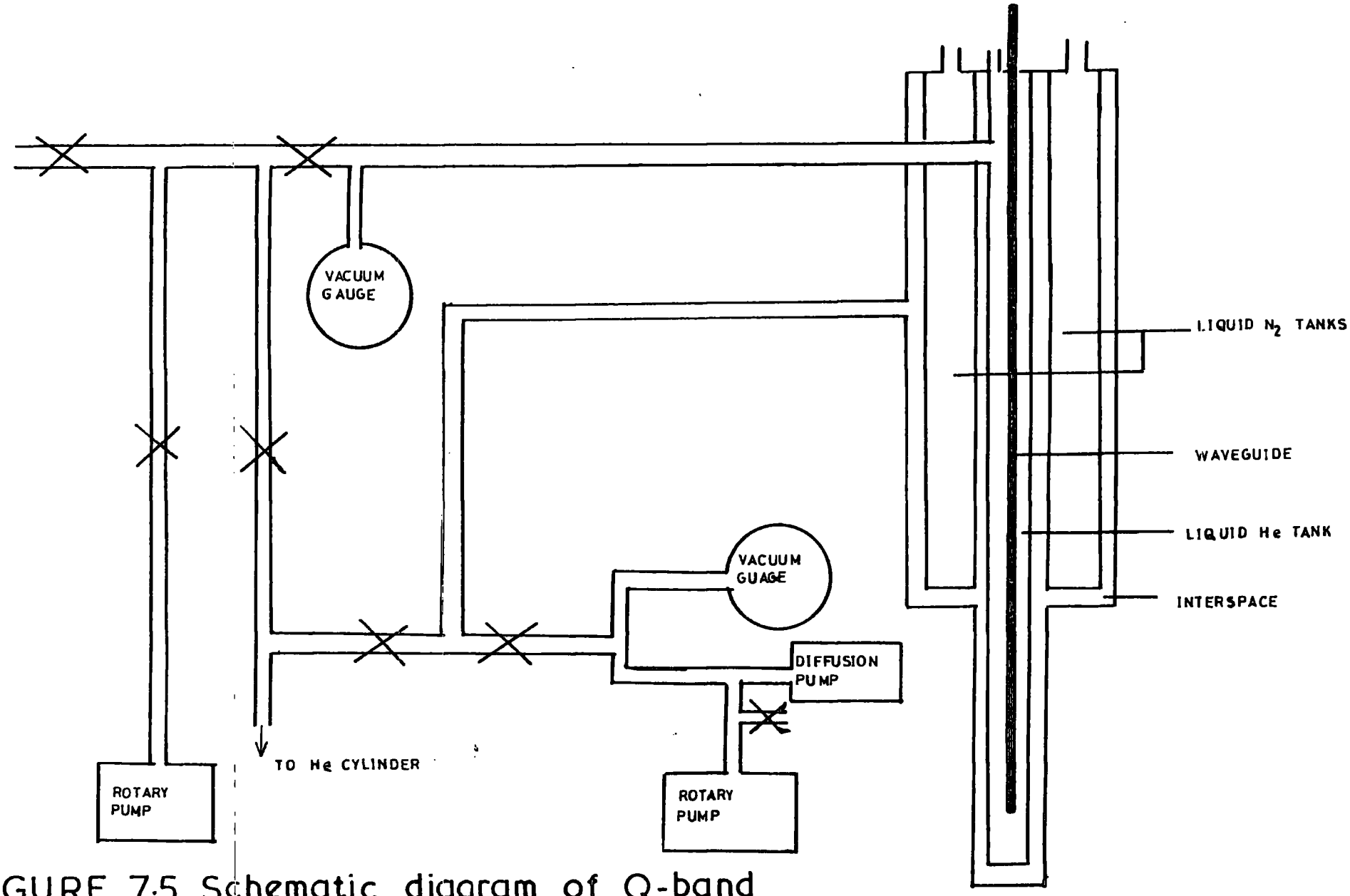

FIGURE 7.5 Schematic diagram of Q-band spectrometer cryogenics

the conduction band is not expected to occur until approximately 10^5 K, and so some other mechanism must be responsible for the observed behaviour.

One suggestion is that impurities diffuse into the MgO lattice from the sheath of the element, and that these could provide a means of conduction consistant with the observed data; so far this has not been proved, nor are the details of possible conduction mechanisms fully understood. Work on the elucidation of this problem has so far been confined to the study of single crystals, doped with a specific impurity ion, at higher concentrations than would normally be expected in the electrical grade magnesia used in industrial heating element manufacture. Indeed, the present e.s.r. work largely followed this pattern, since the interpretation of data is less complex with samples of single crystal form, than with powdered specimens, in which the micro-crystals are randomly oriented.

The donation (by Graham Fletcher) of a kettle element which had failed after some fifteen years of domestic use prompted investigation of a powder specimen. The element was cut open and the magnesium oxide insulation removed. It was noted that, to the eye, the interior of the sheath appeared to be made largely of copper, as was the filament. The spectrum of this powder was recorded at X-band and 4.2 K, and compared with that of pure MgO powder, obtained from B.D.H. These two spectra are shown in Figure 7.6.

The salient problem in the interpretation of a spectrum is to decide which species gives rise to which line. This is assisted by considering three factors; the g-values, the number of lines, and their relative intensities (the A-factor). The g-values is defined by the energy equation

$$h\nu = g\beta H$$

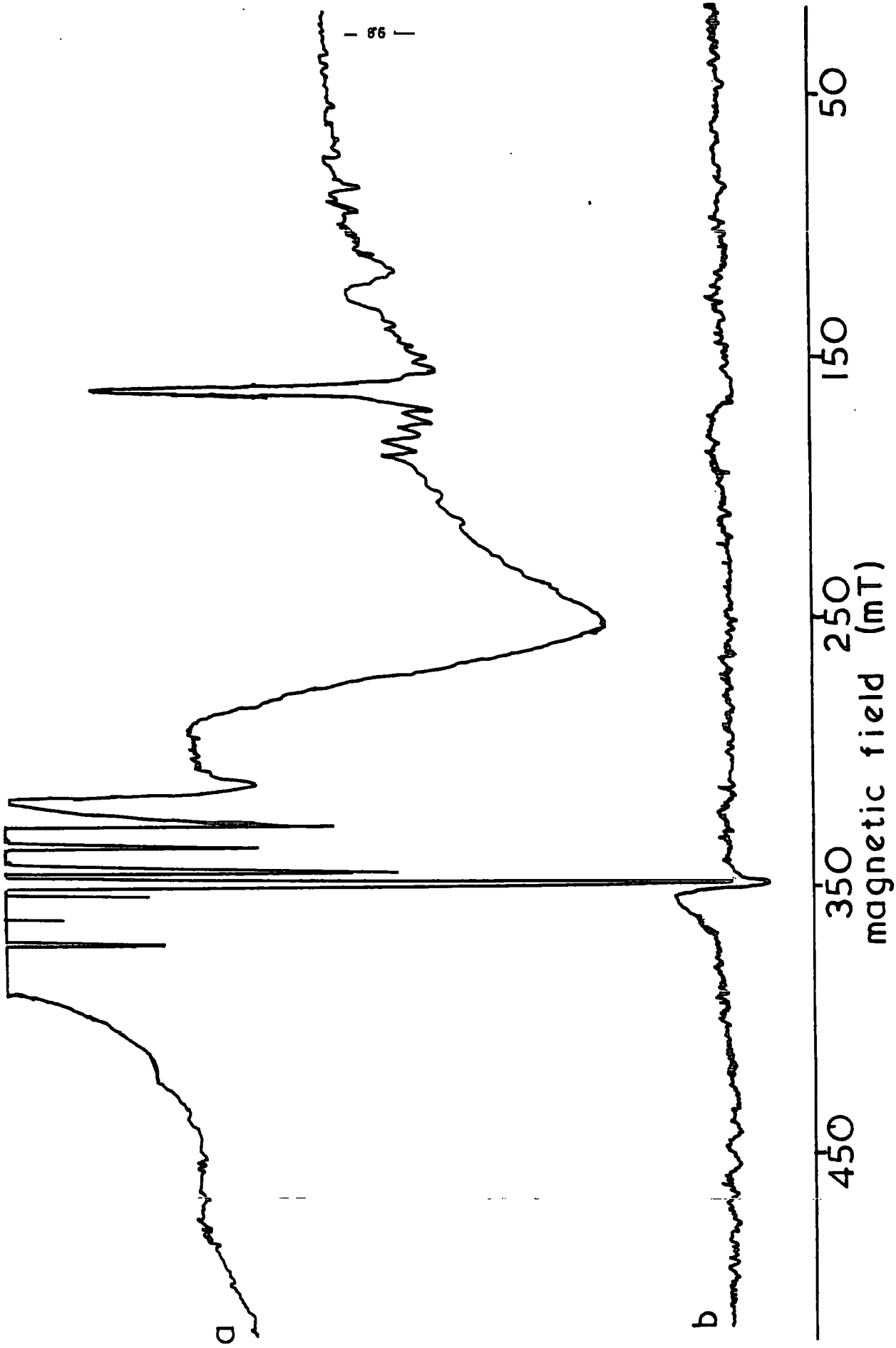

FIGURE 7.6 X-band e.s.r. spectrum of a) MgO powder from a kettle element after 15 years operation, and b) pure MgO supplied by B.D.H. All conditions identical 4.2K

and often can give a good clue to the nature of the line concerned, since the g-value of many species are known (7·2).

The number of lines and their relative intensities are also important in unambiguously assigning a line. Two distinct effects may give rise to multiplets, viz:- fine and hyperfine structure respectively. Fine structure can occur when $S > \frac{1}{2}$. An example of this occurs with Fe^{3+} in MgO (7·3) and an energy level diagram and corresponding spectrum is shown in Figure 7.7. Hyperfine structure occurs when the nucleus of the paramagnetic species has $I > 0$, when $(2I + 1)$ components of equal intensity are seen. An example is Co^{2+} in MgO. The ^{59}Co nucleus has $I = {}^{7}/_{2}$, and consequently eight lines are seen (7·4). An interesting example of a case where both fine and hyperfine structure are seen in some orientations is Mn^{3+}, which has $S = {}^{5}/_{2}$, $I = 5/2$ which gives rise to six components of five lines, a total of thirty lines in all, if fully resolved. If a particular species has hyperfine structure it can be further characterised by the energy separation of the components. This is termed the A-value, and is constant in units of frequency.

Returning to the MgO powder spectra. One feature is immediately noticeable, and that is the number of species present in the MgO from the failed cooker element, compared to that in the pure MgO specimen. At low fields (160 mT), (Figure 7.8), the spectrum is seen to consist of one of intense central line, and, arrowed, some of the components of an octet. This octet has a g-value of 4.25 so can be assigned to Co^{2+}. At present the strongly asymmetric line which appears in this region has not been identified.

A second area of interest is at about 340 mT. Using the g-values and the hyperfine structure, these lines can easily be assigned as shown in Figure 7.8. The six hyperfine lines of Mn^{2+} are easy to pick out, and the remaining lines with g = 1.9 and 2.0 are assigned to Cr^{3+}

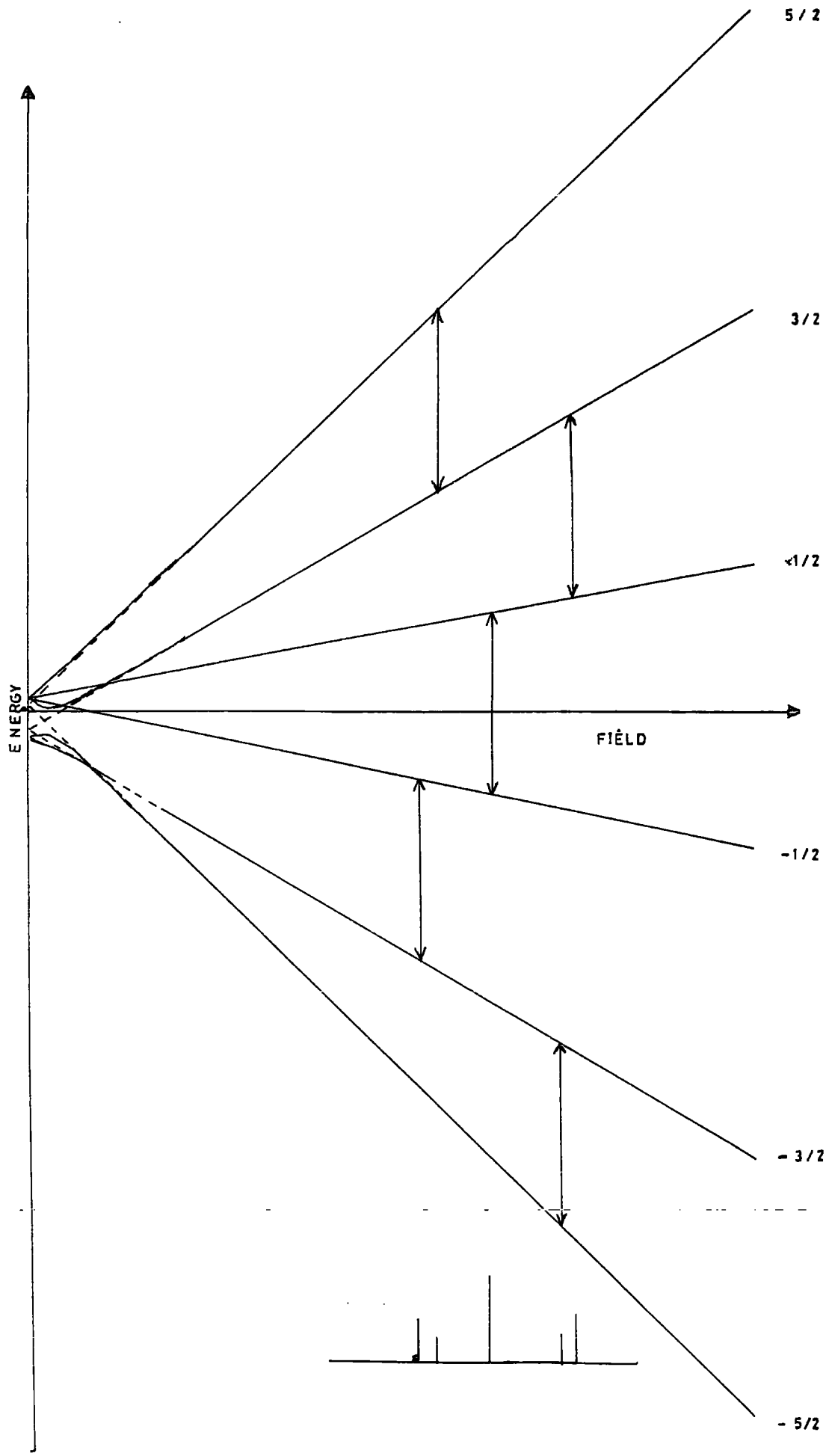

FIGURE 7·7 ZEEMAN ENERGY LEVEL DIAGRAM FOR Fe IN MgO SHOWING THE FIVE TRANSITIONS OBSERVED

and Fe^{3+} respectively. The only line left to be accounted for is the broad and intense line at g = 2.6. At present this line cannot be assigned unambiguously. It is interesting to note that it is much broader than the others, and this may be due to an isotropic spectrum, being superimposed over all orientations in the powder.

When this spectrum is compared with that of pure MgO recorded under identical conditions, it is immediately apparent that the spectrum of the failed element shows many extra impurities.

In the present research a study in greater depth of two ions. chromium and cobalt, has been made.

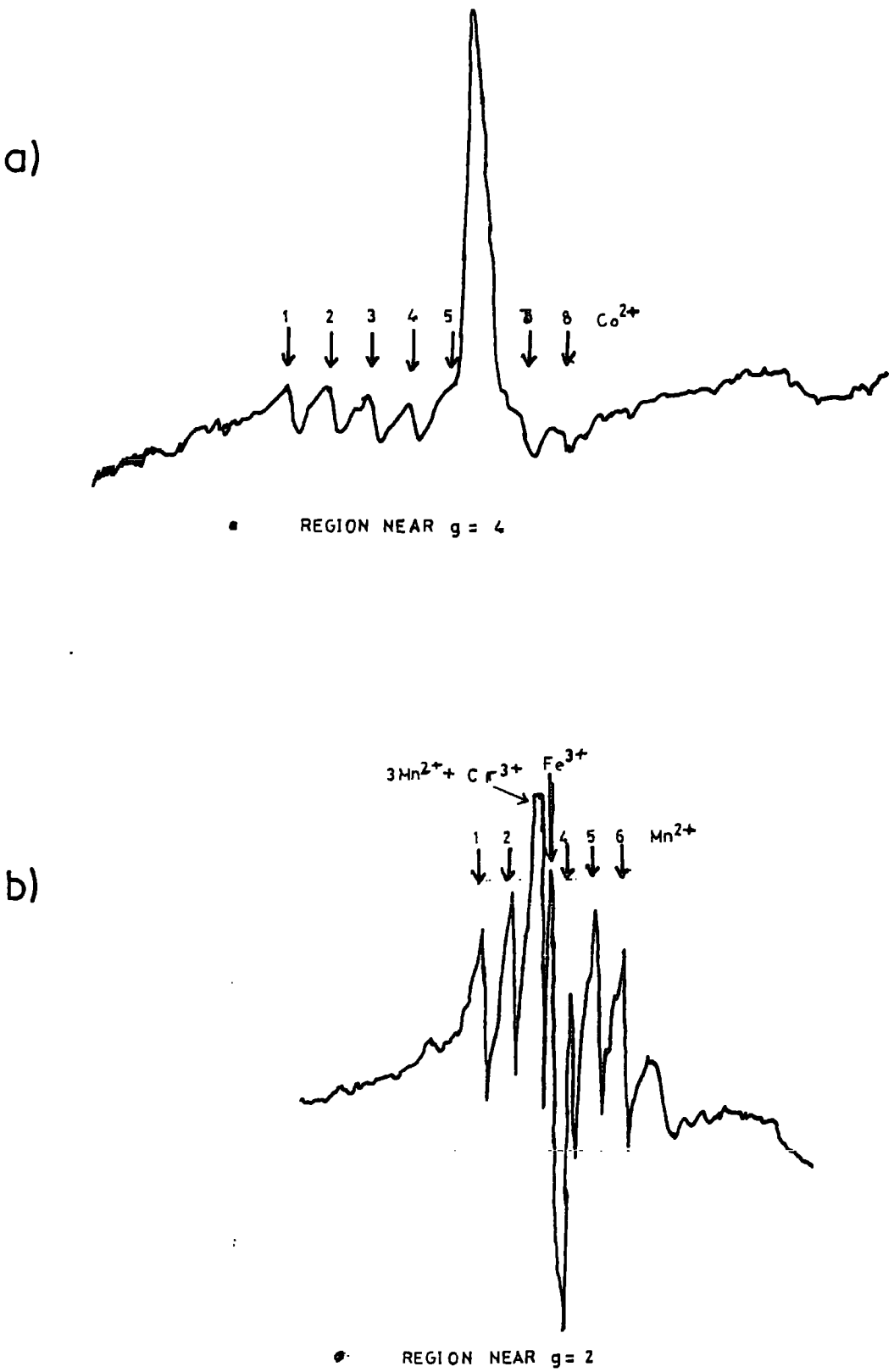

FIGURE 7.8 The spectrum of the failed element a) near g=4, and b) near g=4 X-band 4.2K

CHAPTER EIGHT

ELECTRON SPIN RESONANCE OF MgO:Cr

The electron spin resonance spectrum of Cr^{3+} in MgO has been reported previously by many workers. Investigations have mainly been devoted to two fields; in early work emphasis was placed on the determination of the spectral parameters g and A, the spectroscopic splitting factor and the hyperfine structure constant respectively, (8.1) whilst later work has largely been concerned with the spectra of Cr-Cr pairs, and Cr with other associated vacancies. (8.2)

The present work has been concerned with the lineshape analysis of the Cr^{3+} spectrum in order to investigate the nature of the exchange interactions; the method outlined in Chapter 6 was followed. The spectra were taken at two microwave frequencies, X-band ($\sim$9.5 GHz) and Q-band ($\sim$35 GHz).

8.1 X-BAND RESULTS

The spectra of all the MgO:Cr crystals were recorded on the Varian spectrometer at room temperature. A typical spectrum is shown in Figure 8.1. It consists of an intense line at g = 1.800, which is isotropic, together with four satellite lines of much lower intensity, which are evenly spaced, with two on either side of the main line.

This spectrum is in perfect agreement with that reported by Low (8.1) and assignment can be made in the same manner.

The spin-Hamiltonian for a d^3 ion in a cubic field is given by

$$\hat{H}_s = g\beta \underline{H} \cdot \hat{\underline{S}} + A\hat{\underline{I}} \cdot \hat{\underline{S}} \qquad (8.1)$$

which gives transitions at

$$\Delta E = g\beta H - AM_I + (A^2/2H)\left[I(I+1) - M_I^2 + M_I(2M_s - 1)\right] \qquad (8.2)$$

since the selection rules are $\Delta M_S = \pm 1$, $\Delta M_I = 0$.

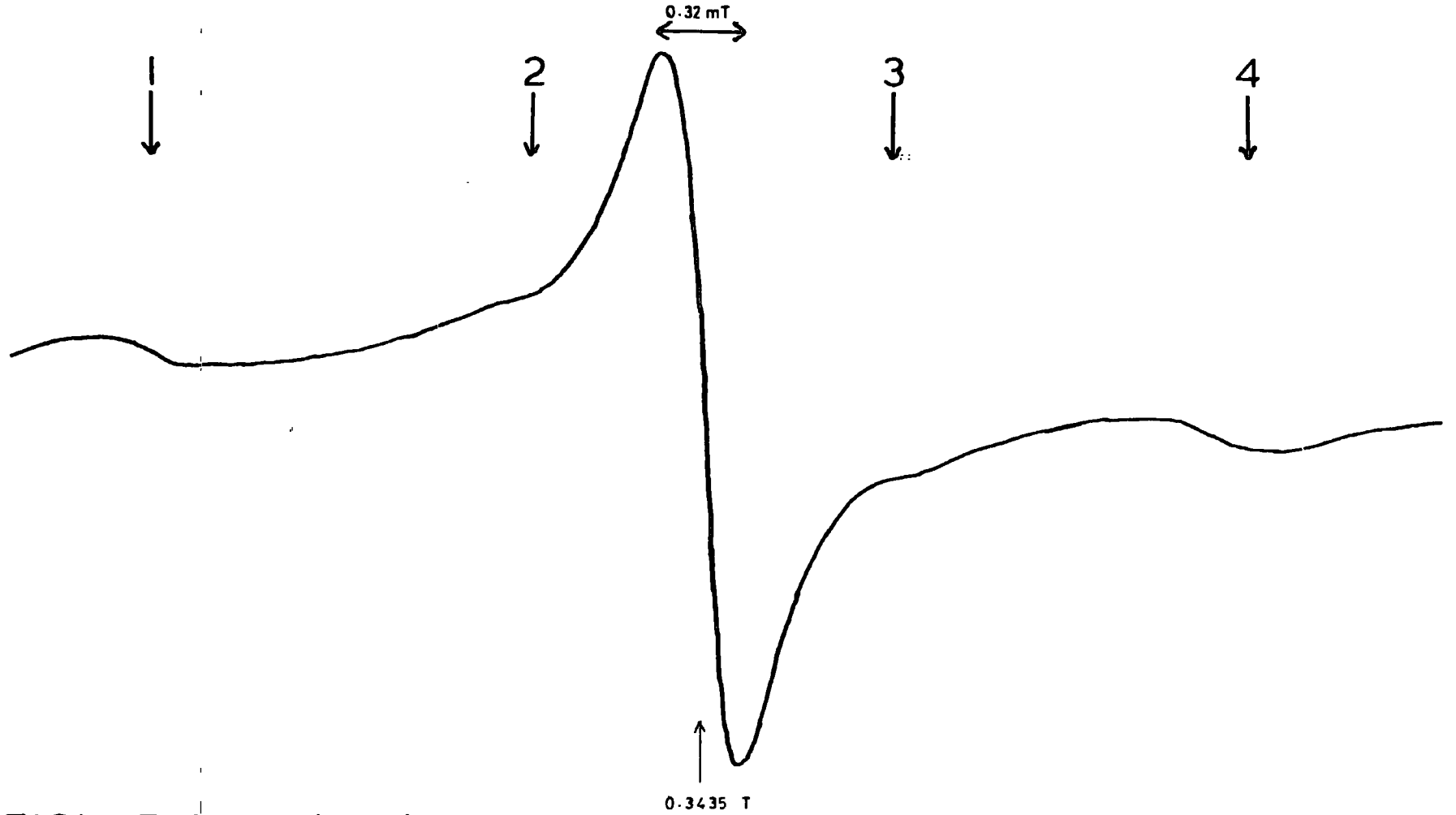

FIGURE 8.1 X-band e.s.r. spectrum of MgO:Cr(9500ppm). ν=9.520GHz 298K

Chromium has one stable isotope, ^{53}Cr, with I = 3/2 (9.5% abundant) whilst the rest have I = 0. Thus the transitions are given by

$$I = 0$$

$$h\nu_o = g\beta H \tag{8.3}$$

$$I = 3/2 \quad (M_I = 3/2)$$

$$\left.\begin{aligned} h\nu_1 &= g\beta H - \tfrac{3}{2}A + \frac{3A^2}{4H} \\ h\nu_2 &= g\beta H - \tfrac{3}{2}A - \frac{3A^2}{4H} \\ h\nu_3 &= g\beta H - \tfrac{3}{2}A - \tfrac{9}{4}\frac{A^2}{H} \end{aligned}\right\} \tag{8.4}$$

$$I = 3/2 \quad (M_I = 1/2)$$

$$\left.\begin{aligned} h\nu_4 &= g\beta H - \tfrac{1}{2}A + \frac{7A^2}{4H} \\ h\nu_5 &= g\beta H - \tfrac{1}{2}A + \frac{5A^2}{4H} \\ h\nu_6 &= g\beta H - \tfrac{1}{2}A + \frac{3A^2}{4H} \end{aligned}\right\} \tag{8.5}$$

$$I = 3/2 \quad (M_I = -1/2)$$

$$\left.\begin{aligned} h\nu_7 &= g\beta H + \tfrac{1}{2}A + \frac{7A^2}{4H} \\ h\nu_8 &= g\beta H + \tfrac{1}{2}A + \frac{9A^2}{4H} \\ h\nu_9 &= g\beta H + \tfrac{1}{2}A + \frac{11A^2}{4H} \end{aligned}\right\} \tag{8.6}$$

$$I = 3/2 \quad (M_I = -3/2)$$

$$\left.\begin{aligned} h\nu_{10} &= g\beta H + \tfrac{3}{2}A + \frac{3A^2}{4H} \\ h\nu_{11} &= g\beta H + \tfrac{3}{2}A + \frac{9A^2}{4H} \\ h\nu_{12} &= g\beta H + \tfrac{3}{2}A + \frac{15A^2}{4H} \end{aligned}\right\} \tag{8.7}$$

Immediately one notes if A << H (as is usually the case), the (8.4), (8.5), (8.6) and (8.7) collapse to give

$$h\nu_a = g\beta H - \tfrac{3}{2} A \qquad (8.4a)$$

$$h\nu_b = g\beta H - \tfrac{1}{2} A \qquad (8.5a)$$

$$h\nu_c = g\beta H + \tfrac{1}{2} A \qquad (8.6a)$$

$$h\nu_d = g\beta H + \tfrac{3}{2} A \qquad (8.7a)$$

The accepted energy level diagram for this system is given in Figure 8.2 along with the observed transitions.

As expected, theory predicts an intense singlet at $h\nu = g\beta H$ due to the even isotopes of Cr^{3+}, and a less intense quartet, centered on $h\nu = g\beta H$, with separation A, due to the isotope ^{53}Cr. This is exactly as observed. Comparison of the spectrum with the energy level diagram of Figure 8.2 shows that the lines can be assigned exactly thus:-

$h\nu_a = g\beta H - \frac{3}{2}A$: $|-\frac{1}{2}\ \frac{3}{2}\rangle \leftarrow |-\frac{3}{2}\ \frac{3}{2}\rangle$

$|\frac{3}{2},-\frac{3}{2}\rangle \leftarrow |\frac{1}{2}\ -\frac{1}{2}\rangle$

$h\nu_b = g\beta H - \frac{1}{2}A$: $|-\frac{1}{2},\ \frac{1}{2}\rangle \leftarrow |-\frac{3}{2}\ \frac{1}{2}\rangle$

$|\frac{3}{2},-\frac{1}{2}\rangle \leftarrow |\frac{1}{2},-\frac{1}{2}\rangle$

$h\nu = g\beta H$: $|-\frac{1}{2}\ 0\rangle \leftarrow |-\frac{3}{2}\ 0\rangle$

$|\frac{1}{2}\ -\frac{3}{2}\rangle \leftarrow |-\frac{1}{2}\ -\frac{3}{2}\rangle$

$|\frac{1}{2}\ -\frac{1}{2}\rangle \leftarrow |-\frac{1}{2}\ -\frac{1}{2}\rangle$

$|\frac{1}{2}\ 0\rangle \leftarrow |-\frac{1}{2}\ 0\rangle$

$|\frac{1}{2}\ \frac{1}{2}\rangle \leftarrow |-\frac{1}{2}\ \frac{1}{2}\rangle$

$|\frac{1}{2}\ -\frac{3}{2}\rangle \leftarrow |-\frac{1}{2}\ -\frac{3}{2}\rangle$

$|\frac{3}{2}\ 0\rangle \leftarrow |\frac{1}{2}\ 0\rangle$

$$h\nu = g\beta H + \tfrac{1}{2}A \quad : \quad |-\tfrac{1}{2}\ \tfrac{1}{2}> \ \leftarrow\ |-\tfrac{3}{2}\ \tfrac{1}{2}>$$

$$|\ \tfrac{3}{2}\ -\tfrac{1}{2}> \ \leftarrow\ |\ \tfrac{1}{2}\ -\tfrac{1}{2}>$$

$$h\nu = g\beta H + \tfrac{3}{2}A \quad : \quad |-\tfrac{1}{2}\ -\tfrac{3}{2}> \ \leftarrow\ |-\tfrac{3}{2}\ -\tfrac{3}{2}>$$

$$|\ \tfrac{3}{2}\ \tfrac{3}{2}> \ \leftarrow\ |\ \tfrac{1}{2}\ \tfrac{3}{2}>$$

where a state is designated by $|M_S\ M_I>$.

As can be seen there are many coincidences in this spectrum. This fact together with the observation that the spectrum is isotropic to a high degree of precision is strong evidence for the earlier assumptions that the Cr^{3+} ion is in a field of high cubic symmetry.

Another item of interest is the evaluation of the spin-orbit coupling constant, λ. As described in Chapter 3, the lowest optical energy level of the Cr^{3+} ion in an octahedral field is the $^4A_2(^4F)$ state, and it is, of course, from this state that the energy level diagram of Figure 8.2 was derived. The next highest optical energy level is the $^4T_{2g}(^4F)$ state, which is separated from the ground by the energy Δ, the crystal field separation energy. Theory states (8.3) that the contribution of this triplet to the orbital moment of the ground state is expressed in the deviation of the g factor from the free electron value, i.e.

$$g - g_s = -8\lambda/\Delta \qquad (8.8)$$

Taking $g_s = 2.0023$, and $\Delta = 16130\ cm^{-1}$ (as evaluated in Chapter 4), gives a value for the spin-orbit coupling, λ, 45.0 cm^{-1}.

8.1.1 X-band Lineshape Analysis

One of the most striking features of the x-band spectra is the virtual independence of linewidth of concentration of Cr^{3+} in the crystal.

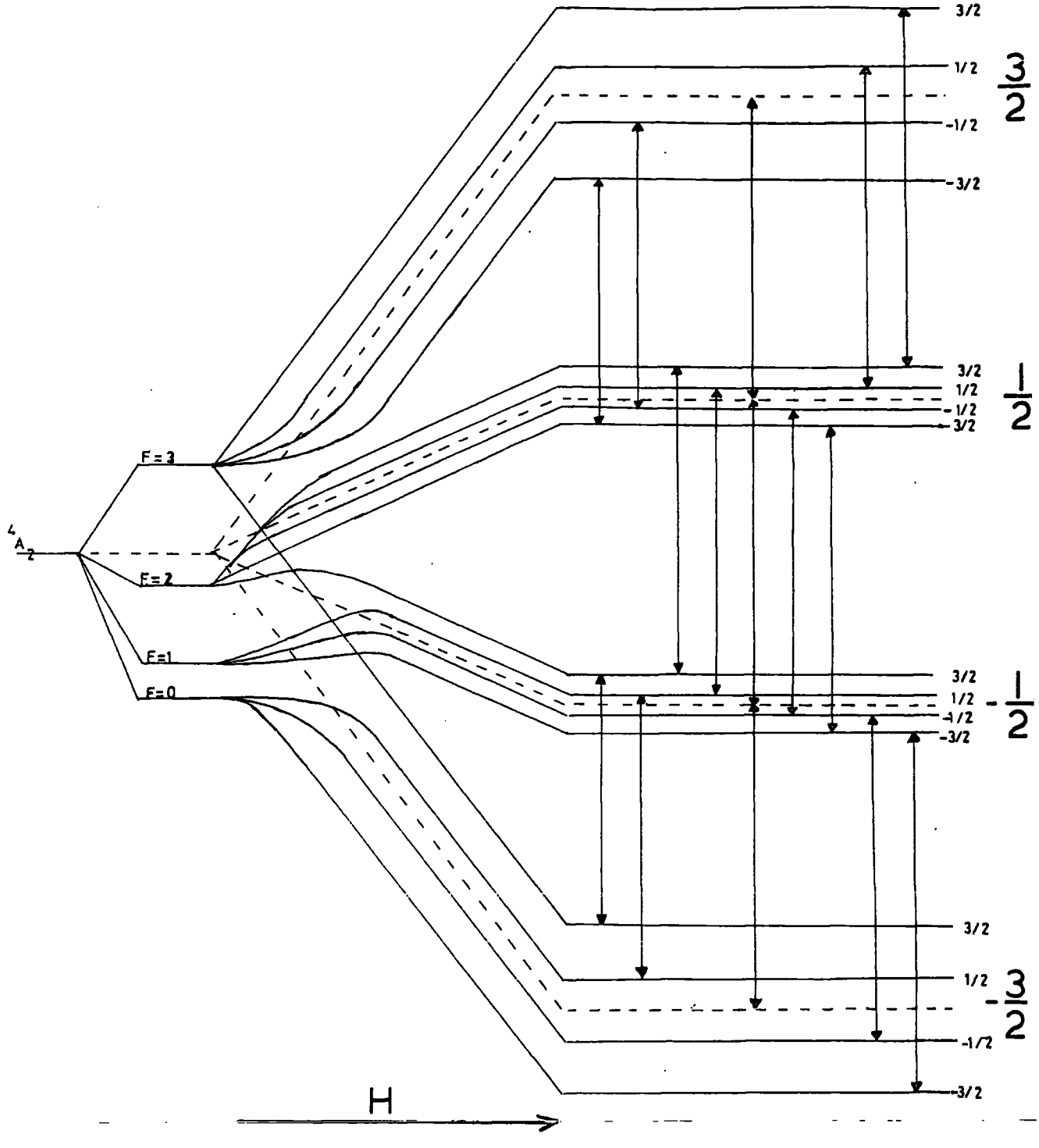

FIGURE 8.2 Schematic diagram of the Zeeman energy levels of MgO:Cr. Even isotopes are represented by dotted lines, ^{53}Cr with I=3/2 by solid lines. Observed transitions shown by arrows.

This is in direct conflict with the data calculated from the dipolar broadening theory of Chapter 6. This is tabulated below (Table 8.1) and also shown diagrammatically in Figure 8.3.

Concentration (ppm)	Hpp (observed (mT)	Hpp (calculated) (mT)
800	0.44	19.31
1300	0.47	24.61
3600	0.73	40.95
4200	0.39	44.23
5000	0.65	48.26
6200	0.46	53.74
7400	0.46	58.71
9500	0.32	66.52
15100	0.39	83.87

Table 8.4: Linewidth data for MgO:Cr

This effect has been seen previously in a similar system by Thorp et al (1.2) when investigating MgO:Fe. They ascribe the effect to exchange narrowing, and substantiate this by a method of moments analysis. A similar approach was used here. In doing so the central line of the spectrum was used, since it was the most intense and could readily be obtained with a good signal to noise ratio.

The spectra were integrated numerically using Simpson's rule. Evenly spaced ordinates were taken along the first derivative trace, typically 60-100 ordinates to each spectrum. These were then integrated on the University's IBM 390 computer, using the following algorithms

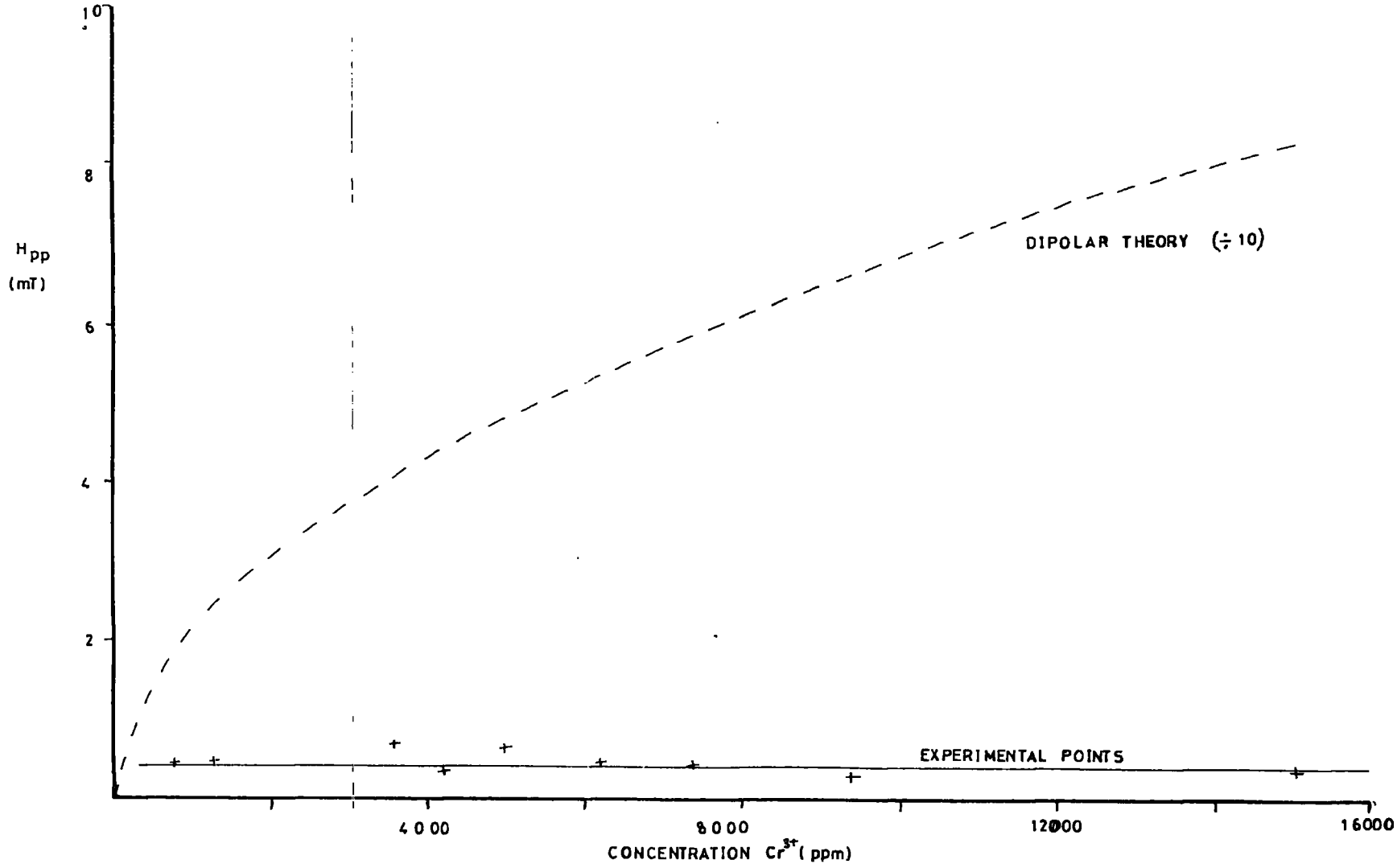

FIGURE 8.3 Variation of linewidth with concentration Cr^{3+} in MgO
9.5155 GHz 298K

$$\left.\begin{aligned} I_4 &= \frac{h}{3}\left\{y_o + 4y_1 + 2y_2 + 4y_3 + y_4\right\} \\ I_{2n} &= I_{2(n-1)} + \frac{h}{3}\left\{y_{2n-2} + 4y_{2n-1} + y_{2n}\right\} \end{aligned}\right\} \quad (8.9)$$

where I represents the integral of the function (see Figure 8.4 for clarification). Plotting the values of I_M against M gives the integrated spectrum and these points were used in the following analysis. For the sake of presentation a further computer programme was used to smooth the data by cubic interpolation; these smoothed integrated spectra are shown in Figures 8.5 to 8.13.

The next stages are to evaluate the first, second, third and fourth moments, the coefficient of kurtosis and also the coefficient of skewness. This is done in two steps. First the moments are evaluated about an arbitrary point (these are designated M'_n) and then are corrected to obtain the moments about the mean. The formula for this is given below (8.4)

$$\bar{x} = \sum_{i=1}^{m} x_i f_i \Big/ \sum_{i=1}^{m} f_i$$

$$M'_1 = \bar{x} \; ; \quad M'_n = \sum_{i=1}^{m} x_i^n f_i \Big/ \sum_{i=1}^{m} f_i$$

$$M_1 = 0$$

$$M_2 = M'_2 - (M'_1)^2$$

$$M_3 = M'_3 - 3M'_1M'_2 + 2(M'_1)^3$$

$$M_4 = M'_4 - 4M'_1M'_3 + 6(M'_1)^2M'_2 + 3(M'_1)^4$$

$$\text{kurtosis} = M_4/(M_2)^2 \quad ; \quad \text{skewness} = M_3/(M_2)^{\frac{3}{2}}$$

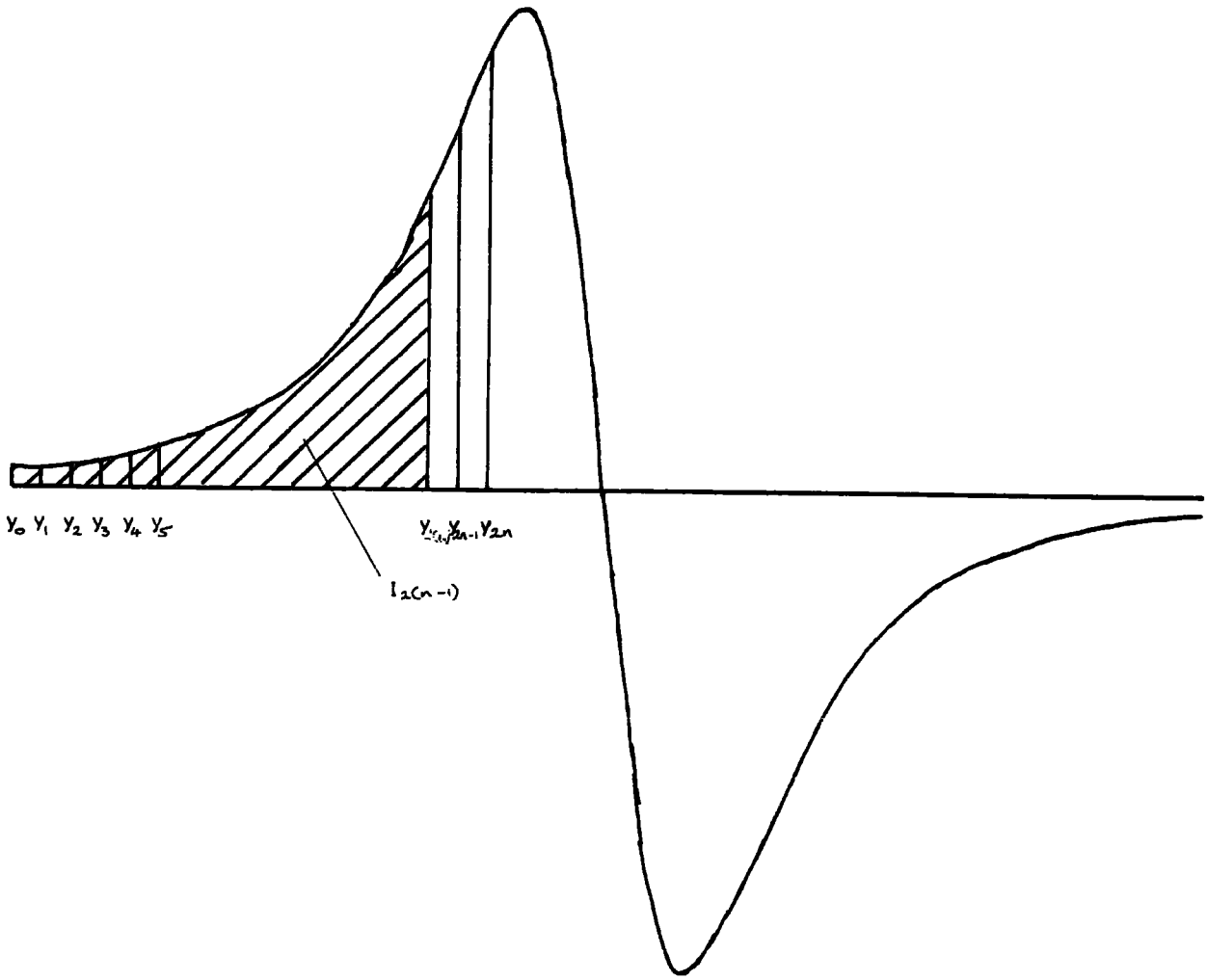

FIGURE 8.4 Clarification of method of integration

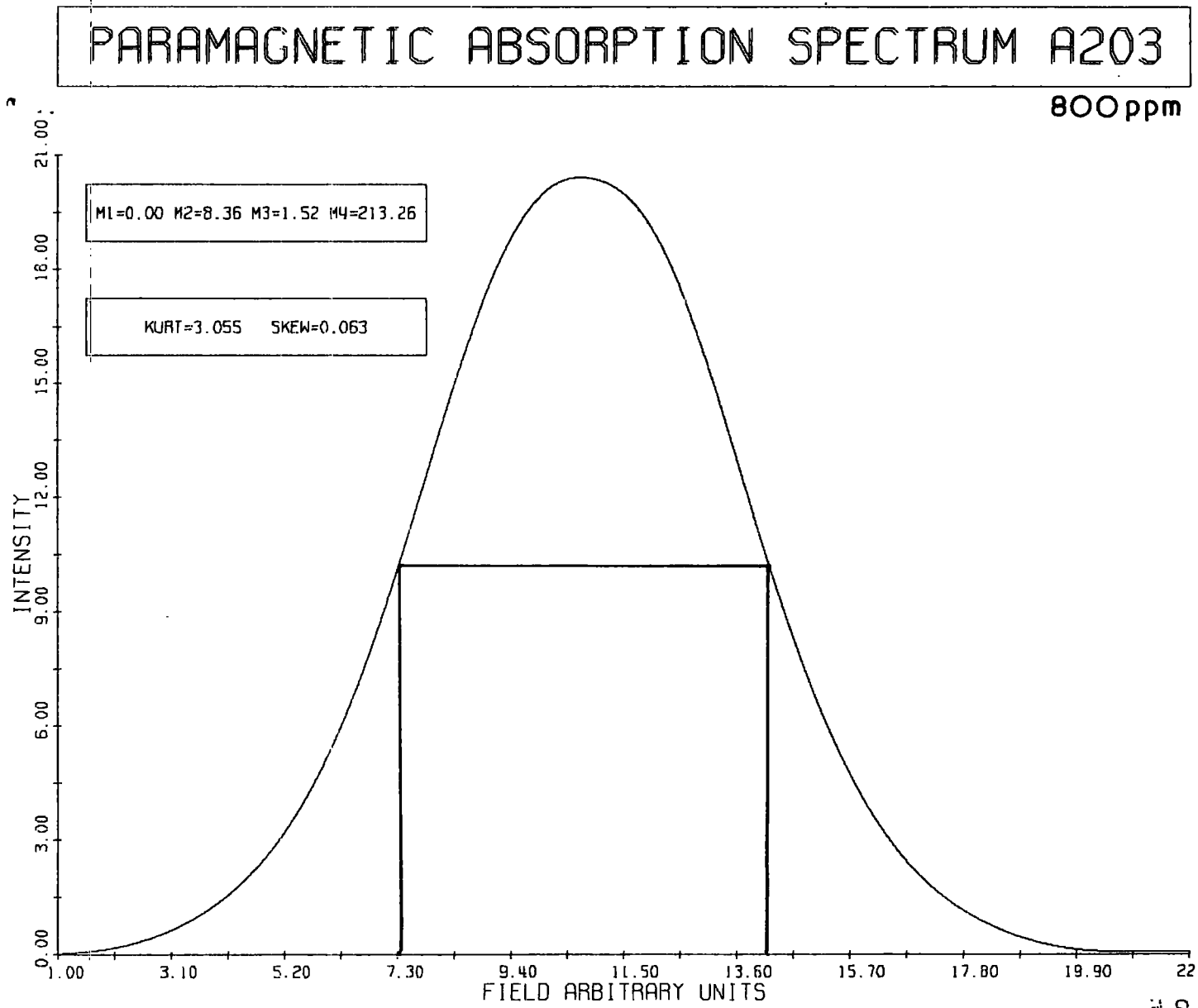

FIG 8.5

FIGURE 8.5

*DURPLOT output for job APL4 on SEP 18, 1978 at 16:52:12

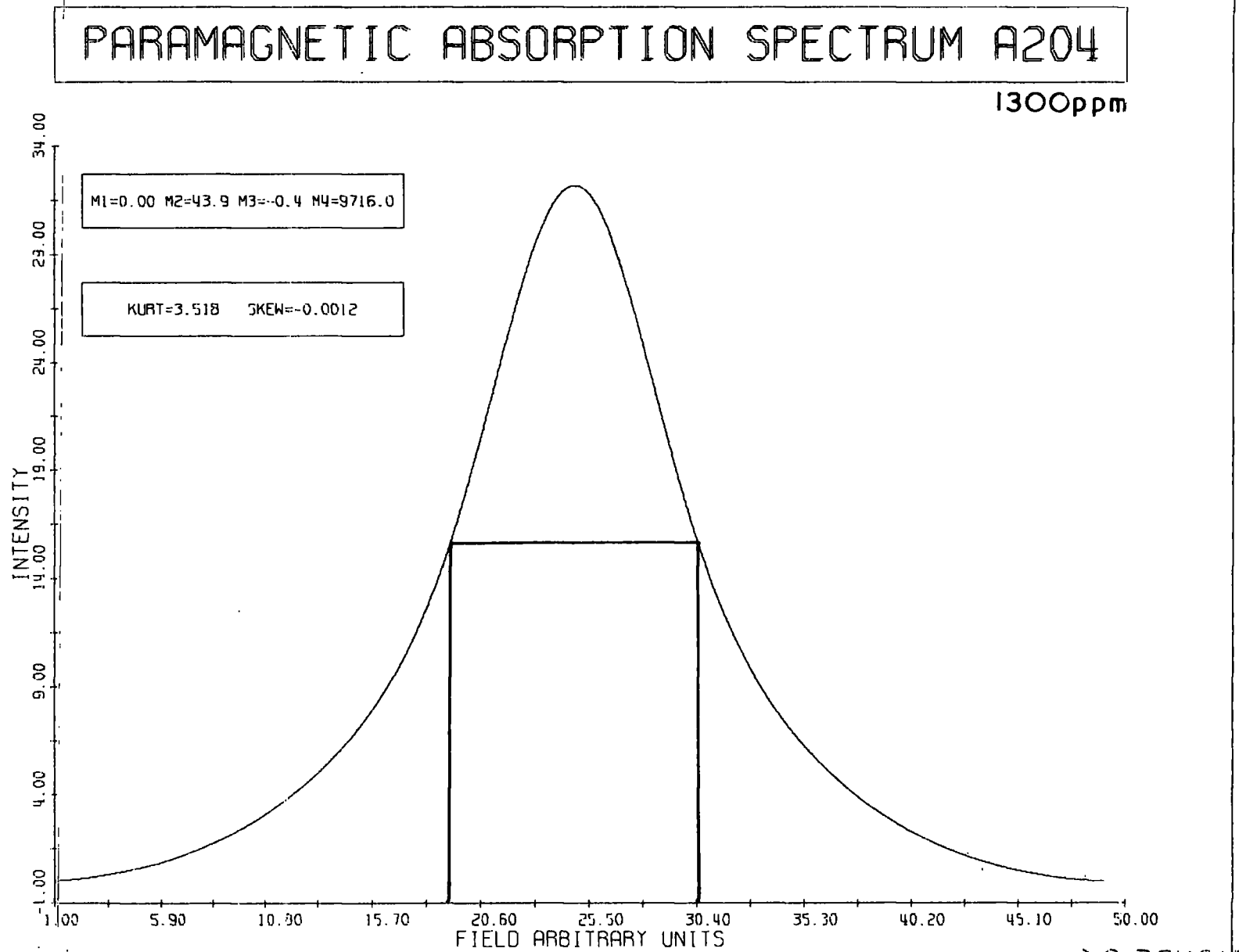

FIG 8.6

FIGURE 8.6

*DURPLOT output for job APL4 on SEP 12, 1978 at 15:25:11

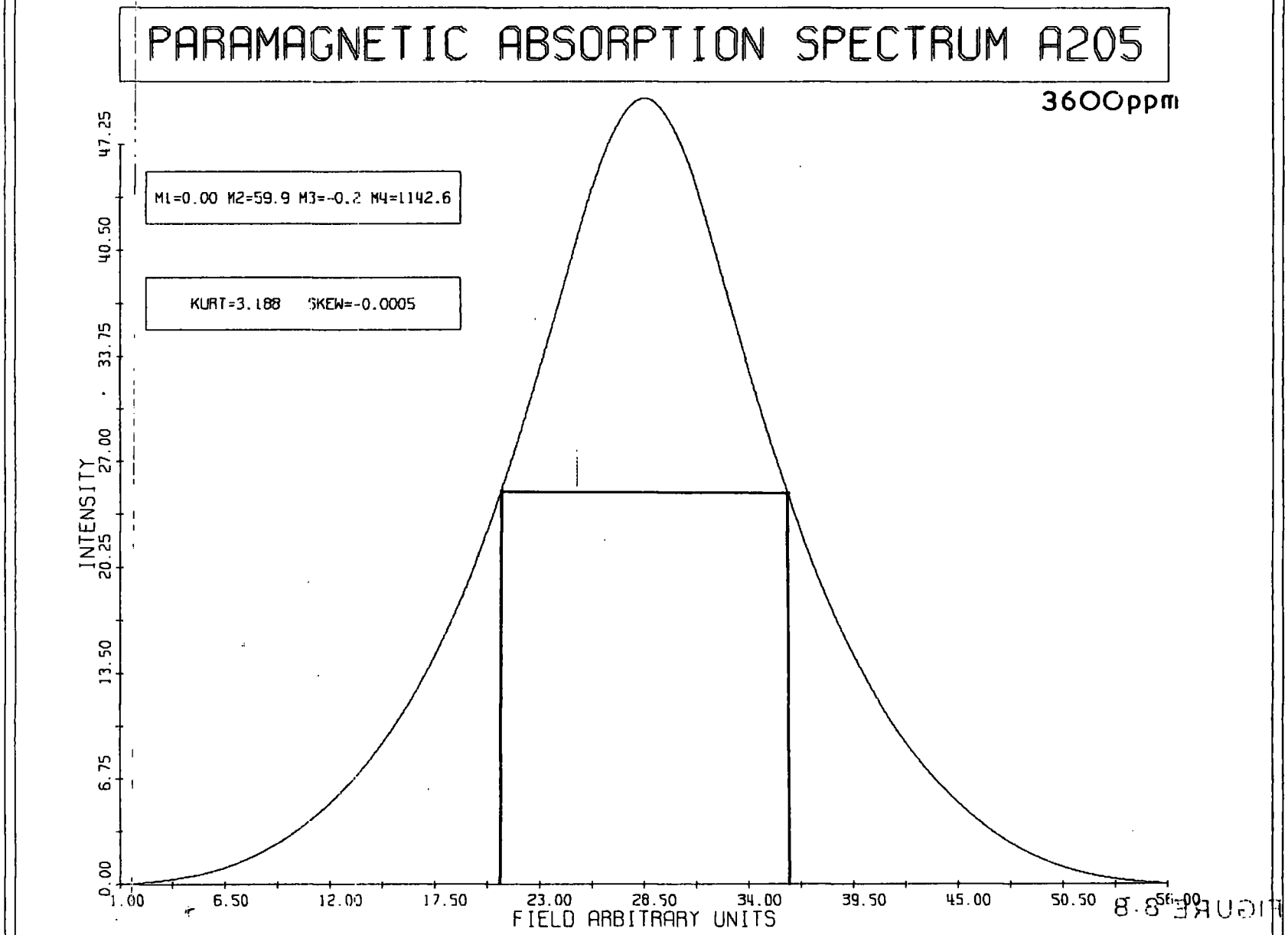

FIG 8.7

FIGURE 8.8

*CURPLOT output for job APL4 on SEP 19, 1978 at 15:33:15

PARAMAGNETIC ABSORPTION SPECTRUM A206

4200ppm

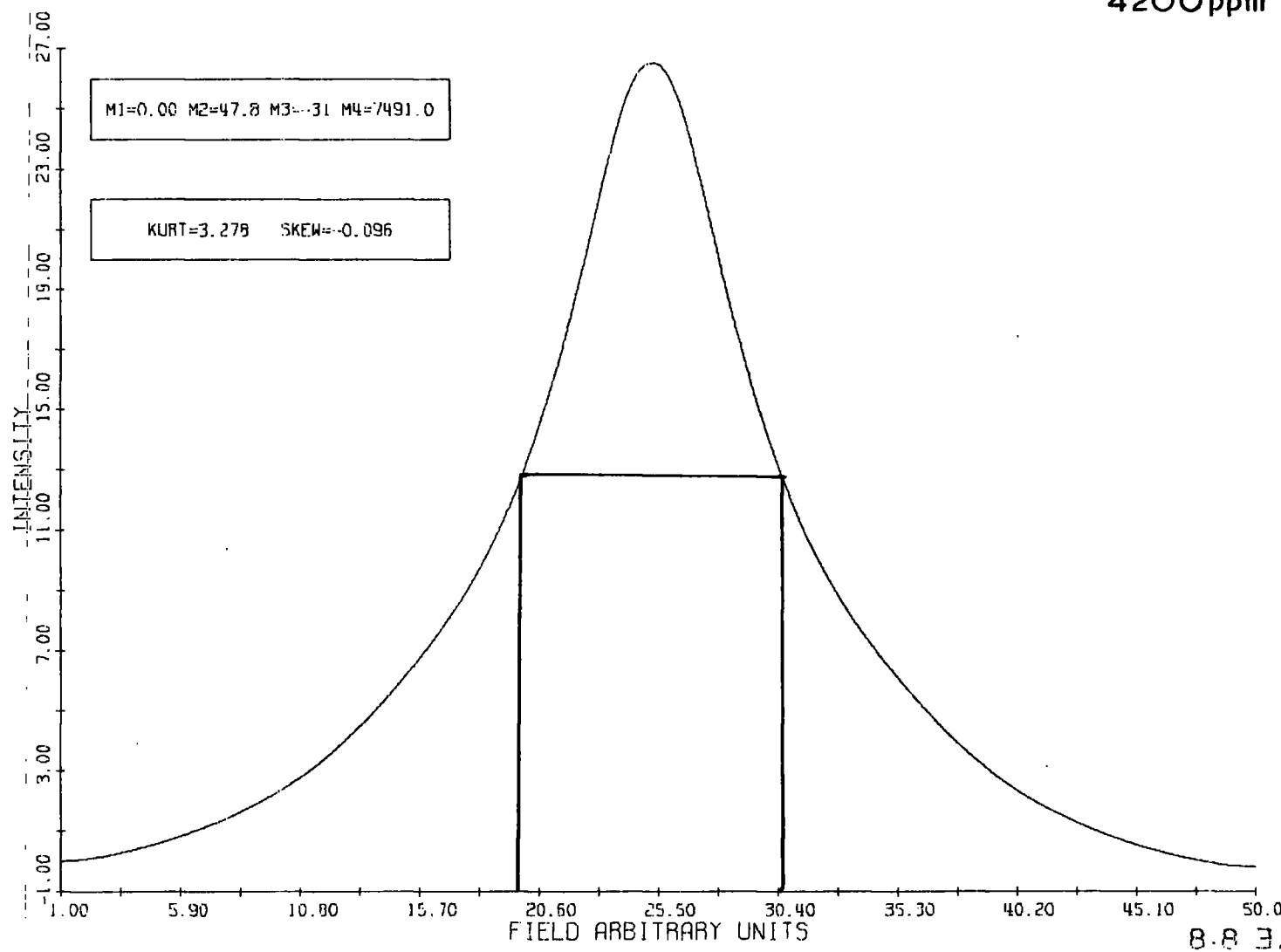

FIG 8.8

FIGURE 8.8

*DURPLOT output for job APL4 on SEP 21, 1978 at 16:09:30

PARAMAGNETIC ABSORPTION SPECTRUM A207

5000ppm

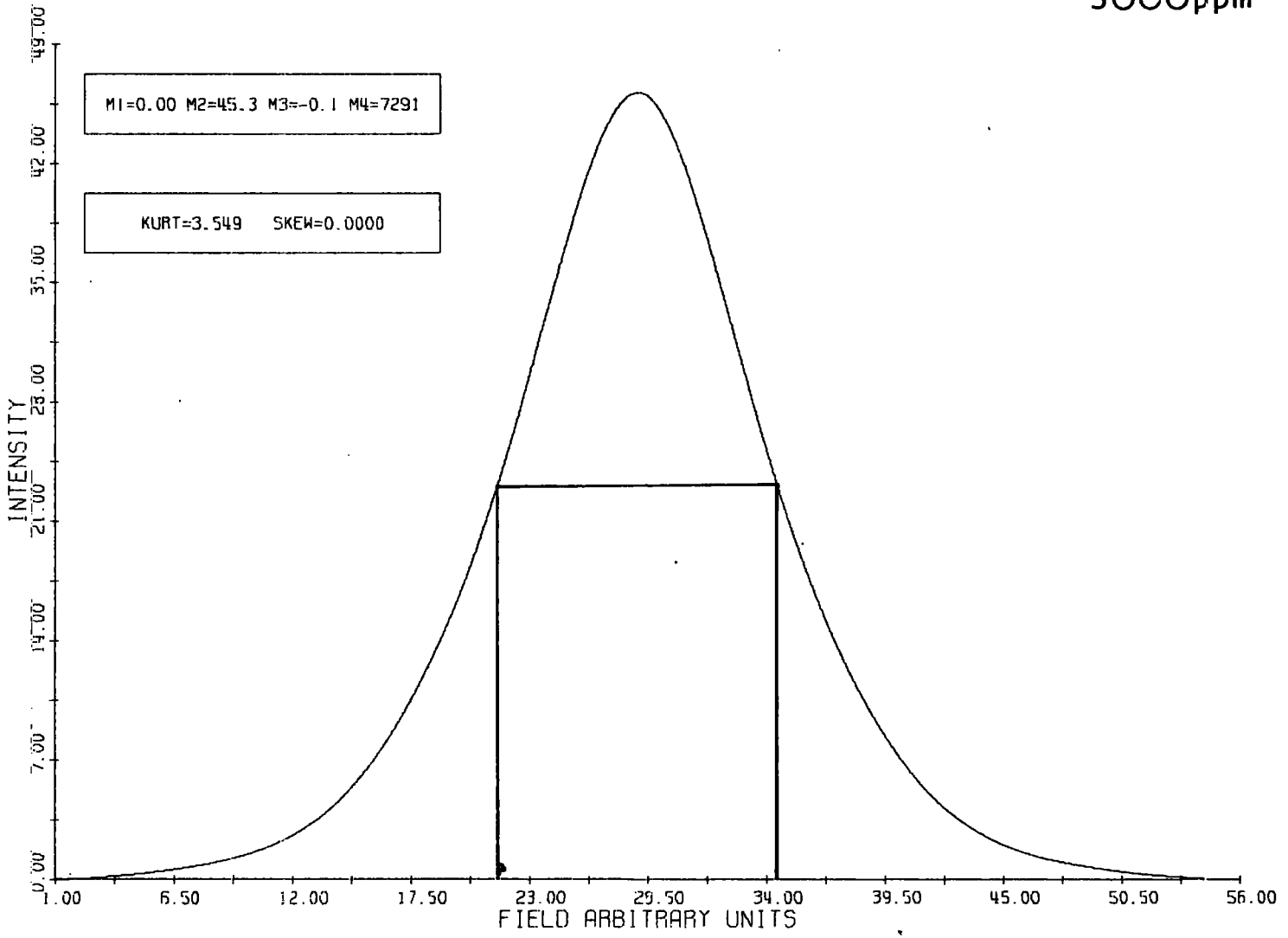

FIG 8.9

FIGURE 8.9

*DURPLOT output for job APL4 on SEP 19, 1978 at 10:53:29

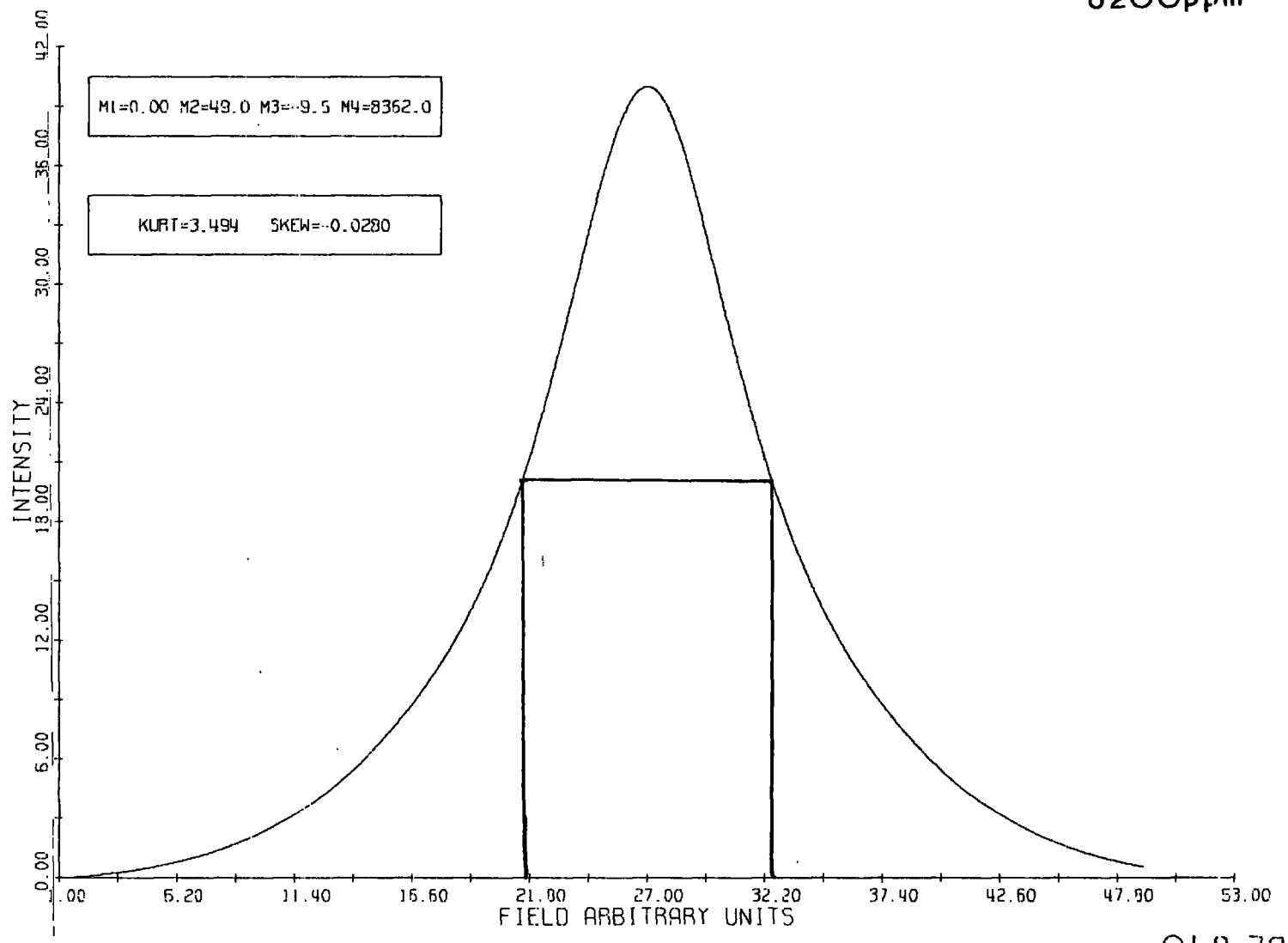

FIG 8.10

FIGURE 8.10

*DURPLOT output for job APL4 on SEP 19, 1978 at 12:09:02

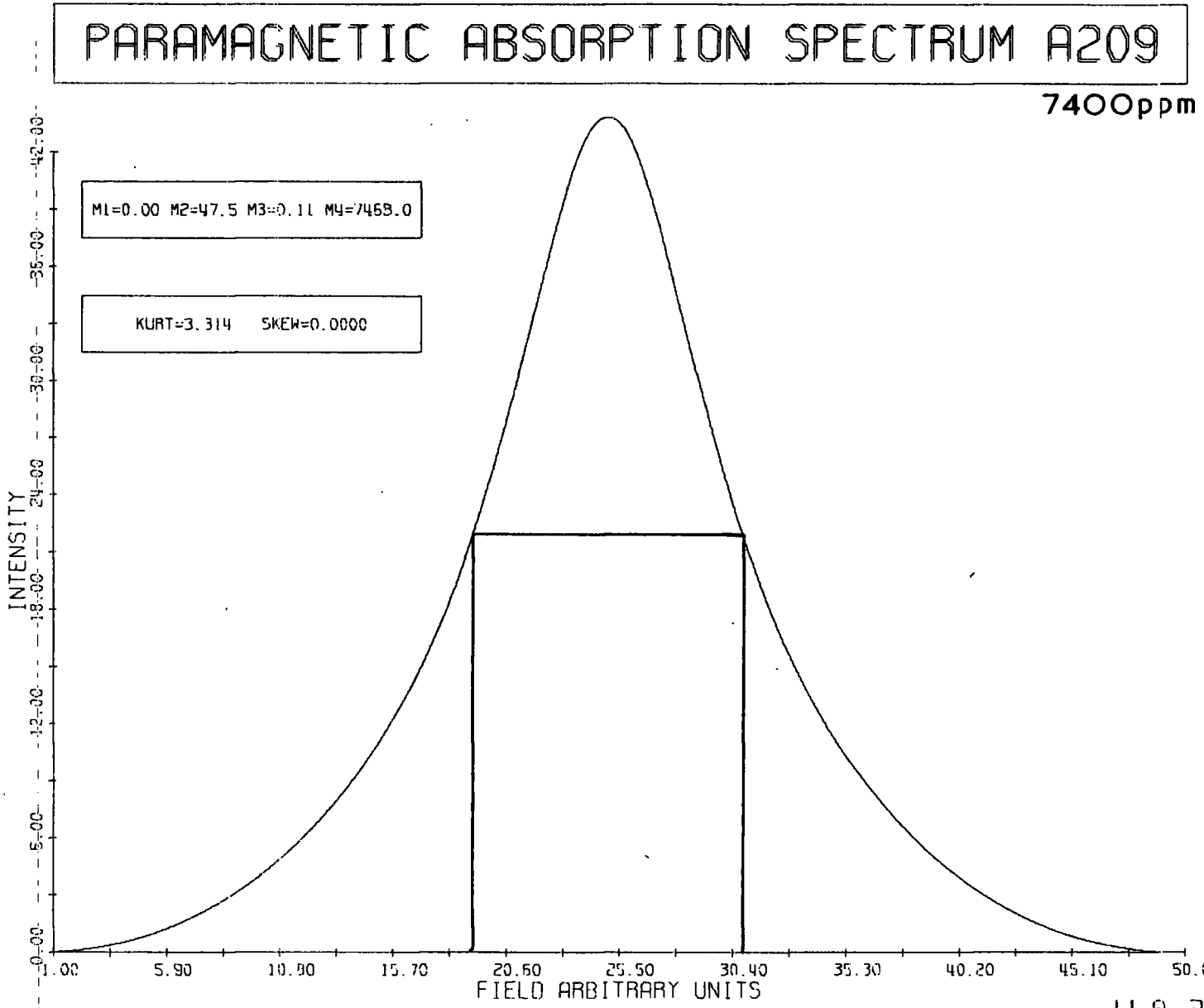

FIG 8.11

FIGURE 8.11

*DURPLOT output for job APL4 on SEP 20, 1978 at 10:35:08

PARAMAGNETIC ABSORPTION SPECTRUM A210

9500ppm

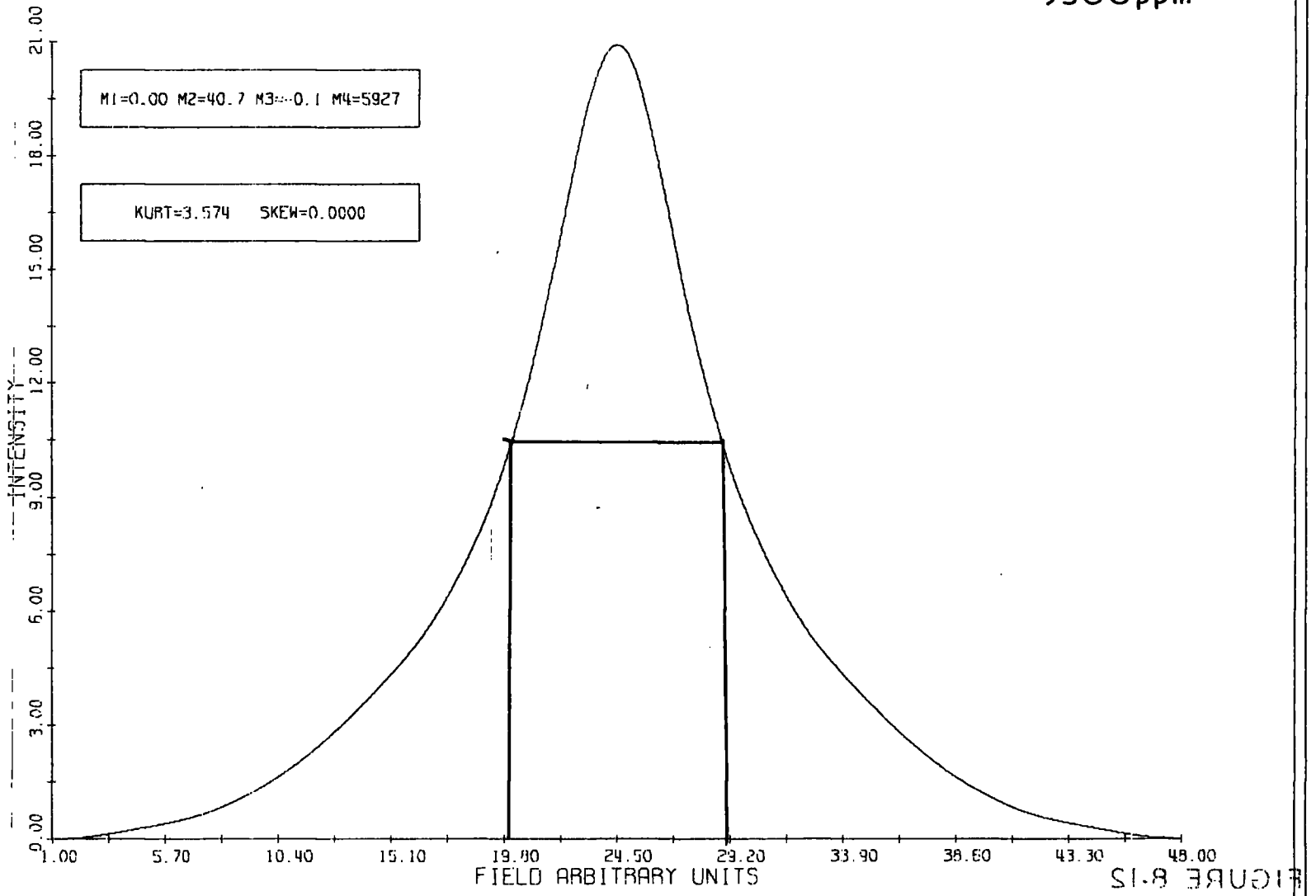

FIG 8.12

FIGURE 8.12

*DURPLOT output for job APL4 on SEP 18, 1978 at 10:43:33

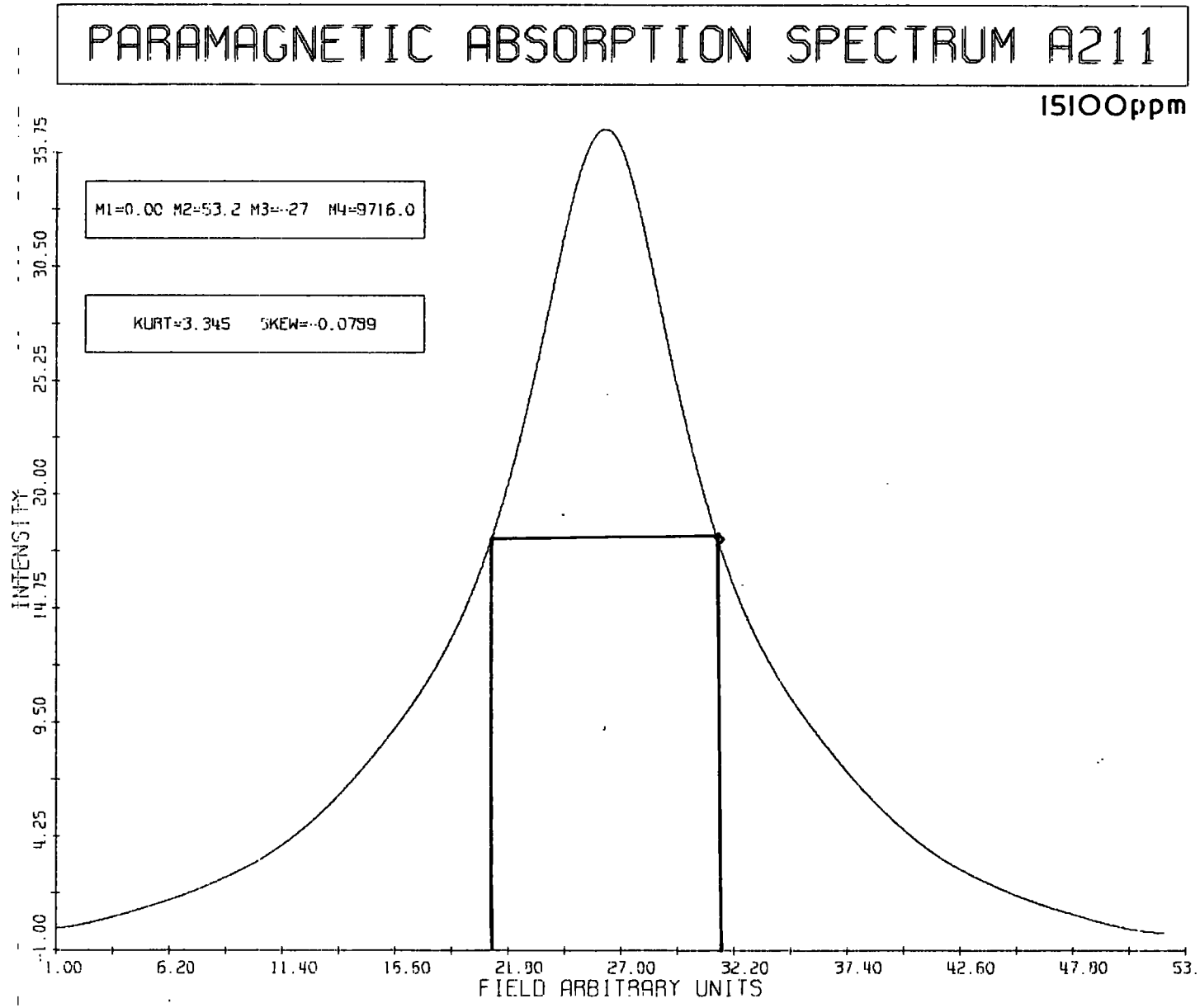

FIG 8.13

FIGURE 8.13

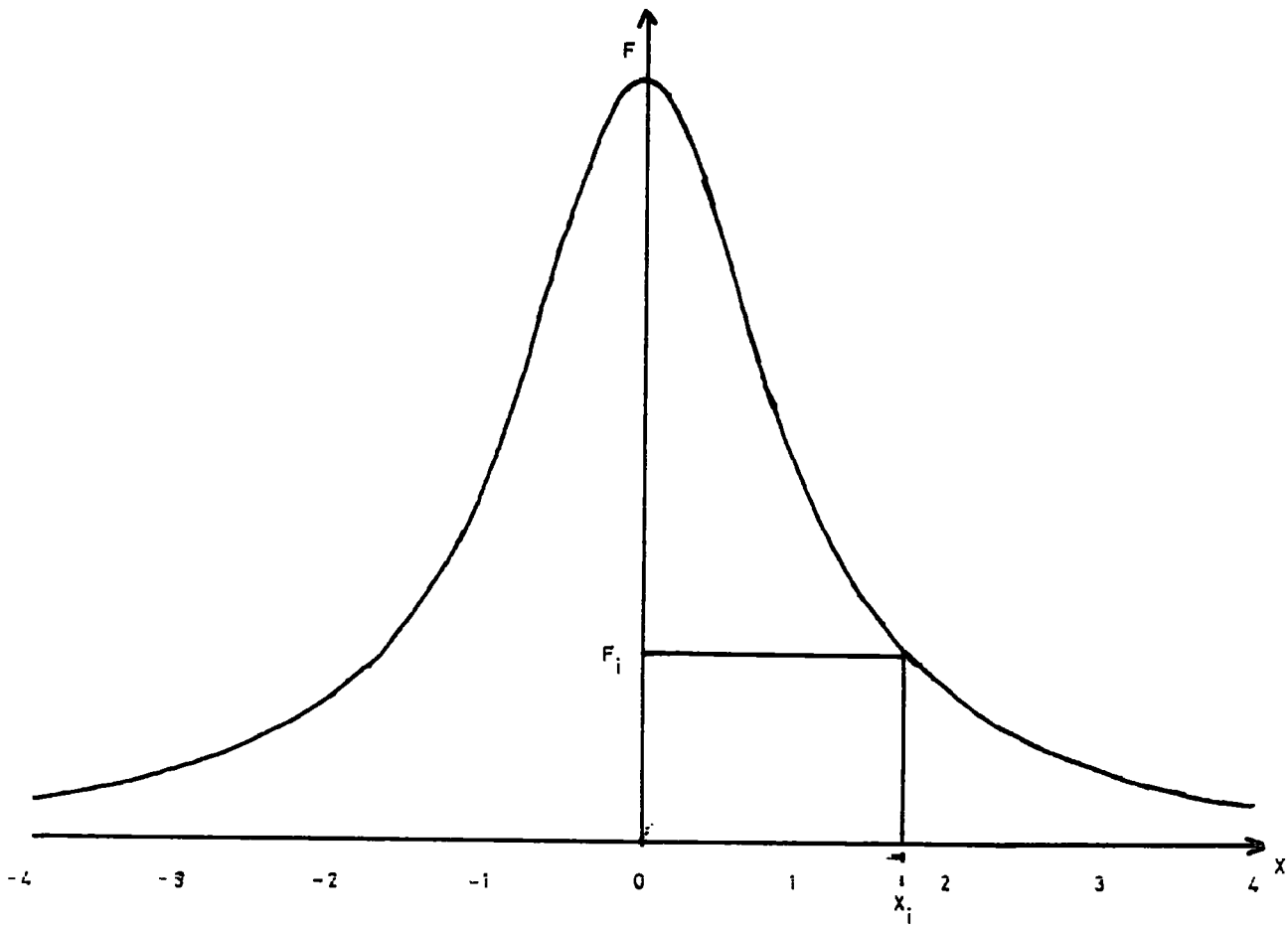

FIGURE 8.14 Characterising an absorption curve

The computer programmes used in these calculations were formulated with the help of P. Waite and B. Shaw, and are given in Appendix 3. Use of the equations derived in Chapter 6 then enabled the parameter J" to be calculated. The lineshape data is tabulated in Table 8.2.

Column one gives the concentration of the Cr^{3+} ions in the specimen, expressed in p.p.m. It is important to recall that the fraction of atomic sites occupied by the dopant species is given by p.p.m. x 10^{-6}.

Columns two and three give the parameters M_2 and ΔHpp, the second moment, and the peak to peak linewidth of the first derivative, as calculated by the dipolar broadening theory of Section 6.3.

Column four gives the observed ΔHpp, for comparison with column three. These two columns, three and four, merely form a repetition of Table 8.1, but are reproduced here for convenience.

Column five gives the value of ΔH, the width at half height, as observed from the integrated spectra given in Figures 8.5 to 8.13. This allows a first insight into the lineshape factor, since from the equations for Gaussian and Lorentzian functions the parameter ΔHpp/ΔH can be evaluated. This has the value 0.577 for a pure Lorentzian curve, and 0.846 for a pure Gaussian, and these values can be compared with the observed ratios given in column six.

The next important parameters are the observed coefficients of kurtosis. The coefficient of kurtosis for a pure Gaussian is equal to three, and any narrowing effect on the line, i.e. trend to Lorentzian, will manifest itself as an increase in this coefficient. These are listed for the observed lines in column seven.

The final piece of information is the coefficient J", the isotropic exchange energy. For a purely dipolar system there is no exchange, and hence this would be equal to zero. The equation for J" is given by (6.36),

Sample Concentration	M_2 $(Hz)^2$	ΔHpp (calc) mT	ΔHpp (obs) mT	ΔH (obs) mT	$\frac{\Delta Hpp}{\Delta H}$ (obs)	kurtosis	J" (Hz)
800	7.20×10^{16}	19.31	0.444	1.044	0.425	3.055	2.49×10^{9}
1300	1.17×10^{17}	24.61	0.466	0.842	0.554	3.518	5.02×10^{9}
3600	3.24×10^{17}	40.95	0.728	1.133	0.642	3.188	1.03×10^{10}
4200	3.78×10^{17}	44.23	0.393	0.819	0.480	3.278	1.67×10^{10}
5000	4.50×10^{17}	48.26	0.648	0.958	0.678	3.549	1.70×10^{10}
6200	5.58×10^{17}	53.74	0.458	0.814	0.563	3.494	2.47×19^{10}
7400	6.66×10^{17}	58.71	0.456	0.856	0.532	3.314	2.81×10^{10}
9500	8.55×10^{17}	66.52	0.326	0.667	0.479	3.574	4.63×10^{10}
15100	1.36×10^{18}	83.87	0.386	0.771	0.470	3.455	6.36×19^{10}

Table 3.2: Lineshape Data for MgO:Cr^{3+}. X-Band, Room Temperature

and one uses the equation of transformation, $h\nu = g\beta H$ to go from ΔH, the half-width in units of field, to $\Delta\nu$, the half-width in units of frequency.

Table 8.2 reveals several important features. Firstly, the observed values of ΔHpp are by no means in good agreement with the ΔHpp calculated by the dipolar broadening theory; secondly the experimental values seem largely independent of sample concentration (in contrast to the theoretical values which are proportional to concentration to the half) and thirdly the experimental values are much smaller than those predicted by the dipolar theory.

Exchange narrowing would cause the line to adopt a near Lorentzian shape and this is substantiated by column six, as the values of $\Delta Hpp/\Delta H$ are much more akin to the Lorentzian value than the Gaussian.

Even more convincing are the values obtained for the kurtosis of the lines. These are consistently greater than the Gaussian value of 3.00, and in fact compare favourably with values of kurtosis obtained for exchange narrowed lines obtained by Van Vleck (6.4) which are given below

Salt	ΔHpp(obs) MT	ΔHpp(calc) MT	kurtosis
$MnCl_2$	75.0	295	3.84
$MnSO_4$	66.5	352	3.32
$MnCO_3$	46.0	446	4.18
MnF_2	47.0	702	3.73
MnS	78.0	752	3.84

Table 8.3: Van Vleck's Data for Exchanged Narrowed Lines (adapted to follow the present units and notation).

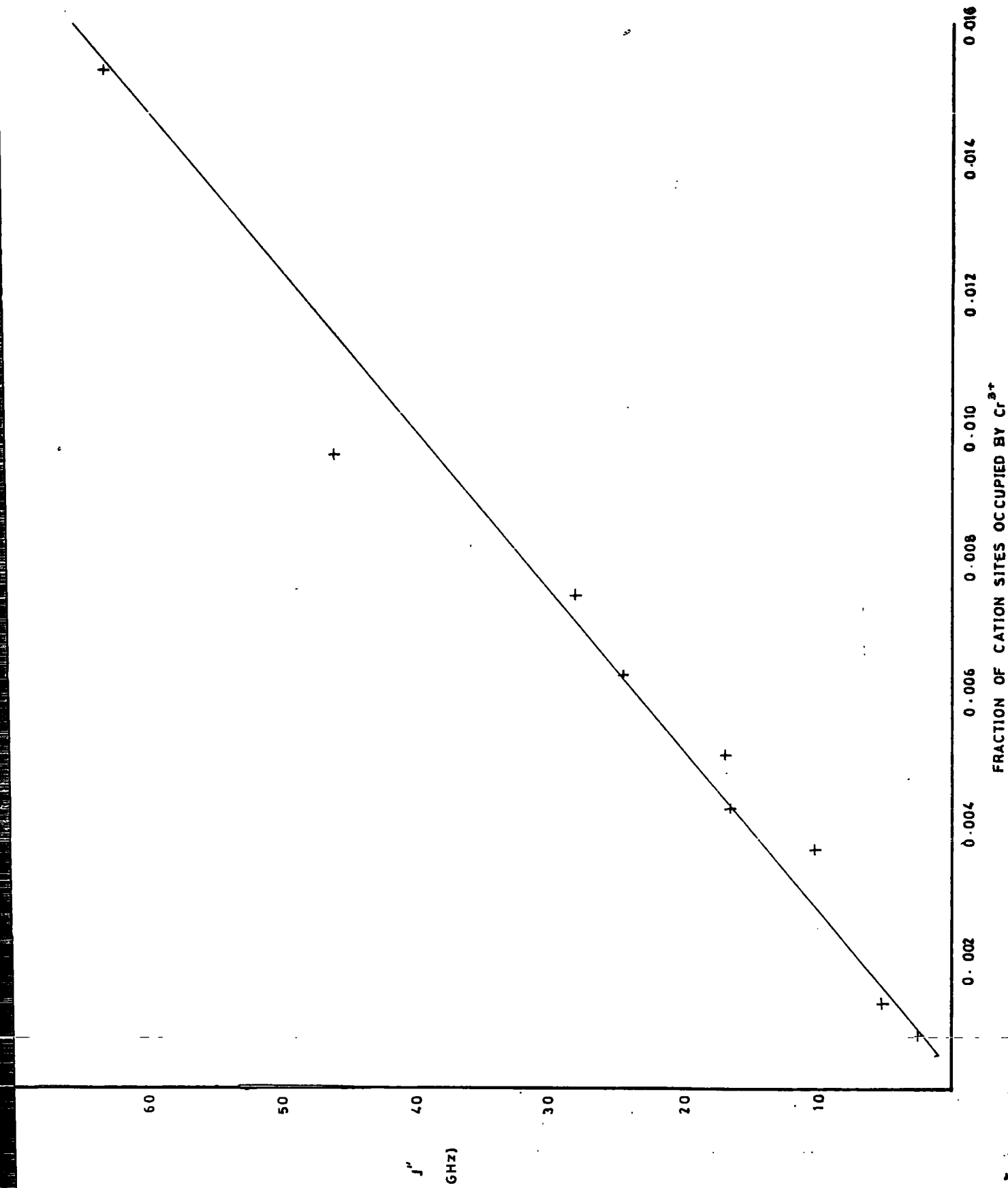

FIGURE 8.15 Plot of isotropic exchange exchange energy versus concentration for Cr^{3+} in MgO. Data obtained at 298K and 9.5155GHz

Further evidence is obtained from evaluation of the exchange interaction energy, J". This has a quite large numerical value, $\sim$ 10 GHz. Further, a plot of J" against concentration (Figure 8.15) gives a straight line to a high degree of confidence (correlation coefficient 0.989). If this line is extrapolated to 66.6% of the cation sites occupied by Cr^{3+}, i.e. to the point corresponding to pure Cr_2O_3, an exchange energy of 2.9×10^{12} Hz is obtained which is in excellent agreement with the literature value for Cr_2O_3 of $\sim 1.5 \times 10^{12}$ Hz (8.5) as estimated from magnetic susceptibility measurements.

The conclusions are that the Cr^{3+} ion in magnesium oxide exists in a relatively strong internal exchange field, which is linearly dependent on chromium concentration in the range measured, and that the electron spin resonance linewidth of Cr^{3+} in MgO is substantially reduced by exchange narrowing from that predicted by assuming a purely dipolar interaction.

8.2 Q-BAND RESULTS

The spectra of the MgO:Cr crystals were recorded on the Q-band spectrometer at room temperature and also at liquid nitrogen temperatures. At high gain a large number of lines were seen, as at X-band, and for completeness the Q-band spectrum is shown in Figure 8.16. One important point to note with all the Q-band spectra presented here is that the field markings provided are by no means as accurate as those at X-band. The reason for this is that the low fields needed for X-band spectroscopy may be measured with great accuracy by a proton magnetometer, but at the higher fields needed for Q-band ($\sim$ 1.6 T) the proton magnetometer can no longer be used. For high accuracy field measurements a magnetic resonance technique using lithium nuclei is required and a Lithium magnetometer was not available. The values that are quoted in the Q-band work were measured with a Hall probe.

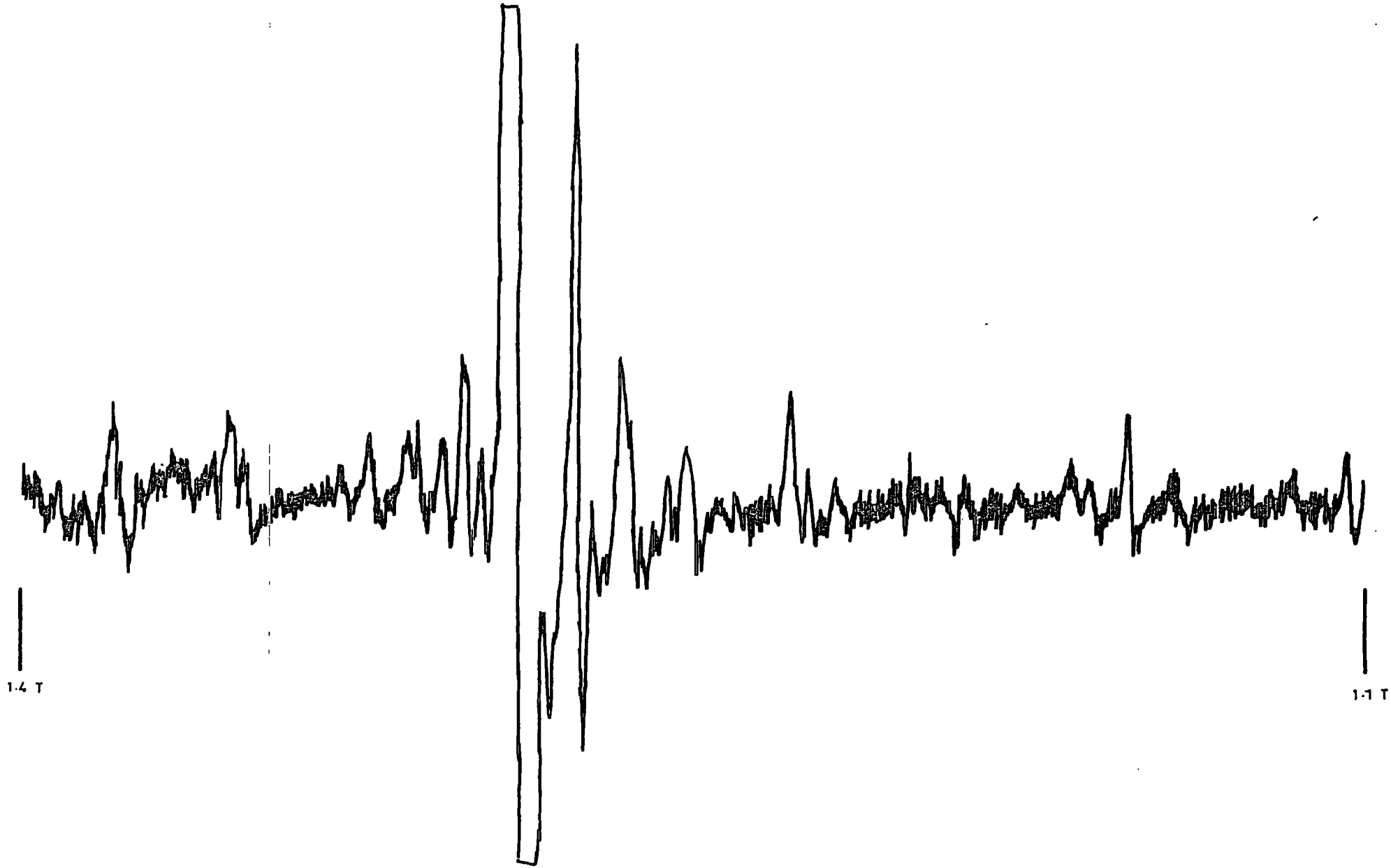

FIGURE 8·16 High gain spectrum of MgO:Cr(3600ppm) 298K 35·5GHz

By reducing the gain considerably it was possible to study only those lines due to Cr^{3+}, as these were the most intense. The spectrum could easily be fitted to the same energy level digram. On all the crystals investigated one further line appeared to low field, as shown in a typical spectrum (Figure 8.18). Without know the exact field at which this line occurs it is extremely difficult to identify the species responsible, but as it is to low field the g-value must be higher than that of Cr^{3+}, and it is tempting to ascribe the new line to Fe^{3+} (G = 2.0037).

8.2.1 Q-band Lineshape Analysis

The Q-band spectra again reveal the apparent independence of concentration of the linewidth. Despite the difficulty in measuring field accurately, the linewidth could be estimated using the Hall probe as being less than 0.9 mT.

The problem of not knowing the linewidths exactly has been overcome by taking the mean of the X-band linewidths, and normalising the arbitrary units of the Q-band data to this, using the mean of that data; i.e. if the units of field for the Q-band data (experimentally the number of squates on the recorder chart corresponding to 1 T) be denoted γ_Q, then

$$k\gamma_Q = 1 \text{ T}$$

where k is the conversion factor, defined as

$$k = \frac{\overline{\Delta Hpp} \text{ (x-band)}}{\overline{\Delta Hpp} \text{ (Q-band)}} \cdot T\gamma_Q^{-1}$$

Whilst recognising that this is a large assumption, which will tend to place less credance on the data obtained at Q-band, it is reasonable because there is no frequency term in the theoretical formulae for linewidth, and hence it would be generally expected that no change would be

observed in going from X-band to Q-band.

The Q-band analogue of the X-band data is given in Table 8.4. It should be said at this point that no observable difference was recorded between the spectra obtained at room temperature and those at 77 K, so for this reason, only the room temperature results will be discussed.

The integration and moment evaluations were performed on a Texas SR56 programmable calculator, using the same algorithms as at X-band.

Table 8.4 shows the same trends as observed at X-band. The values for the coefficient of kurtosis and $\Delta Hpp/\Delta H$ give firm evidence for a line which is strongly tending towards a Lorentzian lineshape. Again the linewidth seems almost concentration independent, and certainly is narrower than predicted by dipolar theory.

The dependence of J" on concentration is shown in Figure 8.17. Again it can be seen to be linear, with correlation coefficient $r = 0.951$. The value of J" at $c = 0.66$ (i.e. pure Cr_2O_3) is 3.8×10^{12} Hz, in good agreement with the value obtained at X-band of 2.9×10^{12} Hz, and the literature value of $\sim 1.5 \times 10^{12}$ Hz, obtained by magnetic susceptibility measurements.

The data obtained at Q-band provides excellent support for the X-band results, and gives additional evidence for the strong exchange field experienced by the Cr^{3+} ion in magnesium oxide.

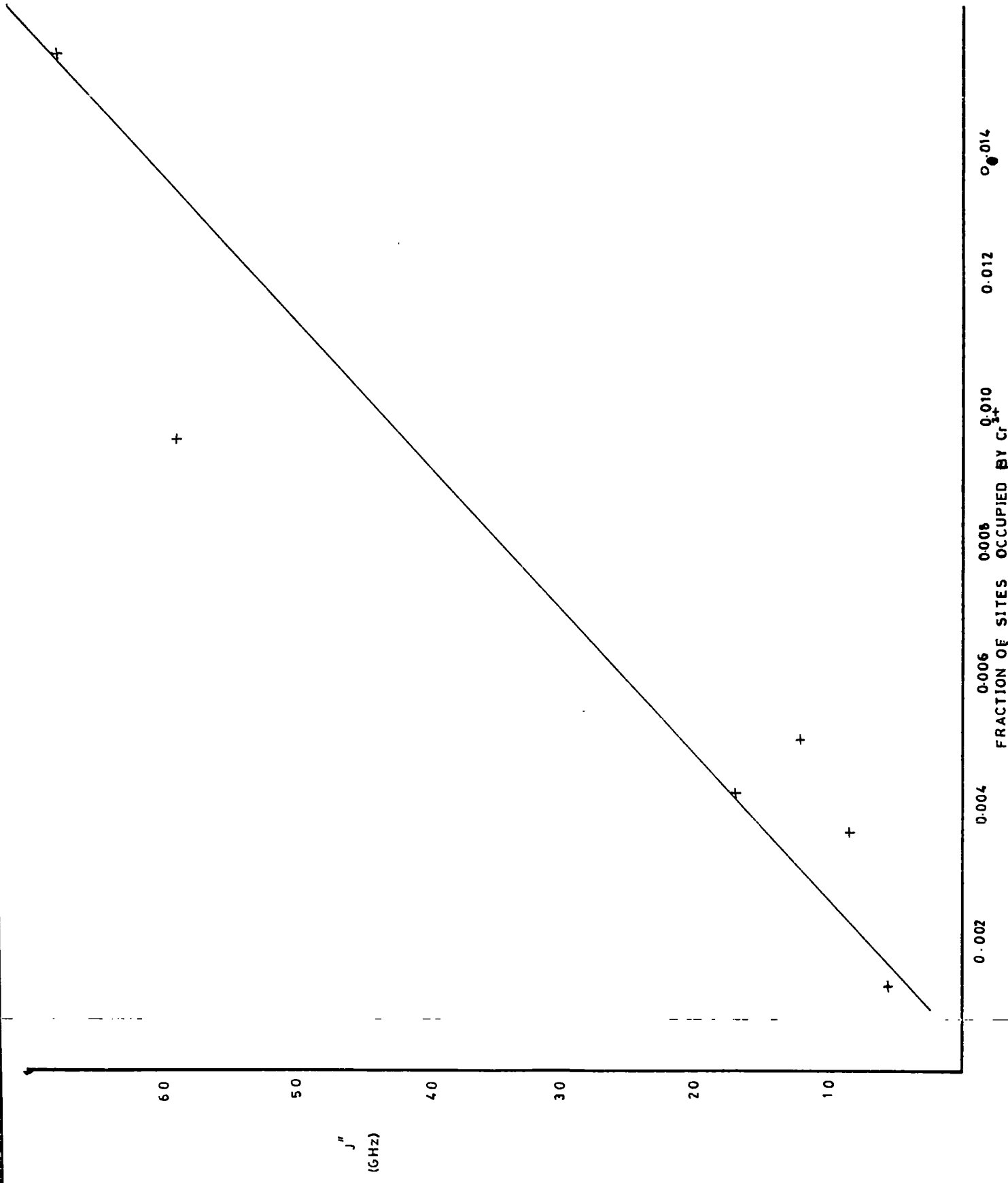

FIGURE 8·17 Plot of isotropic exchange energy versus concentration for Cr^{3+} in MgO. Data obtained at 298K and 35·5GHz

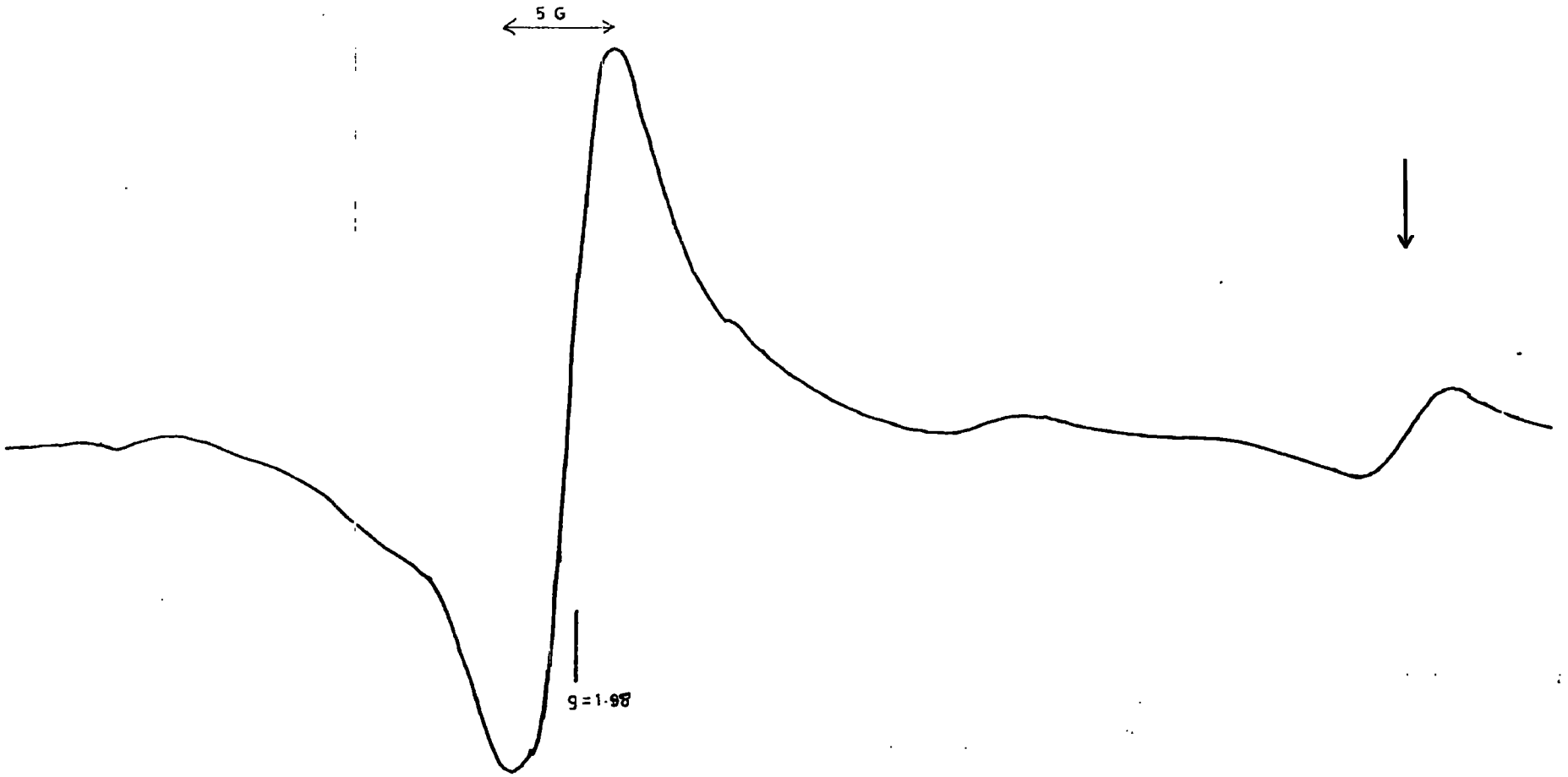

FIGURE 8.18 35.5GHz spectrum of MgO:Cr(3600ppm) 298K Note the line to low field (arrowed)

Sample Concentration	M_2 $(Hz)^2$	Hpp (calc) mT	ΔHpp^* (obs mT	ΔH^* (obs) mT	$\frac{\Delta Hpp}{\Delta H}$ (obs)	kurtosis	J" (Hz)
1300	1.17×10^{17}	24.61	0.39	0.76	0.51	3.88	5.56×10^{9}
3600	3.24×10^{17}	40.95	0.63	1.35	0.47	3.85	8.66×10^{9}
4200	3.78×10^{17}	44.23	0.43	0.79	0.54	3.48	1.73×10^{10}
5000	4.50×10^{17}	48.26	0.68	1.33	0.51	3.07	1.22×10^{10}
9500	8.55×10^{17}	66.52	0.28	0.52	0.54	4.01	5.93×10^{10}
15100	1.36×19^{18}	83.87	0.31	0.72	0.43	3.79	6.82×10^{10}

Table 8.4: Lineshape Data for $MgO:Cr^{3+}$, Q-Band.

(* See comment in text)

CHAPTER NINE

ELECTRON SPIN RESONANCE OF MgO:Co

The electron spin resonance spectrum of Co^{2+} in MgO was first observed by Low in 1958 (9.1). His main interest was the determination of the g-factor, and of the hyperfine interaction coefficient. This latter parameter has been measured to greater precision by the ENDOR experiments of Fry and Llewellyn (9.2).

The purpose of the present study has been to investigate the line-shape of the absorption signal in order to understand the nature of the exchange interactions, as was done for MgO: r. The cobalt spectrum in MgO is not observable at temperatures above about 65 K, and for this reason it was impossible to record the spectra at Q-band, and so the results to be discussed here are those obtained at X-band on the commercial Varian spectrometer, using the continuous flow cryostat described in Chapter 7.

9.1 PRELIMINARY COMMENTS

As discussed when dealing with the optical spectroscopy of the MgO:Co crystals, the effect of the crystal field is to split the free ionic ^4F state into two triplets and a singlet. These are, in order of increasing energy from the ground state, $^4T_1(F)$, $^4T_2(F)$ and $^4A_2(F)$. Since electron spin resonance experiments normally apply to transitions within the ground term manifold, it is the $^4T_1(F)$ term which is of interest here.

The $^4T_1(F)$ term is a triplet, and is also four-fold spin degenerate, giving a total degeneracy of twelve. As pointed out in Chapter 5, evidence from optical spectroscopy shows that the effects of spin-orbit coupling are by no means negligible in the MgO:Co system. This spin-orbit coupling causes the twelve-fold degeneracy of the ground term to be partially lifted. Consequently there remains, again in order of increasing energy, a doublet,

a quartet, and a sextet. This splitting of the energy levels by the spin-orbit interaction is shown in Figure 9.1, along with the energies of the states, in terms of λ , the spin orbit coupling constant. These energies have been evaluated following the method of Abragam and Pryce (9.3), and are calculated ignoring any admixture of the ^4P Stark state with the ground $^4T_1(F)$ term.

It can be seen that the next set of energy levels above the ground doublet is a quartet, and they are spaced by $^9/4\ \lambda$. If one takes $\lambda = -180\ cm^{-1}$, i.e. the value of the spin-orbit coupling constant of the free Co^{2+} ion (neglecting for the moment that the numerical value of this parameter is normally reduced by the nephelauxectic effect of liquids in a complex), it is found that the first excited level is about 400 cm^{-1} above the ground state. Since this corresponds to radiation of frequency $\sim 10^{13}$ Hz, which is three orders of magnitude greater than the microwave frequency used in the e.s.r. experiments performed here, it is only necessary to consider transitions in the ground doublet.

Since the only natural isotope of cobalt is ^{59}Co, which has a nuclear spin of $^7/2$, considerable hyperfine interaction is expected. This is illustrated in Figure 9.2, which shows the expected spectrum of MgO:Co as an octet, of separation A cm^{-1}.

9.2 EXPERIMENTAL RESULTS

The spectra of the MgO:Co crystals were taken at X-band and at various temperatures between 4.2 and 70 K. Even at high gain the crystals showed only lines due to Co^{2+}, and a weak line due to iron, which suggests that these crystals are of a higher degree of perfection than the corresponding MgO:Cr samples. This is possibly due to the fact that, since the Co^{2+} ion is doubly charged, direct substitution into the MgO lattice is

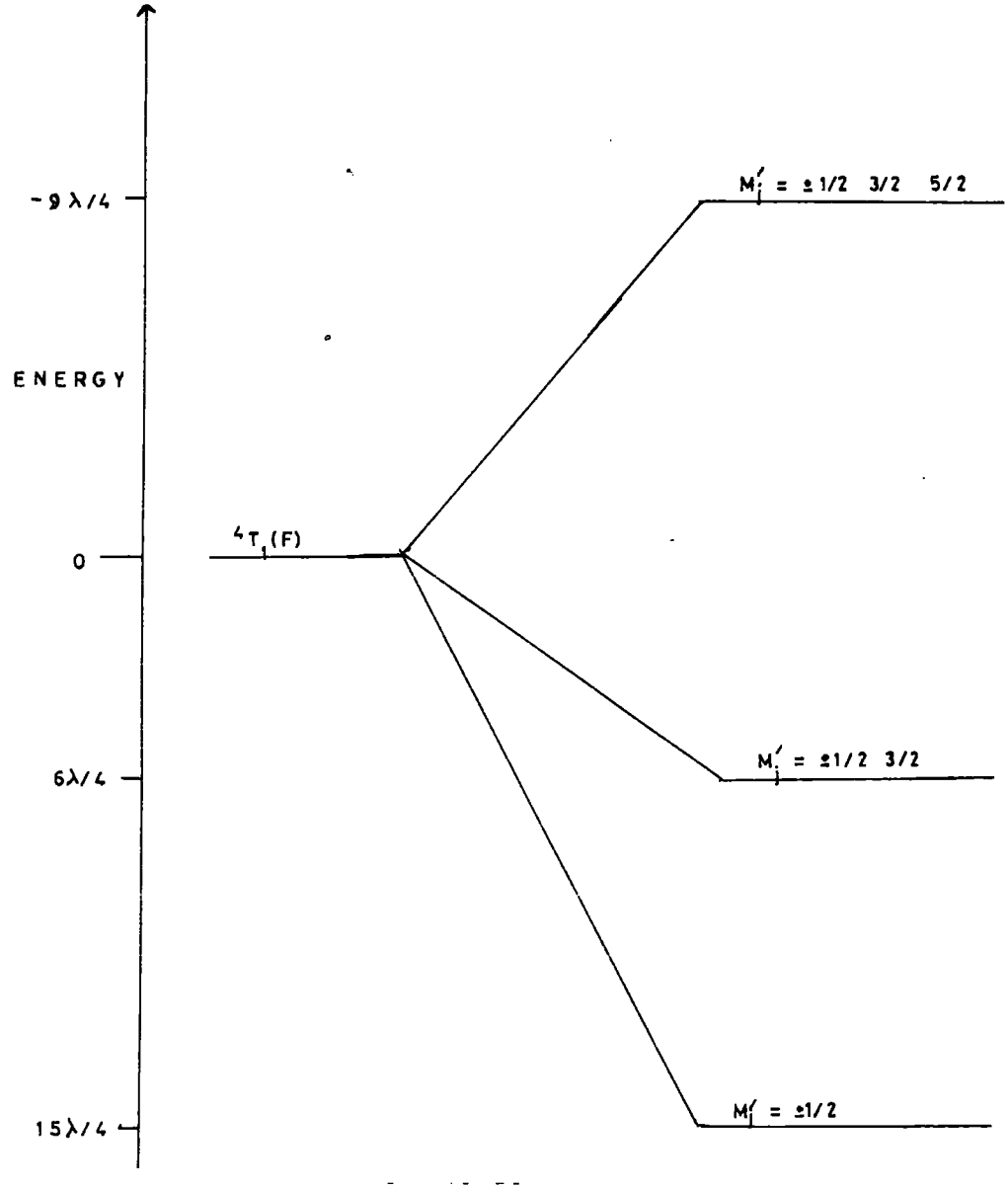

FIGURE 9.1 Fine structure splitting of the ground state Stark level of Co^{2+} under the combined action of an octahedral field and spin-orbit coupling

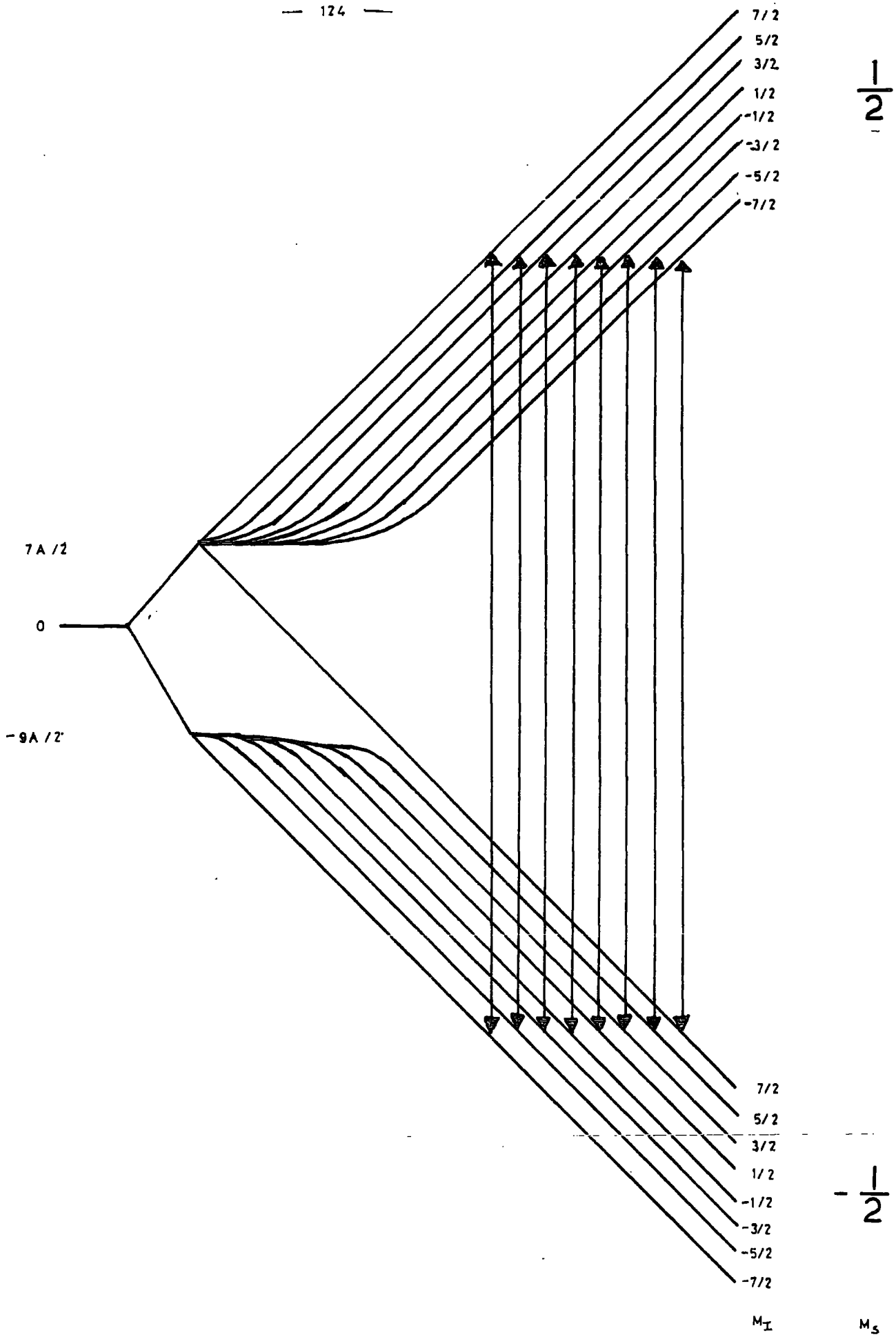

FIGURE 9.2 The electronic and nuclear Zeeman levels of Co^{2+} showing the eight transitions observed in e.s.r.

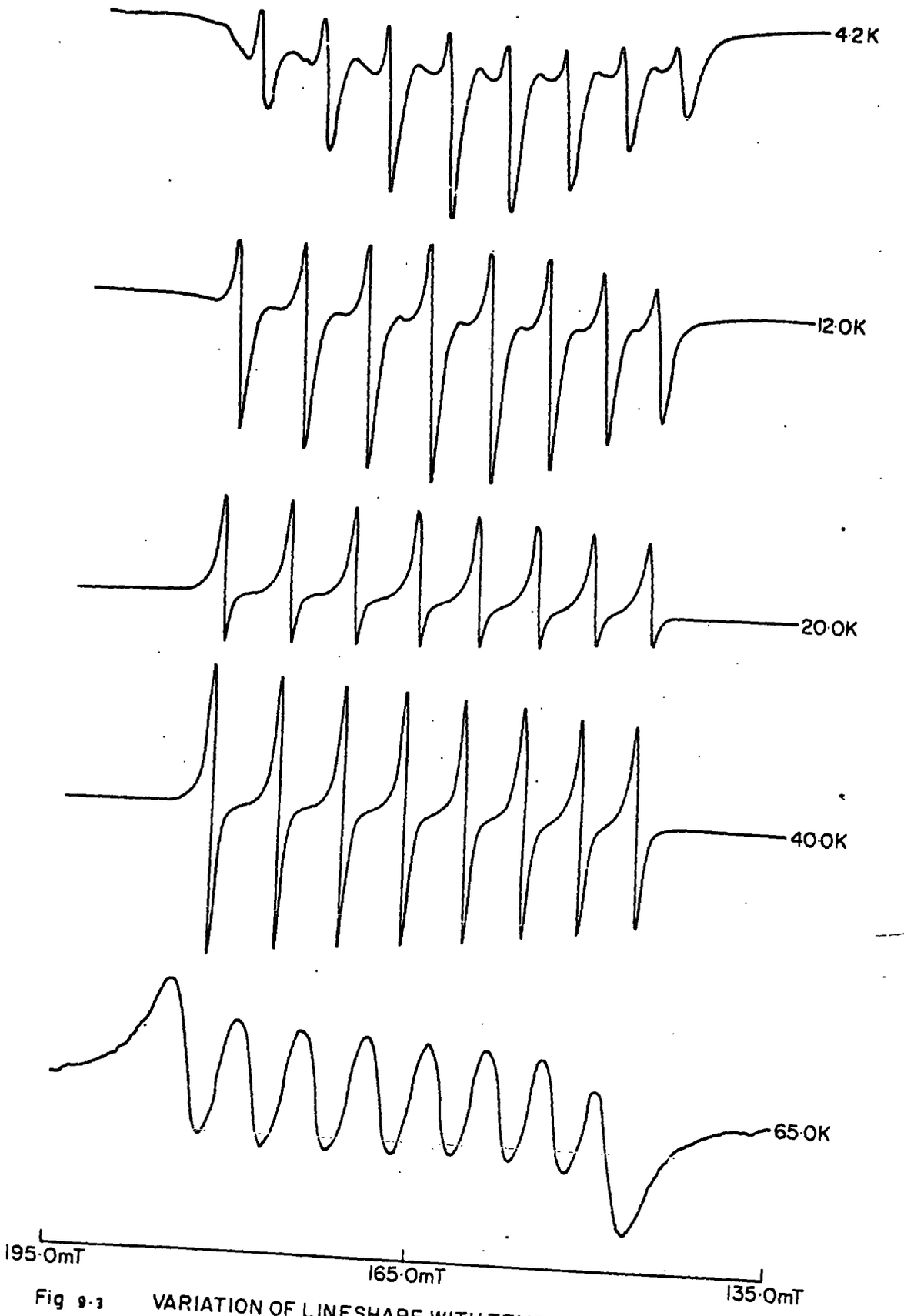

Fig 9·3 VARIATION OF LINESHAPE WITH TEMPERATURE
Mgo: Co (310ppm), 9·5155 GHz

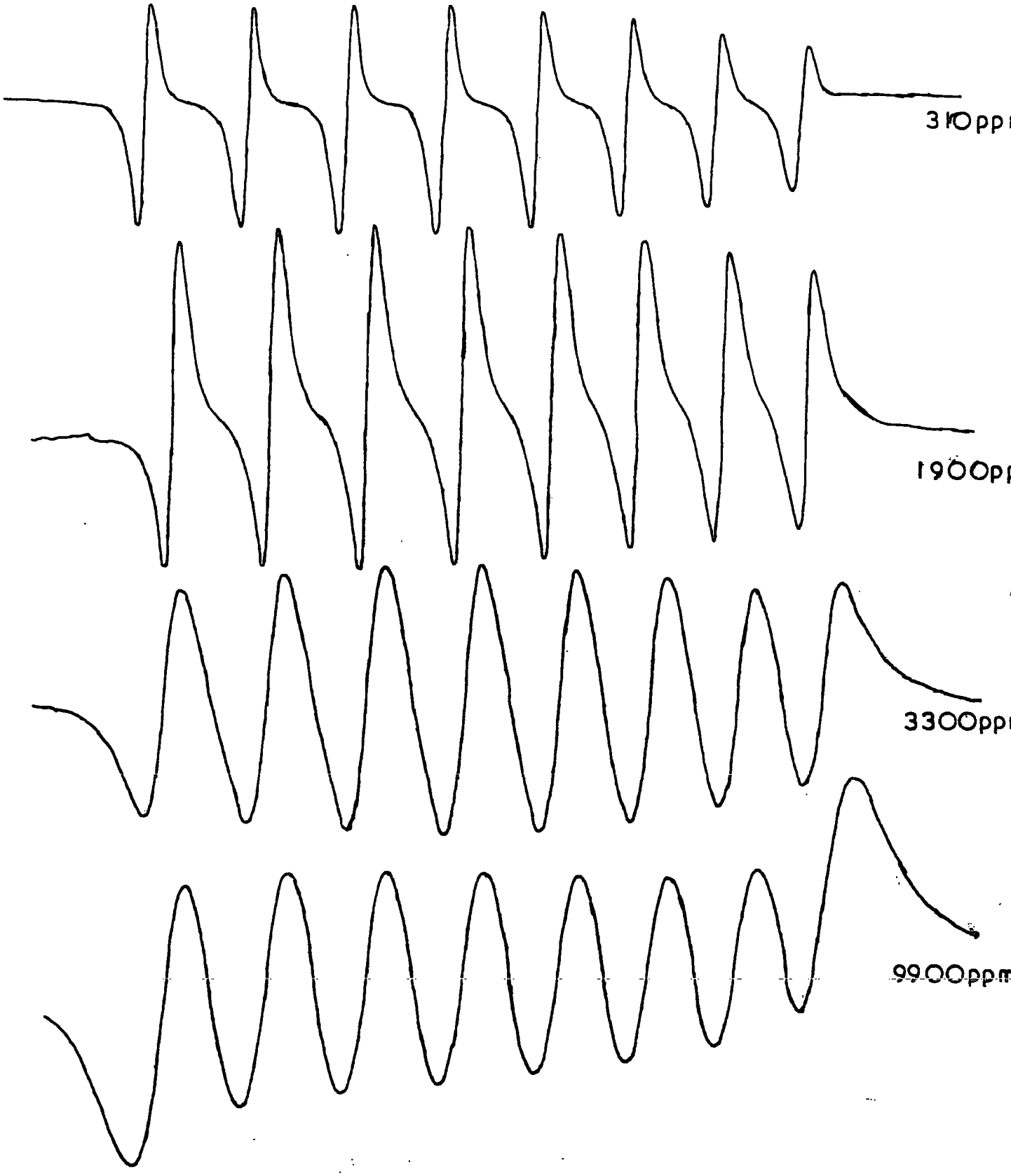

FIG 9.4 VARIATION OF LINESHAPE WITH CONCENTRATION
MgO:Co 20K 9.5155GHz

possible without the need for charge compensating vacancies. As before the spectra to be used for the lineshape analysis were recorded at low gain.

Immediately it was seen that the data recorded needed more complex analysis than obtained in the chromium doped case. By inspection the linewidth and lineshape of the Co^{2+} spectrum seem to be functions both of dopant concentration and temperature. To show this, the as recorded derivative spectra are shown as a function of temperature in Figure 9.3, and as a function of concentration in Figure 9.4. One other fact is also strikingly obvious from these spectra, viz:- the low concentration samples, at very low temperatures, give a severely distorted spectrum. Whether this 'distortion' is in fact a correct representation of an exceptionally asymmetric spectrum, or merely an infidelity in recording a normal spectrum, has not yet been fully ascertained. However, some evidence suggests the former possibility.

There are three common causes of instrumental distortion of lineshape. The first is modulation broadening. This, as previously mentioned, is caused by having too high a modulation field at the sample, which present a false electrical signal to the phase sensitive detector. As is implicit in its name, it causes the e.s.r. signal to be broadened. The second is power saturation. This arises from using too high an incident microwave power level, which causes the populations of the upper and lower states between which transitions are induced, to approach each other. The incident radiation is then able to stimulate almost as many emissive transitions as absorptive ones, with a corresponding reduction in the net power absorbed. The third common error leading to distortion is scanning the line too quickly, so that the rate of change of the quantity used to characterise the spectrum is faster than the time constant of the instrument. In other words the line is scanned so quickly, the spectrometer is

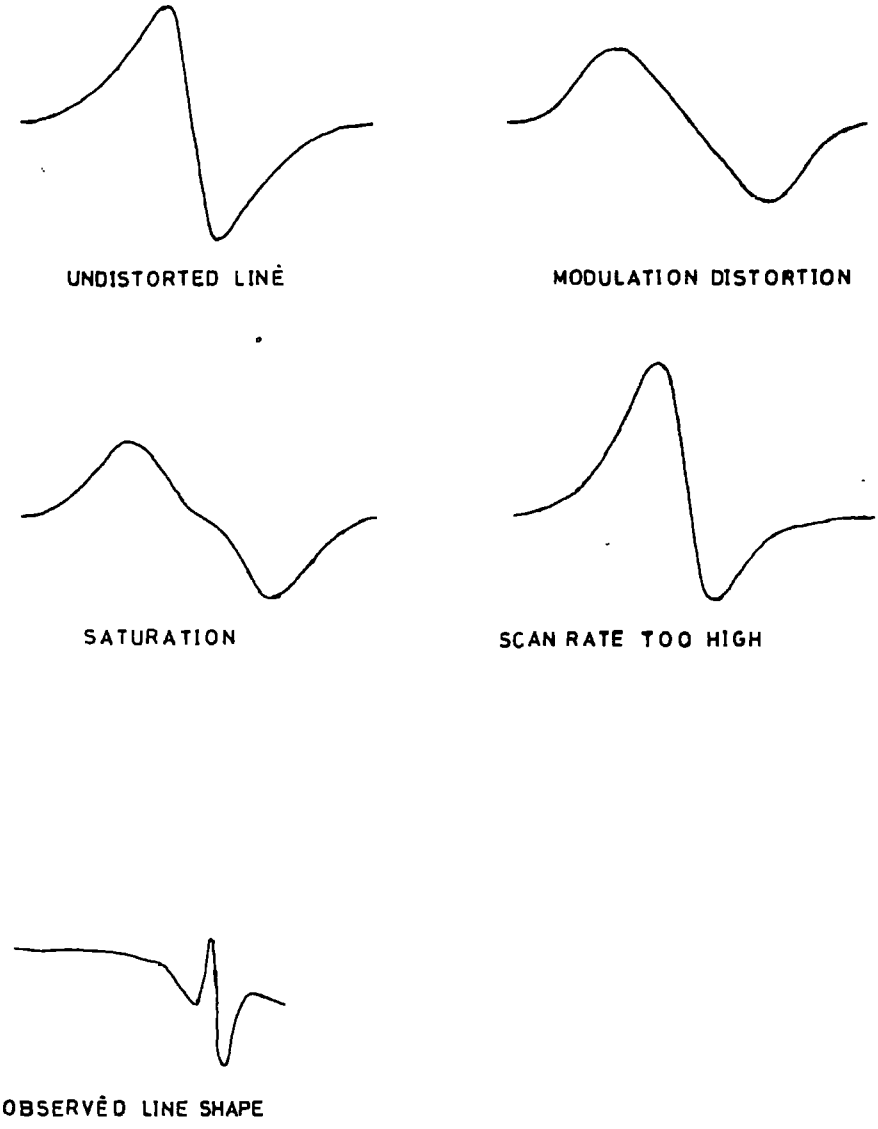

FIGURE 9.5 Comparison of common instrumental distortions with the observed lineshape for Co^{2+} in MgO (310ppm) at 4.2K and 9.5155 GHz

unable to respond fully to it. Of course every precaution was taken when recording our MgO:Co spectra to avoid the effects outlined above. These three types of distortion are shown in Figure 9.5, along with the spectra recorded. None of them satisfactorily accounts for the observations, and hence the most likely conclusion is that the tracings recorded are true representations of the absorption.

9.3 COMMENTS ON THE TEMPERATURE DEPENDENCE

The striking temperature dependence of the linewidth of the signal, particularly as the temperature approached 70 K, has already been noted. One particular crystal, containing 8200 ppm of cobalt, was studied in detail in this region, and its behaviour seems typical. This gave a spectrum which was intense at 60 K, but at temperatures above this the intensity decreased rapidly, as the linewidth increased. At 63 K it was only just possible to observe all eight components of the octet, but at 65 K these had become so broad that the spectrum appeared as a single, broad line, of very low intensity. At 67 K the spectrum was unobservable. The full temperature dependence of this crystal is shown graphically in Figure 9.6.

The marked decrease in intensity of the line and its associated increase in width can be ascribed to one of two causes. The first of these is that low lying energy states might begin to become populated at this temperature to a significant extent, which causes a reduction in intensity of the signal due to transitions between the ground Zeeman states. However a temperature of 65 K corresponds to thermal quanta of about 50 cm^{-1}, and since the lowest lying excited state is $\sim$ 400 cm^{-1} above the ground state, the Boltzman population law shows that at 65 K this state will be populated to a negligible extent. The other possible explanation is that there is a significant change in the relaxation

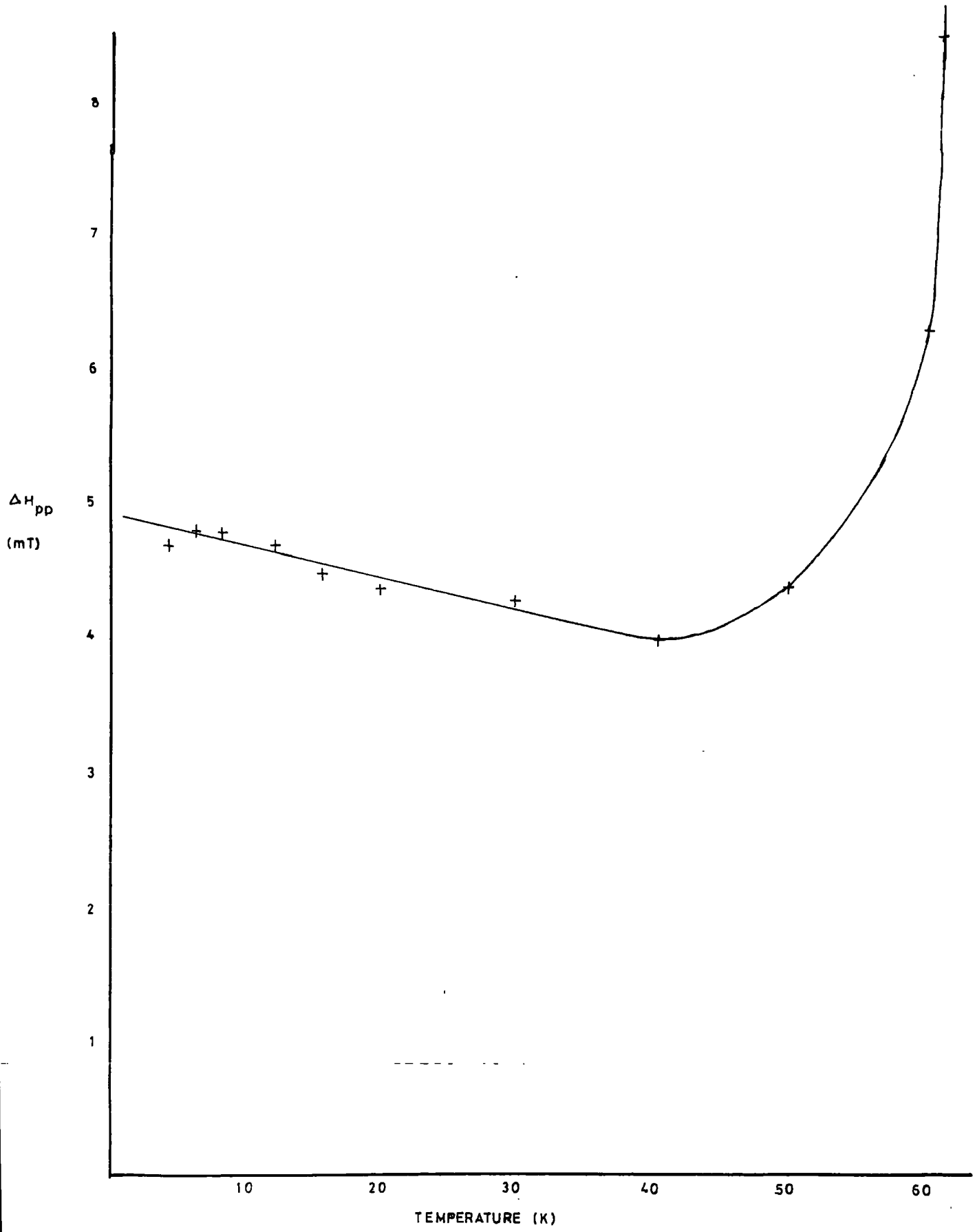

FIGURE 9.6 The temperature dependance of the linewidth for Co^{2+} in MgO. Data obtained at 9.5155GHz. Co concentration 8200ppm

behaviour in the temperature range under consideration. Paramagnetic relaxation can occur by three mechanisms:- spin-spin relaxation, in which an excited system decays to thermal equilibrium within the spin system itself; cross-relaxation, where the thermal equilibrium is attained between spins of different species, and spin-lattice relaxation, where energy is transferred to the lattice. Since this is a system in which the vast majority of spins are due to Co^{2+} a cross-relaxation mechanism may be neglected; further, the spin-spin relaxation time is almost independent of temperature, consequently the effect must be concerned with a change in spin-lattice relaxation behaviour.

Van Vleck (9.8) in 1940 fathered the quantitative formulation of the theory of spin-lattice relaxation, since when the theory has been extended by many others, notably Orbach (9.4). In the majority of cases the temperature dependence of the spin-lattice relaxation time may be written as:

$$1/T_1 = AT + BT^n + C\exp(-E/kT) \qquad (9.1)$$

where the various terms in temperature arise from the three main processes possible.

The first of these is the Direct process, by which the relaxing spin emits a phonon into one of the lattice modes of the appropriate frequency. This is linear in temperature. Secondly, there is the Raman process where the spin interacts directly with two phonons, whose frequency difference is the resonance frequency. The probability of this process varies with T^7 or T^9. The usual net result of these two effects is that the direct process dominates at about liquid helium temperatures and the Raman mechanism at higher temperatures.

The Orbach process accounts for the third term. This involves absorption of a phonon by a direct process to excite the spin system to

a much higher energy level. These spins then relax to the lower level by emitting a phonon of slightly higher frequency. This 'resonant two-phonon process' is only possible if there is another energy level at $E < k\theta_D$ where θ_D is the Debye temperature, so that phonons are available to cause this transition. If it is assumed that the Debye temperature of MgO:Co is close to that of pure MgO (θ_D = 946 K) the requirement is for a first excited state less than about 650 cm^{-1} above the ground level. Here, as already shown, the first excited 'spin-orbit' state is $\sim$400 cm^{-1} above the ground level, and so this Orbach process must be considered.

A method exists of measuring T_1, the spin-lattice relaxation time directly. This is the pulse saturation technique (9.5) and work using this method has been performed in this Department (9.6) on various materials, including iron-doped MgO (9.7). Unfortunately there were no facilities readily available for this work, although construction of a suitable spectrometer is planned for the near future, when it is hoped that the doped MgO crystals used in the present work will be further investigated.

At the moment therefore a different approach must be used which, although not as accurate as full T_1 measurements, will give some insight into the processes involved, and perhaps serve as a useful precursor to full relaxation time experiments. The dependence of the linewidth on spin-spin interactions has already been discussed and formulae derived relating the linewidth to various parameters. It is helpful to discuss an idea first introduced in Chapter 6. It was pointed out there that the relaxation time of the spins gives a 'residual linewidth' to any e.s.r. line, and that this width is given by

$$\Delta\nu = \frac{1}{2\pi\tau} \qquad (6.11)$$

Up to now it has been assumed that this is a small contribution to the total linewidth, and hence negligible when compared to the dipolar linewidth.

This has been justified up to now as the lines showed no obserable temperature dependence, and the 'spin-spin term' follows this behaviour, whereas the 'relaxation term' does not.

It is now postulated that for MgO:Co this is no longer the case, and that the equation for the linewidth of the e.s.r. line must be written as :

$$\Delta\nu = \Delta\nu_{SPIN-SPIN} + \Delta\nu_{RELAXATION} \qquad (9.2)$$

Hence in the analysis of the result a method of separating the two components must be found.

In order to justify the validity of this argument consider the linewidth dependence on relaxation time, equation (9.1) and assume that in the majority of temperature ranges one relaxation mechanism dominates. This is usually the case. In MgO:Fe for instance below about 20 K the direct process is dominant, while between 25 K and 50 K the Raman process is followed (9.8). Hence the temperature dependence of the relaxation time, T_1 for three cases can be written in the following way:-

(1) Direct case

$$\text{Log } T_1 = -\text{Log } T - \text{Log } A$$

(2) Raman case

$$\text{Log } T_1 = -n \text{ Log } T - \text{Log } B \qquad (9.3)$$

(3) Orbach case

$$\text{Log } T_1 = \frac{E}{kT} - \text{Log } C$$

Now from equation (6.11)

$$\Delta\nu_{RELAXATION} = \frac{1}{2\pi T_1}$$

Hence $T_1 = -\text{Log}\ \Delta\nu_{RELAXATION} - \text{Log}\ 2\pi$,

and since $h\nu = g\beta H$

$$\text{Log}\ T_1 = -\text{Log}\ \Delta H_{RELAXATION} + \text{Log}\ (^{h}/_{g\beta}),$$

and as $\alpha\Delta Hpp = \Delta H$, where α is a function of the lineshape (α = 0.577 for a Lorentzian, 0.846 for a Gaussian) :

$$\text{Log}\ T_1 = -\text{Log}(\Delta Hpp)_{RELAXATION} + \text{Log}\ (^{h}/_{\alpha g\beta}) \qquad (9.4)$$

Substitution of (9.4) into (9.3) gives

(1) Direct case

$$\text{Log}\ (\Delta Hpp)_{RELAXATION} = \text{Log}\ T + \text{Log}\ (^{Ah}/_{\alpha g\beta})$$

(2) Raman case (9.5)

$$\text{Log}\ (\Delta Hpp)_{RELAXATION} = n\,\text{Log}\ T + \text{Log}\ (^{Bh}/_{\alpha g\beta})$$

(2) Orbach case

$$\text{Log}\ (\Delta Hpp)_{RELAXATION} = {}^{-E}/_{kT} - \text{Log}\ (^{h}/_{\alpha g\beta})$$

The remaining problem is to separate $(\Delta Hpp)_{RELAXATION}$ from the total linewidth. Consideration shows that if the lowest value of ΔHpp, measured for each sample, is taken as the value for spin-spin interaction the best value for $(\Delta Hpp)_{RELAXATION}$ will be obtained. Plots of Log $(\Delta Hpp)_{RELAXATION}$ vs both $^{1}/_{T}$, and also Log T should then give an idea of which process is dominant in temperature range. This is shown in Table 9.1 for the 8200 p.p.m. crystal. Combined with Figure 9.7, which shows the plots, the evidence leads to the conclusion that at temperatures above 45 K the relaxation follows the law

$$\text{Log}\ (\Delta Hpp)_{RELAXATION} = \frac{-260}{T} + 1.8 \quad \text{Correlation coefficient } 0.9996)$$

This suggests that the dominant relaxation mechanism between 45 K and 65 K is the Orbach process. Further support for this can be seen by comparison

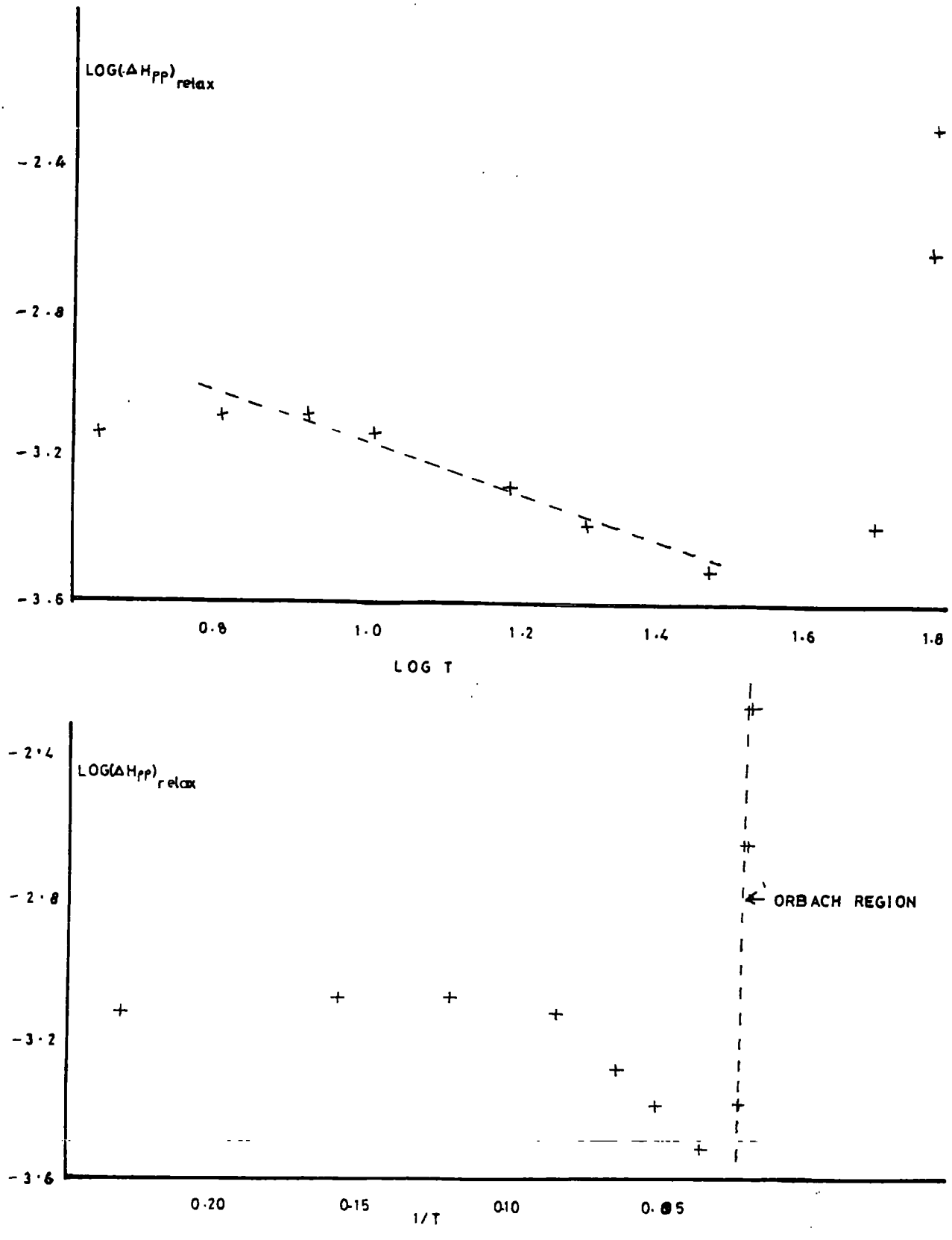

FIGURE 9.7 The temperature dependance of the relaxation of MgO:Co(8200ppm) 9.5155 GHz

T (K)	ΔHpp (mT)	$\Delta Hpp_{(Relax)}$ (mT)	Log T	$Log(\Delta Hpp)_{Relax}$	$^1/_T$ (k^{-1})
4.3	4.7	0.7	0.633	-3.155	0.233
6.3	4.8	0.8	0.799	-3.097	0.159
8.3	4.8	0.8	0.919	-3.097	0.120
12.1	4.7	0.7	1.083	-3.155	0.083
15.8	4.5	0.5	1.198	-3.301	0.063
20.0	4.4	0.4	1.301	-3.398	0.050
30.0	4.3	0.3	1.477	-3.523	0.033
40.3	4.0	-	1.605	-	0.025
50.0	4.4	0.4	1.699	-3.398	0.020
60.0	6.3	2.3	1.778	-2.638	0.017
62.0	8.5	4.5	1.792	-2.347	0.016

Table 9.1: The temperature dependence of ΔHpp for MgO:Co (8200 p.p.m.)

with equation (9.5). One obtains

$$E/k = 260\ K^{-1} ,$$

giving a value for E, the energy above the ground state of the first excited states, of about 200 cm^{-1}. This is in excellent agreement with the calculated value of $\sim 400\ cm^{-1}$ (especially since this calculated value has already been conceded to be slightly high).

At temperatures betweek 5 and 40 K the relaxation seems to follow the law

$$Log(\Delta Hpp)_{RELAXATION} = -0.65\ Log\ T - 2.52 \quad \text{(Correlation coefficient = 0.96)}$$

This suggests that $T_1 \propto T^{-0.65}$, a surprising result as yet unexplained, but the slight various of ΔHpp with T in this range suggests that the Direct process is dominant.

Although this discussion of experimental results has largely been concerned with one crystal, the 8200 p.p.m. specimen, preliminary investigations have shown that a very similar behaviour is observed for all the samples.

9.4 SPIN-SPIN INTERACTIONS IN MgO:Cr

The linewidth of the cobalt signal from the MgO:Co system is a function both of temperature and concentration and for this reason the analysis of the spin-spin interactions is more difficult than the MgO:Cr case, where the measured linewidth could be related to the exchange energy.

In order to gain information about the exchange interaction in MgO:Co it is necessary to place greater credance on the lineshape analysis, in particular the coefficient of kurtosis and regard, at least for the moment, the linewidth data as being somewhat less reliable. Consequently the data has been obtained by considering that in all cases an undistorted line may be obtained by integrating the leading (or trailing) half of the

first (or last) line of the octet. This gives one side of the absorption line, when integrated; it is also assumed that the line is symmetrical about the mid-point. The moments can then be evaluated, and used to characterize the absorption line.

The integrations and moment analysis was once more performed on a Texas SR 56 programmable calculator, the results from this agreeing perfectly with one trial calculation performed on the University's computer

The results in Table 9.2 show that the line due to Co^{2+} in MgO is narrower at all temperatures and concentrations than that predicted by a pure dipolar theory; the lineshape parameters indicate a substantial trend towards a Lorentzian lineshape, the value of the kurtosis being consistently greater than 3 at all temperatures.

One other broad trend noticable is that the value of the coefficient of kurtosis can be linked to the observed linewidth. In general a narrower line gives rise to a greater kurtosis, amongst data for a particular concentration. This data suggests that cobalt, like iron and chromium, in MgO has a line which is exchange narrowed, following the same reasoning used in Chapter 8. This appears to be the case at all temperatures between 4.2 K and 65 K, even though that at the high end of this temperature range, there is a marked temperature dependence on the lineshape which it was feared might mask any exchange effect.

Finally an attempt can be made to evaluate the parameter J" for Co^{2+} in MgO. To do this a value for ΔH must be chosen. The reasoning of the previous section has shown that there are two components to the observed linewidth, one due to spin-spin interaction, and one to a relaxation effect. There the minimum measured value of ΔHpp was used as being equal to that component due to spin-spin interactions, and that is the approach adopted here. This is not totally accurate, but it should yield estimates accurate to about 20%. The results are given in Table 9.3,

Sample Concentration	Temperature (K)	M_2 $(Hz)^2$	ΔHpp(calc) (MT)	ΔHpp(obs) (MT)	ΔH(obs) (MT)	$\frac{\Delta Hpp}{\Delta H}$(obs)	Kurtosis
310	4.2	6.09×10^{17}	26.00	2.0	3.5	0.57	4.41
310	8.0	6.09×10^{17}	26.00	1.8	3.4	0.53	4.90
310	12.0	6.09×10^{17}	26.00	1.2	2.1	0.58	5.10
310	16.0	6.09×10^{17}	26.00	1.0	1.8	0.55	4.16
310	20.0	6.09×10^{17}	26.00	0.8	1.4	0.57	3.83
310	40.0	6.09×10^{17}	26.00	1.5	2.9	0.52	3.43
310	60.0	6.09×10^{17}	26.00	2.4	3.9	0.6	3.80
310	65.0	6.09×10^{17}	26.00	4.6	7.1	0.65	3.98
1250	4.2	2.46×10^{18}	52.16	2.9	5.0	0.58	3.41
1250	20.0	2.46×10^{18}	52.16	2.1	3.8	0.55	3.99
1900	4.2	3.73×10^{18}	64.31	1.5	2.6	0.58	4.41
1900	8.0	3.73×10^{18}	64.31	1.6	2.9	0.56	4.56
1900	20.0	3.73×10^{18}	64.31	1.0	1.7	0.60	4.53
1900	35.0	3.73×10^{18}	64.31	0.8	1.5	0.53	3.94
1900	60.2	3.73×10^{18}	64.31	3.7	6.9	0.54	3.38
1900	65.0	3.73×10^{18}	64.31	6.0	11.0	0.55	3.27
2500	4.2	4.91×10^{18}	73.76	2.9	6.0	0.48	3.48
2500	20.0	4.91×10^{18}	73.76	2.1	3.3	0.64	3.96
3300	4.2	6.49×10^{18}	84.75	2.7	5.7	0.47	3.76
3300	20.0	6.49×10^{18}	84.75	2.0	3.9	0.51	3.75
3300	40.0	6.49×10^{18}	84.75	1.6	3.1	0.52	4.61
8200	4.3	1.61×10^{19}	133.59	4.7	6.8	0.69	3.52
8200	6.3	1.61×10^{19}	133.59	4.8	6.7	0.71	3.41
8200	8.3	1.61×10^{19}	133.59	4.8	7.1	0.68	4.09
8200	12.1	1.61×10^{19}	133.59	4.7	7.0	0.67	3.71
8200	15.8	1.61×10^{19}	133.59	4.5	6.7	0.67	3.49
8200	20.0	1.61×10^{19}	133.59	4.4	6.8	0.65	4.22
8200	30.0	1.61×10^{19}	133.59	4.3	6.2	0.69	4.46
8200	40.3	1.61×10^{19}	133.59	4.0	6.1	0.66	4.74
8200	50.0	1.61×10^{19}	133.59	4.4	7.6	0.58	4.53
8200	60.0	1.61×10^{19}	133.59	6.3	10.2	0.62	4.06
8200	62.0	1.61×10^{19}	133.59	8.5	12.5	0.68	3.38
9900	4.2	1.95×10^{19}	146.79	4.9	7.8	0.63	3.33
9900	20.0	1.95×10^{19}	146.79	4.0	6.5	0.62	3.54
9900	40.0	1.95×10^{19}	146.79	3.5	6.0	0.59	3.56
9900	60.0	1.95×10^{19}	146.79	4.9	7.3	0.67	3.79
9900	65.0	1.95×10^{19}	146.79	10.5	15.3	0.69	3.38

Table 9.[illegible]: X-band lineshape data for [illegible] at various temperatures.

Concentration (ppm)	J" (Hz)
310	7.26×10^{9}
1250	1.08×10^{70}
1900	4.15×10^{10}
2500	2.48×10^{10}
3300	3.50×10^{10}
8200	4.41×10^{10}
9900	5.43×10^{10}

Table 9.3: Exchange energy for Co^{2+} in MgO at various concentrations.

A plot of J" vs c is given in Figure 9.8; with the exception of the 1900 p.p.m. crystal the data fits a straight line of gradient 4.53×10^{12} Hz. On the basis of this evidence it may be concluded that Co^{2+} in MgO (like Cr^{3+}), is subject to a strong internal exchange field, which is linearly dependent on the concentration of Co^{2+}.

9.5 COMPARISON OF VARIOUS IONS IN THE MgO LATTICE

Having obtained results for Co^{2+} and Cr^{3+} in the MgO lattice, it is instructive to compare the results obtained for these two ions, at the same time reconsidering some results obtained for Fe^{3+} in MgO a few years ago in this Department. The work on MgO:Fe performed then showed that the iron spectrum was indeed exchanged narrowed. Unfortunately

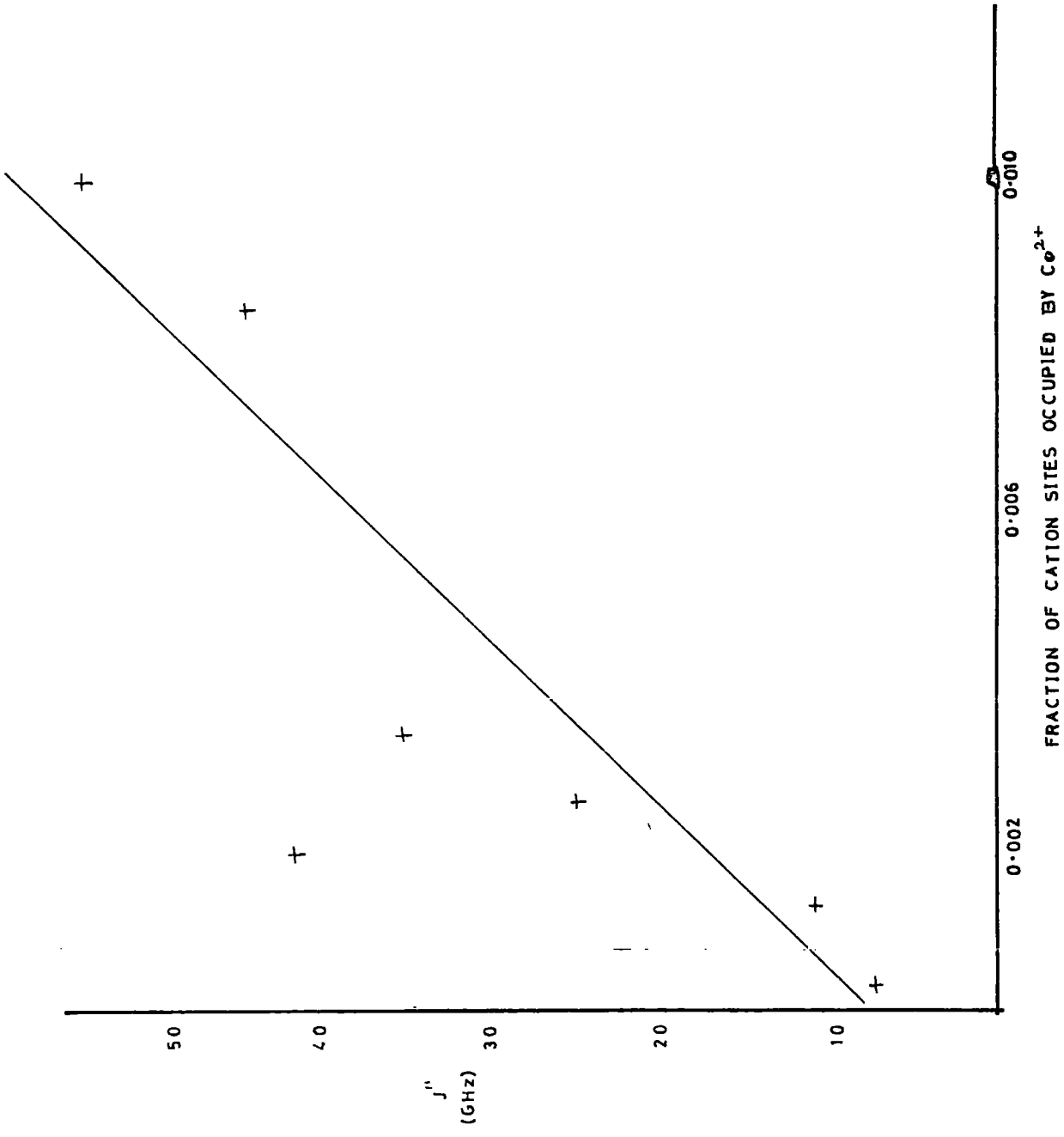

FIGURE 9.8 Plot of isotropic exchange energy versus concentration for Co^{2+} in MgO. 9.5155GHz

the original spectra were unavailable, but values of Hpp(obs) and the kurtosis for each line were at hand. It has been assumed that the ratio $\frac{\Delta Hpp}{\Delta H}$ is the same for Fe^{3+} as the mean value for Cr^{3+}; (this is not unreasonable at this parameter is a function of lineshape, and the values for kurtosis suggest that the lines due to these ions are almost identical in shape). Bearing this in mind, values of J" can be derived as shown in Table 9.4.

A plot of J" versus concentration, and this is shown in Figure 9.9. The best way of comparing ions is in terms of the gradient of such plots and this gives

Ion	$J''/_c$ (Hz)
Fe^{2+}	1.14×10^{13}
Cr^{3+}	4.45×10^{12}
Co^{2+}	4.53×10^{12}

This shows that the exchange forces are strongest for Fe^{3+}, with Cr^{3+} and Co^{2+} approximately equal, but weaker. There has also recently been the opportunity to investigate briefly a crystal of $MgO:Mn^{2+}$ (courtesy of the Clarendon Laboratory), of unknown concentration. It is interesting to note that examination of one of the most prominent peaks gave a coefficient of kurtosis of 3.68, suggesting that it too may be exchange narrowed.

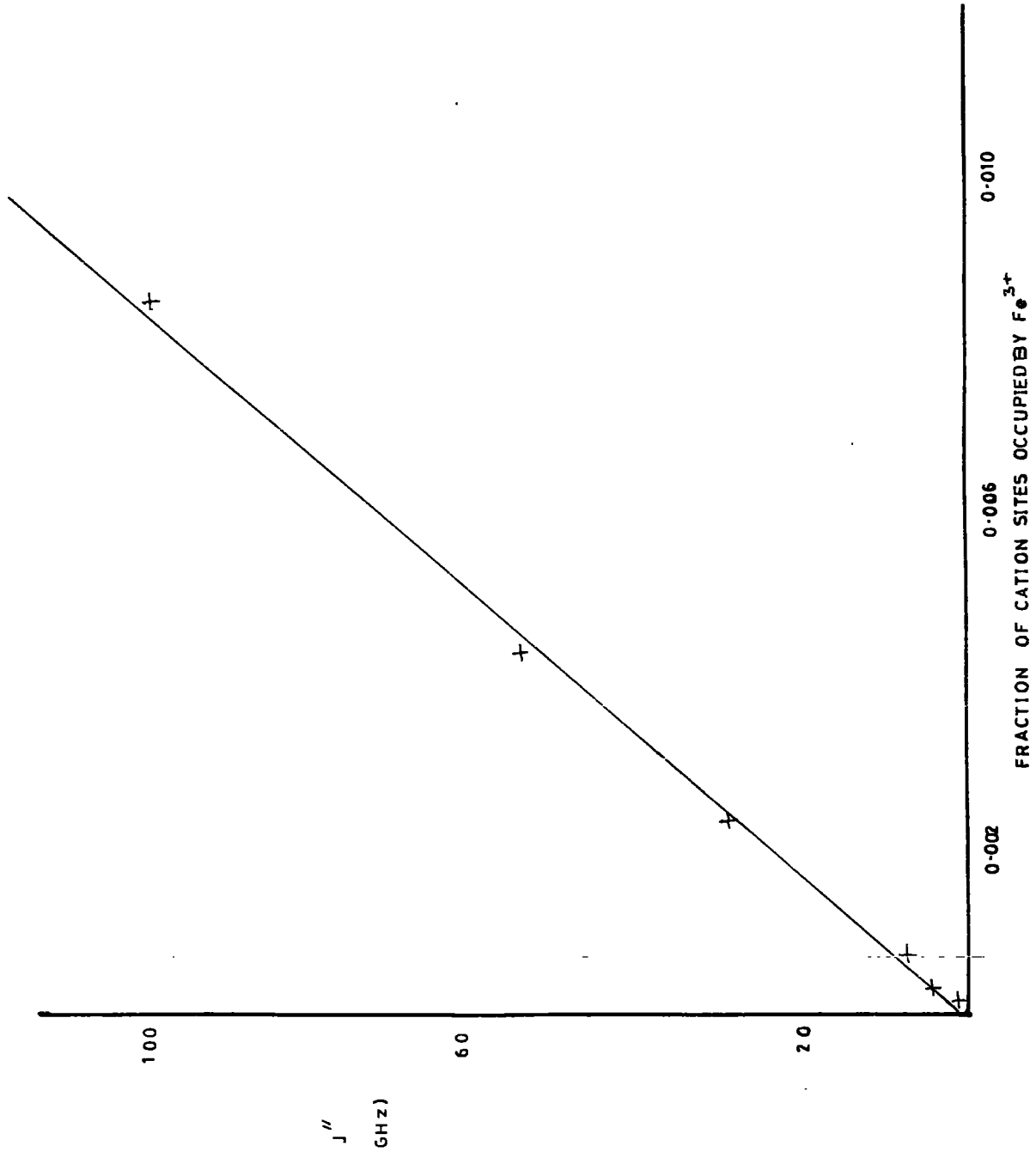

FIGURE 9.9 Plot of isotropic exchange energy versus concentration for Fe^{3+} in MgO. 298K 9.10GHz

Sample Concentration	M_2(calc) $(Hz)^2$	Hpp(calc) (mT)	Hpp(obs) (mT)	H(obs) * (mT)	Kurtosis	J" (Hz)
140	6.77×10^{16}	12.56	0.85	1.59	3.22	1.51×10^{9}
310	1.50×10^{17}	18.69	0.64	1.19	3.42	4.47×10^{9}
710	3.45×10^{17}	28.28	0.86	1.61	3.13	7.56×10^{9}
2300	1.11×10^{18}	50.91	0.74	1.38	4.80	2.86×10^{10}
4300	2.08×10^{18}	69.61	0.75	1.40	4.07	5.27×10^{10}
8500	4.11×10^{18}	97.86	1.51	2.81	3.32	9.65×10^{10}

Table 9.4: Room temperature x-band lineshape data for MgO:Fe.

*See Text

APPENDIX ONE

Table 1: Taking 64 unit cells of MgO the Magnesium sites are indexed thus, with their radius from the central ion in units of a_o and the value of n_{ij}.

a	b	c	r	n_{ij}	a	b	c	r	n_{ij}
2	2	2	3.4641	0.5774	-2	2	-1	3.0000	-0.3333
-2	2	2	3.4641	0.5774	2	-2	-1	3.0000	-0.3333
2	-2	2	3.4641	0.5774	-2	-2	-1	3.0000	-0.3333
-2	-2	2	3.4641	0.5774	1	2	-2	3.0000	-0.6667
2	2	-2	3.4641	-0.5774	-1	2	-2	3.0000	-0.6667
-2	2	-2	3.4641	-0.5774	2	1	-2	3.0000	-0.6667
2	-2	-2	3.4641	-0.5774	-2	1	-2	3.0000	-0.6667
-2	-2	-2	3.4641	-0.5774	2	-1	-2	3.0000	-0.6667
					-2	-1	-2	3.0000	-0.6667
1	2	2	3.0000	0.6667	1	-2	-2	3.0000	-0.6667
-1	2	2	3.0000	0.6667	-1	-2	-2	3.0000	-0.6667
2	1	2	3.0000	0.6667					
-2	1	2	3.0000	0.6667	$\frac{3}{2}$	$\frac{3}{2}$	2	2.9155	0.6860
2	-1	2	3.0000	0.6667	$-\frac{3}{2}$	$\frac{3}{2}$	2	2.9155	0.6860
-2	-1	2	3.0000	0.6667	$\frac{3}{2}$	$-\frac{3}{2}$	2	2.9155	0.6860
1	-2	2	3.0000	0.6667	$-\frac{3}{2}$	$-\frac{3}{2}$	2	2.9155	0.6860
-1	-2	2	3.0000	0.6667	$\frac{3}{2}$	2	$\frac{3}{2}$	2.9155	0.5145
-2	2	1	3.0000	0.3333	$-\frac{3}{2}$	2	$\frac{3}{2}$	2.9155	0.5145
-2	2	1	3.0000	0.3333	2	$\frac{3}{2}$	$\frac{3}{2}$	2.9155	0.5145
2	-2	1	3.0000	0.3333	-2	$\frac{3}{2}$	$\frac{3}{2}$	2.9155	0.5145
-2	-2	1	3.0000	0.3333	2	$-\frac{3}{2}$	$\frac{3}{2}$	2.9155	0.5145
2	2	-1	3.0000	-0.3333	-2	$-\frac{3}{2}$	$\frac{3}{2}$	2.9155	0.5145

a	b	c	r	n_{ij}	a	b	c	r	n_{ij}
$\frac{3}{2}$	-2	$\frac{3}{2}$	2.9155	0.5145	$\frac{1}{2}$	$\frac{3}{2}$	2	2.5495	0.7845
$-\frac{3}{2}$	-2	$\frac{3}{2}$	2.9155	0.5145	$-\frac{1}{2}$	$\frac{3}{2}$	2	2.5495	0.7845
$\frac{3}{2}$	2	$-\frac{3}{2}$	2.9155	-0.5145	$\frac{3}{2}$	$\frac{1}{2}$	2	2.5495	0.7845
$-\frac{3}{2}$	2	$-\frac{3}{2}$	2.9155	-0.5145	$-\frac{3}{2}$	$\frac{1}{2}$	2	2.5495	0.7845
2	$\frac{3}{2}$	$-\frac{3}{2}$	2.9155	-0.5145	$\frac{3}{2}$	$-\frac{1}{2}$	2	2.5495	0.7845
-2	$\frac{3}{2}$	$-\frac{3}{2}$	2.9155	-0.5145	$-\frac{3}{2}$	$-\frac{1}{2}$	2	2.5495	0.7845
2	$-\frac{3}{2}$	$-\frac{3}{2}$	2.9155	-0.5145	$\frac{1}{2}$	$-\frac{3}{2}$	2	2.5495	0.7845
-2	$-\frac{3}{2}$	$-\frac{3}{2}$	2.9155	-0.5145	$-\frac{1}{2}$	$-\frac{3}{2}$	2	2.5495	0.7845
$\frac{3}{2}$	-2	$-\frac{3}{2}$	2.9155	-0.5145	$\frac{1}{2}$	2	$\frac{3}{2}$	2.5495	0.5883
$-\frac{3}{2}$	-2	$-\frac{3}{2}$	2.9155	-0.5145	$-\frac{1}{2}$	2	$\frac{3}{2}$	2.5495	0.5883
$\frac{3}{2}$	$\frac{3}{2}$	-2	2.9155	-0.6860	2	$\frac{1}{2}$	$\frac{3}{2}$	2.5495	0.5883
$-\frac{3}{2}$	$\frac{3}{2}$	-2	2.9155	-0.6860	-2	$\frac{1}{2}$	$\frac{3}{2}$	2.5495	0.5883
$\frac{3}{2}$	$-\frac{3}{2}$	-2	2.9155	-0.6860	2	$-\frac{1}{2}$	$\frac{3}{2}$	2.5495	0.5883
$-\frac{3}{2}$	$-\frac{3}{2}$	-2	2.9155	-0.6860	-2	$-\frac{1}{2}$	$\frac{3}{2}$	2.5495	0.5883
					$\frac{1}{2}$	-2	$\frac{3}{2}$	2.5495	0.5883
0	2	2	2.8284	0.7071	$-\frac{1}{2}$	-2	$\frac{3}{2}$	2.5495	0.5883
2	0	2	2.8284	0.7071	$\frac{3}{2}$	2	$\frac{1}{2}$	2.5495	0.1961
-2	0	2	2.8284	0.7071	$-\frac{3}{2}$	2	$\frac{1}{2}$	2.5495	0.1961
0	-2	2	2.8284	0.7071	2	$\frac{3}{2}$	$\frac{1}{2}$	2.5495	0.1961
2	2	0	2.8284	0.0000	-2	$\frac{3}{2}$	$\frac{1}{2}$	2.5495	0.1961
-2	2	0	2.8284	0.0000	2	$-\frac{3}{2}$	$\frac{1}{2}$	2.5495	0.1961
2	-2	0	2.8284	0.0000	-2	$-\frac{3}{2}$	$\frac{1}{2}$	2.5495	0.1961
-2	-2	0	2.8284	0.0000	$\frac{3}{2}$	-2	$\frac{1}{2}$	2.5495	0.1961
0	2	-2	2.8284	-0.7071	$-\frac{3}{2}$	-2	$\frac{1}{2}$	2.5495	0.1961
2	0	-2	2.8284	-0.7071	$\frac{3}{2}$	2	$-\frac{1}{2}$	2.5495	-0.1961
-2	0	-2	2.8284	-0.7071	$-\frac{3}{2}$	2	$-\frac{1}{2}$	2.5495	-0.1961
0	-2	-2	2.8284	-0.7071	2	$\frac{3}{2}$	$-\frac{1}{2}$	1.5495	-0.1961

a	b	c	r	n_{ij}	a	b	c	r	n_{ij}
-2	$\frac{3}{2}$	$-\frac{1}{2}$	2.5495	-0.1961	-1	2	1	2.4495	0.4082
2	$-\frac{3}{2}$	$-\frac{1}{2}$	2.5495	-0.1961	2	1	1	2.4495	0.4082
-2	$-\frac{3}{2}$	$-\frac{1}{2}$	2.5495	-0.1961	-2	1	1	2.4495	0.4082
$\frac{3}{2}$	-2	$-\frac{1}{2}$	2.5495	-0.1961	2	-1	1	2.4495	0.4082
$-\frac{3}{2}$	-2	$-\frac{1}{2}$	2.5495	-0.1961	-2	-1	1	2.4495	0.4082
$\frac{1}{2}$	2	$-\frac{3}{2}$	2.5495	-0.5883	1	-2	1	2.4495	0.4082
$-\frac{1}{2}$	2	$-\frac{3}{2}$	2.5495	-0.5883	-1	-2	1	2.4495	0.4082
2	$\frac{1}{2}$	$-\frac{3}{2}$	2.5495	-0.5883	1	2	-1	2.4495	-0.4082
-2	$\frac{1}{2}$	$-\frac{3}{2}$	2.5495	-0.5883	-1	2	-1	2.4495	-0.4082
2	$-\frac{1}{2}$	$-\frac{3}{2}$	2.5495	-0.5883	2	1	-1	2.4495	-0.4082
-2	$-\frac{1}{2}$	$-\frac{3}{2}$	2.5495	-0.5883	-2	1	-1	2.4495	-0.4082
$\frac{1}{2}$	-2	$-\frac{3}{2}$	2.5495	-0.5883	2	-1	-1	2.4495	-0.4082
$-\frac{1}{2}$	-2	$-\frac{3}{2}$	2.5495	-0.5883	-2	-1	-1	2.4495	-0.4082
$\frac{1}{2}$	$\frac{3}{2}$	-2	2.5495	-0.7845	1	-2	-1	2.4495	-0.4082
$-\frac{1}{2}$	$\frac{3}{2}$	-2	2.5495	-0.7845	-1	-2	-1	2.4495	-0.4082
$\frac{3}{2}$	$\frac{1}{2}$	-2	2.5495	-0.7845	1	1	-2	2.4495	-0.8165
$-\frac{3}{2}$	$\frac{1}{2}$	-2	2.5495	-0.7845	-1	1	-2	2.4495	-0.8165
$\frac{3}{2}$	$-\frac{1}{2}$	-2	2.5495	-0.7845	1	-1	-2	2.4495	-0.8165
$-\frac{3}{2}$	$-\frac{1}{2}$	-2	2.5495	-0.7845	-1	-1	-2	2.4495	-0.8165
$\frac{1}{2}$	$-\frac{3}{2}$	-2	2.5495	-0.7845					
$-\frac{1}{2}$	$-\frac{3}{2}$	-2	2.5495	-0.7845	1	$\frac{3}{2}$	$\frac{3}{2}$	2.3452	0.6396
					-1	$\frac{3}{2}$	$\frac{3}{2}$	2.3452	0.6396
1	1	2	2.4495	0.8165	$\frac{3}{2}$	1	$\frac{3}{2}$	2.3452	0.6396
-1	1	2	2.4495	0.8165	$-\frac{3}{2}$	1	$\frac{3}{2}$	2.3452	0.6396
1	-1	2	2.4495	0.8165	$\frac{3}{2}$	-1	$\frac{3}{2}$	2.3452	0.6396
-1	-1	2	2.4495	0.8165	$-\frac{3}{2}$	-1	$\frac{3}{2}$	2.3452	0.6396
-1	-1	2	2.4495	0.8165	$-\frac{3}{2}$	-1	$\frac{3}{2}$	2.3452	0.6396
1	2	1	2.4495	0.4082	1	$-\frac{3}{2}$	$\frac{3}{2}$	2.3452	0.6396

a	b	c	r	n_{ij}	a	b	c	r	n_{ij}
-1	$-\frac{3}{2}$	$\frac{3}{2}$	2.3452	0.6396	-1	2	0	2.2361	0.0000
$\frac{3}{2}$	$\frac{3}{2}$	1	2.3452	0.4264	2	1	0	2.2361	0.0000
$-\frac{3}{2}$	$\frac{3}{2}$	1	2.3452	0.4264	-2	1	0	2.2361	0.0000
$\frac{3}{2}$	$-\frac{3}{2}$	1	2.3452	0.4264	2	-1	0	2.2361	0.0000
$-\frac{3}{2}$	$-\frac{3}{2}$	1	2.3452	0.4264	-2	-1	0	2.2361	0.0000
$\frac{3}{2}$	$\frac{3}{2}$	-1	2.3452	-0.4264	1	-2	0	2.2361	0.0000
$-\frac{3}{2}$	$\frac{3}{2}$	-1	2.3452	-0.4264	-1	-2	0	2.2361	0.0000
$\frac{3}{2}$	$-\frac{3}{2}$	-1	2.3452	-0.4264	0	2	-1	2.2361	-0.4472
$-\frac{3}{2}$	$-\frac{3}{2}$	-1	2.3452	-0.4264	2	0	-1	2.2361	-0.4472
1	$\frac{3}{2}$	$-\frac{3}{2}$	2.3452	-0.6396	-2	0	-1	2.2361	-0.4472
-1	$\frac{3}{2}$	$-\frac{3}{2}$	2.3452	-0.6396	0	-2	-1	2.2361	-0.4472
$\frac{3}{2}$	1	$-\frac{3}{2}$	2.3452	-0.6396	0	1	-2	2.2361	-0.8944
$-\frac{3}{2}$	1	$-\frac{3}{2}$	2.3452	-0.6396	1	0	-2	2.2361	-0.8944
$\frac{3}{2}$	-1	$-\frac{3}{2}$	2.3452	-0.6396	-1	0	-2	2.2361	-0.8944
$-\frac{3}{2}$	-1	$-\frac{3}{2}$	2.3452	-0.6396	0	-1	-2	2.2361	-0.8944
1	$-\frac{3}{2}$	$-\frac{3}{2}$	2.3452	-0.6396					
-1	$-\frac{3}{2}$	$-\frac{3}{2}$	2.3452	-0.6396	$\frac{1}{2}$	$\frac{1}{2}$	2	2.1213	0.9428
					$-\frac{1}{2}$	$\frac{1}{2}$	2	2.1213	0.9428
0	1	22	2.2361	0.8944	$\frac{1}{2}$	$-\frac{1}{2}$	2	2.1213	0.9428
1	0	2	2.2361	0.8944	$-\frac{1}{2}$	$-\frac{1}{2}$	2	2.1213	0.9428
-1	0	2	2.2361	0.8944	0	$\frac{3}{2}$	$\frac{3}{2}$	2.1213	0.7071
0	-1	2	2.2361	00.8944	$\frac{3}{2}$	0	$\frac{3}{2}$	2.1213	0.7071
0	2	1	2.2361	0.4472	$-\frac{3}{2}$	0	$\frac{3}{2}$	2.1213	0.7071
2	0	1	2.2361	0.4472	0	$-\frac{3}{2}$	$\frac{3}{2}$	2.1213	0.7071
-2	0	1	2.2361	0.4472	$\frac{1}{2}$	2	$\frac{1}{2}$	2.1213	0.2357
0	-2	1	2.2361	0.4472	$-\frac{1}{2}$	2	1	2.1213	0.2357
1	2	0	2.2361	0.0000	2	$\frac{1}{2}$	$\frac{1}{2}$	2.1213	0.2357

a	b	c	r	n_{ij}
-2	$\frac{1}{2}$	$\frac{1}{2}$	2.1213	0.2357
2	$-\frac{1}{2}$	$\frac{1}{2}$	2.1213	0.2357
-2	$-\frac{1}{2}$	$\frac{1}{2}$	2.1213	0.2357
$\frac{1}{2}$	-2	$\frac{1}{2}$	2.1213	00.2357
$-\frac{1}{2}$	-2	$\frac{1}{2}$	2.1213	0.2357
$\frac{3}{2}$	$\frac{3}{2}$	0	2.1213	0.0000
$-\frac{3}{2}$	$\frac{3}{2}$	0	2.1213	0.0000
$\frac{3}{2}$	$-\frac{3}{2}$	0	2.1213	0.0000
$-\frac{3}{2}$	$-\frac{3}{2}$	0	2.1213	0.0000
$\frac{1}{2}$	2	$-\frac{1}{2}$	2.1213	-0.2357
$-\frac{1}{2}$	2	$-\frac{1}{2}$	2.1213	-0.2357
2	$\frac{1}{2}$	$-\frac{1}{2}$	2.1213	-0.2357
-2	$\frac{1}{2}$	$-\frac{1}{2}$	2.1213	-0.2357
2	$-\frac{1}{2}$	$-\frac{1}{2}$	2.1213	-0.2357
-2	$-\frac{1}{2}$	$-\frac{1}{2}$	1.1213	-0.2357
$\frac{1}{2}$	-2	$-\frac{1}{2}$	2.1213	-0.2357
$-\frac{1}{2}$	-2	$-\frac{1}{2}$	2.1213	-0.2357
0	$\frac{3}{2}$	$-\frac{3}{2}$	2.1213	-0.7071
$\frac{3}{2}$	0	$-\frac{3}{2}$	2.1213	-0.7071
$-\frac{3}{2}$	0	$-\frac{3}{2}$	2.1213	-0.7071
0	$-\frac{3}{2}$	$-\frac{3}{2}$	2.1213	-0.7071
$\frac{1}{2}$	$\frac{1}{2}$	-2	2.1213	-0.9428
$-\frac{1}{2}$	$\frac{1}{2}$	-2	2.1213	-0.9428
$\frac{1}{2}$	$-\frac{1}{2}$	-2	2.1213	-0.9428
$-\frac{1}{2}$	$-\frac{1}{2}$	-2	2.1213	-0.9428
0	0	2	2.0000	1.0000
0	2	0	2.0000	0.0000
2	0	0	2.0000	0.0000
-2	0	0	2.0000	0.0000
0	-2	0	2.0000	0.0000
0	0	-2	2.0000	-1.0000
$\frac{1}{2}$	1	$\frac{3}{2}$	1.8708	0.8018
$-\frac{1}{2}$	1	$\frac{3}{2}$	1.8708	0.8018
1	$\frac{1}{2}$	1	1.8708	0.8018
-1	$\frac{1}{2}$	$\frac{3}{2}$	1.8708	0.8018
1	$-\frac{1}{2}$	$\frac{3}{2}$	1.8708	0.8018
-1	$-\frac{1}{2}$	$\frac{3}{2}$	1.8708	0.8018
$\frac{1}{2}$	-1	$\frac{3}{2}$	1.8708	0.8018
$-\frac{1}{2}$	-1	$\frac{3}{2}$	1.8708	0.8018
$\frac{1}{2}$	$\frac{3}{2}$	1	1.8708	0.5345
$-\frac{1}{2}$	$\frac{3}{2}$	1	1.8708	0.5345
$\frac{3}{2}$	$\frac{1}{2}$	1	1.8708	0.5345
$-\frac{3}{2}$	$\frac{1}{2}$	1	1.8708	0.5345
$\frac{3}{2}$	$-\frac{1}{2}$	1	1.8708	0.5345
$-\frac{3}{2}$	$-\frac{1}{2}$	1	1.8708	0.5345
$\frac{1}{2}$	$-\frac{3}{2}$	1	1.8708	0.5345
$-\frac{1}{2}$	$-\frac{3}{2}$	1	1.8708	0.5345
1	$\frac{3}{2}$	$\frac{1}{2}$	1.8708	0.2673
-1	$\frac{3}{2}$	$\frac{1}{2}$	1.8708	0.2673
$\frac{3}{2}$	1	$\frac{1}{2}$	1.8708	0.2673
$-\frac{3}{2}$	1	$\frac{1}{2}$	1.8708	0.2673
$\frac{3}{2}$	-1	$\frac{1}{2}$	1.8708	0.2673

a	b	c	r	n_{ij}	a	b	c	r	n_{ij}
$-\frac{3}{2}$	-1	$\frac{1}{2}$	1.8708	0.2673	1	1	1	1.7321	0.5774
1	$-\frac{3}{2}$	$\frac{1}{2}$	1.8708	0.2673	-1	1	1	1.7321	0.5774
-1	$-\frac{3}{2}$	$\frac{1}{2}$	1.8708	0.2673	1	-1	1	1.7321	0.5774
1	$\frac{3}{2}$	$-\frac{1}{2}$	1.8708	-0.2673	-1	-1	1	1.7321	0.5774
-1	$\frac{3}{2}$	$-\frac{1}{2}$	1.8708	-0.2673	1	1	-1	1.7321	-0.5774
$\frac{3}{2}$	1	$-\frac{1}{2}$	1.8708	-0.2673	-1	1	-1	1.7321	-0.5774
$-\frac{3}{2}$	1	$-\frac{1}{2}$	1.8708	-0.2673	1	-1	-1	1.7321	-0.5774
$\frac{3}{2}$	-1	$-\frac{1}{2}$	1.8708	-0.2673	-1	-1	-1	1.7321	-0.5774
$-\frac{3}{2}$	-1	$-\frac{1}{2}$	1.8708	-0.2673					
1	$-\frac{3}{2}$	$-\frac{1}{2}$	1.8708	-0.2673	0	$\frac{1}{2}$	$\frac{3}{2}$	1.5811	0.9487
-1	$-\frac{3}{2}$	$-\frac{1}{2}$	1.8708	-0.2673	$\frac{1}{2}$	0	$\frac{3}{2}$	1.5811	0.9487
$\frac{1}{2}$	$\frac{3}{2}$	-1	1.8708	-0.5345	$-\frac{1}{2}$	0	$\frac{3}{2}$	1.5811	0.9487
$-\frac{1}{2}$	$\frac{3}{2}$	-1	1.8708	-0.5345	0	$-\frac{1}{2}$	$\frac{3}{2}$	1.5811	0.9487
$\frac{3}{2}$	$\frac{1}{2}$	-1	1.8708	-0.5345	0	$\frac{3}{2}$	$\frac{1}{2}$	1.5811	0.3162
$-\frac{3}{2}$	$\frac{1}{2}$	-1	1.8708	-0.5345	$\frac{3}{2}$	0	$\frac{1}{2}$	1.5811	0.3162
$\frac{3}{2}$	$-\frac{1}{2}$	-1	1.8708	-0.5345	$-\frac{3}{2}$	0	$\frac{1}{2}$	1.5811	0.3162
$-\frac{3}{2}$	$-\frac{1}{2}$	-1	1.8708	-0.5345	0	$-\frac{3}{2}$	$\frac{1}{2}$	1.5811	0.3162
$\frac{1}{2}$	$-\frac{3}{2}$	-1	1.8708	-0.4345	$\frac{1}{2}$	$\frac{3}{2}$	0	1.5811	0.0000
$-\frac{1}{2}$	$-\frac{3}{2}$	-1	1.8708	-0.5345	$-\frac{1}{2}$	$\frac{3}{2}$	0	1.5811	0.0000
$\frac{1}{2}$	1	$-\frac{3}{2}$	1.8708	-0.8018	$\frac{3}{2}$	$\frac{1}{2}$	0	1.5811	0.0000
$-\frac{1}{2}$	1	$-\frac{3}{2}$	1.8708	-0.8018	$-\frac{3}{2}$	$\frac{1}{2}$	0	1.5811	0.0000
1	$\frac{1}{2}$	$-\frac{3}{2}$	1.8708	-0.8018	$\frac{3}{2}$	$-\frac{1}{2}$	0	1.5811	0.0000
-1	$\frac{1}{2}$	$-\frac{3}{2}$	1.8708	-0.8018	$-\frac{3}{2}$	$-\frac{1}{2}$	0	1.5811	0.0000
1	$-\frac{1}{2}$	$-\frac{3}{2}$	1.8708	-0.8018	$\frac{1}{2}$	$-\frac{3}{2}$	0	1.5811	0.0000
-1	$-\frac{1}{2}$	$-\frac{3}{2}$	1.8708	-0.8018	$-\frac{1}{2}$	$-\frac{3}{2}$	0	1.5811	0.0000
$\frac{1}{2}$	-1	$-\frac{3}{2}$	1.8708	-0.8018	0	$\frac{3}{2}$	$-\frac{1}{2}$	1.5811	-0.3162
$-\frac{1}{2}$	-1	$-\frac{3}{2}$	1.8708	-0.8018	$\frac{3}{2}$	0	$-\frac{1}{2}$	1.5811	-0.3162

a	b	c	r	n_{ij}
$-\frac{3}{2}$	0	$-\frac{1}{2}$	1.5811	-0.3162
0	$-\frac{3}{2}$	$-\frac{1}{2}$	1.5811	-0.3162
0	$\frac{1}{2}$	$-\frac{3}{2}$	1.5811	-0.9487
$\frac{1}{2}$	0	$-\frac{3}{2}$	1.5811	-0.9487
$-\frac{1}{2}$	0	$-\frac{3}{2}$	1.5811	-0.9487
0	$-\frac{1}{2}$	$-\frac{2}{2}$	1.5811	-0.9847
0	1	1	1.4142	0.7071
1	0	1	1.4142	0.7071
-1	0	1	1.4142	0.7071
0	-1	1	1.4142	0.7071
1	1	0	1.4142	0.0000
-1	1	0	1.4142	0.0000
1	-1	0	1.4142	0.0000
-1	-1	0	1.4142	0.0000
0	1	-1	1.4142	-0.7071
1	0	-1	1.4142	-0.7071
-1	0	-1	1.4142	-0.7071
0	-1	-1	1.4142	-0.7071
$\frac{1}{2}$	$\frac{1}{2}$	1	1.2247	0.8165
$-\frac{1}{2}$	$\frac{1}{2}$	1	1.2247	0.8165
$\frac{1}{2}$	$-\frac{1}{2}$	1	1.2247	0.8165
$-\frac{1}{2}$	$-\frac{1}{2}$	1	1.2247	0.8165
$\frac{1}{2}$	1	$\frac{1}{2}$	1.2247	0.4082
$-\frac{1}{2}$	1	$\frac{1}{2}$	1.2247	0.4082
1	$\frac{1}{2}$	$\frac{1}{2}$	1.2247	0.4082

a	b	c	r	n_{ij}
-1	$\frac{1}{2}$	$\frac{1}{2}$	1.2247	0.4082
1	$-\frac{1}{2}$	$\frac{1}{2}$	1.2247	0.4082
-1	$-\frac{1}{2}$	$\frac{1}{2}$	1.2247	0.4082
$\frac{1}{2}$	-1	$\frac{1}{2}$	1.2247	0.4082
$-\frac{1}{2}$	-1	$\frac{1}{2}$	1.2247	0.4082
$\frac{1}{2}$	$\frac{1}{2}$	-1	1.2247	-0.8165
$-\frac{1}{2}$	$\frac{1}{2}$	-1	1.2247	-0.8169
$\frac{1}{2}$	$-\frac{1}{2}$	-1	1.2247	-0.8165
$-\frac{1}{2}$	$-\frac{1}{2}$	-1	1.2247	-0.8165
$\frac{1}{2}$	1	$-\frac{1}{2}$	1.2247	-0.4028
$-\frac{1}{2}$	1	$-\frac{1}{2}$	1.2247	-0.4028
1	$\frac{1}{2}$	$-\frac{1}{2}$	1.2247	-0.4082
-1	$\frac{1}{2}$	$-\frac{1}{2}$	1.2247	-0.4082
1	$-\frac{1}{2}$	$-\frac{1}{2}$	1.2247	-0.4082
-1	$-\frac{1}{2}$	$-\frac{1}{2}$	1.2247	-0.4082
$\frac{1}{2}$	-1	$-\frac{1}{2}$	1.2247	-0.4082
$-\frac{1}{2}$	-1	$-\frac{1}{2}$	1.2247	-0.4082
0	0	1	1.0000	1.0000
0	1	0	1.0000	0.0000
1	0	0	1.0000	0.0000
-1	0	0	1.0000	0.0000
0	-1	0	1.0000	0.0000
0	0	-1	1.0000	-1.0000
0	$\frac{1}{2}$	$\frac{1}{2}$	0.7071	0.7071
$\frac{1}{2}$	0	$\frac{1}{2}$	0.7071	0.7071
$-\frac{1}{2}$	0	$\frac{1}{2}$	0.7071	0.7071

a	b	c	r	n_{ij}
$-\frac{1}{2}$	0	$\frac{1}{2}$	0.7071	0.7071
0	$-\frac{1}{2}$	$\frac{1}{2}$	0.7071	0.7071
$\frac{1}{2}$	$\frac{1}{2}$	0	0.7071	0.0000
$-\frac{1}{2}$	$\frac{1}{2}$	0	0.7071	0.0000
$\frac{1}{2}$	$-\frac{1}{2}$	0	0.7071	0.0000
$-\frac{1}{2}$	$-\frac{1}{2}$	0	0.7071	0.0000
0	$\frac{1}{2}$	$-\frac{1}{2}$	0.7071	-0.7071
$\frac{1}{2}$	0	$-\frac{1}{2}$	0.7071	-0.7071
$-\frac{1}{2}$	0	$-\frac{1}{2}$	0.7071	-0.7071
0	$-\frac{1}{2}$	$-\frac{1}{2}$	0.7071	-0.7071

APPENDIX TWO

The matrix elements of d^3 in an octahedral field are given

^2H	^2G	^2F	^2D	^2D
$9B+3C-0.335\Delta$	-0.1605Δ	-0.1055Δ	0.730Δ	-0.512Δ
	$4B+6C+0.1680\Delta$	0.2525Δ	-0.2935Δ	0.384Δ
		$24B+3C-0.0335\Delta$	0.5775Δ	0.253Δ
			$20B+5C-X-0.20\Delta$	0.218Δ
$^2T_{2g}$	$X=(193B^2-8BC+4C^2)^{\frac{1}{2}}$			$20B+5C+X\ 0.18\Delta$

---

^2H	^2H	^2G	^2F	^2P
$9B\ 3C\ 0.261\Delta$	$9B+3C$	0.617Δ	0.175Δ	0.0588Δ
	$9B+3C-0.261\Delta$	0.445Δ	-0.064Δ	0.4980Δ
		$4B+6C-0.100\Delta$	-0.173Δ	-0.2780Δ
			$4B+3C+0.100\Delta$	-0.5880Δ
$^2T_{1g}$				$9B+3C$

---

^2H	^2G	^2D	^2D
$9B+3C+0.200\Delta$	0.964Δ	0.548Δ	-0.1195Δ
	$4B+6C-0.029\Delta$	0.586Δ	-0.7660Δ
		$20B+5C-X+0.30\Delta$	-0.3270Δ
^2E_g	$X=(193B^2-8B+4C^2)^{\frac{1}{2}}$		$20B+5C+X-0.272\Delta$

---

^4F	^4P
0.6Δ	0.4Δ
$^4T_{2g}$	$15B$

$^2A_{2g}(^2F)$	$24B+3C-0.2\Delta$
$^2A_1(^2G)$	$4B+6C-0.2\Delta$
$^4T_{2g}(^4F)$	-0.2Δ
$^4A_{2g}(^4F)$	-1.2Δ

The matrices are symmetric and so only the top part is given

APPENDIX THREE

The computer programmes used in the lineshape analysis are given below. They were formulated with the help of Paul Waite and Brendon Shaw, and the programming language used is PL-1.

1. SHAPAN

This programme integrates a function by Simpson's rule, and then evaluates the first four moments of the integrated data about an arbitrary point, in this case zero. It then evaluates the first four moments of the integrated data about the mean, along with the coefficients of kurtosis and skewness. The algorithms are given below.

$$I_4 = \frac{h}{3}\{y_o + 4y_1 + 2y_2 + 4y_3 + y_4\}.$$

$$I_{2m} = I_{2m-2} + \frac{h}{3}\{y_{2m-2} + 4y_{2m-1} + y_{2m}\}.$$

$$3 \leqslant M \leqslant \frac{nn}{2}$$

Arithmetic mean $$\bar{x} = \left(\sum_{i=1}^{nn} x_i f_i\right) / \left(\sum_{i=1}^{nm} f_i\right)$$

Moments about zero

$$M_1' = \bar{x}$$

$$M_j' = \left(\sum_{i=1}^{nn} f_i x_i^j\right) / \left(\sum_{i=1}^{nn} f_i\right) \left[j \neq 1\right].$$

Moments about mean

$$M_1 = 0$$

$$M_2 = M_2' - (M_1')^2$$

$$M_3 = M_3' - 3M_1'M_2' + 2(M_1')^3$$

$$M_4 = M_4' - 4M_1'M_3' + 6(M_1')^2M_2' - 3(M_1')^4.$$

kurtosis $= M_4/M_2^2$; skewness $= M_3/M_2^{\frac{3}{2}}$

```
(SUBRG):
SHAPAN : PROCEDURE OPTIONS (MAIN);
DCL(NN,LIMIT) FIXED BIN, H FLOAT;
    GET LIST (NN,H);
    LIMIT = (NN-5)/2 + 1 ;
        OPEN FILE (INDAT) TITLE ('IN') INPUT ;

BEGIN;
*/THIS SECTION INTEGRATES THE FUNCTION DESCRIBED IN INDAT/*
DCL (ARRAD(NN), SUMM(LIMIT), ARRIN(NN), ARRAY(LIMIT), SUBMOM(4),
    MOM(4)) FLOAT, TEMP(NN)FLOAT INIT ((NN)0);
DCL (I,IJ,IR,IZ,IQ,IP,IT,IB) FIXED BIN, (SUMAR, SIGMA, ANSWER,
    MEAN, KURT, SKEW) FLOAT ;
    END;
N = 0
ARRAD (1) = ARRIN (1);
ARRAD (2) = ARRIN (2)*4 ;
ARRAD (3) = ARRIN (3)*2 ;
ARRAD (4) = ARRIN (4)*4 ;
ARRAD (5) = ARRIN (5) ;
   DO = I = 5 BY 2 TO (NN) ;
              do I_R = 1 TO I ;
               TEMP 1 (I_R) = ARRAD(I_R) ;
               END ;
```

```
            SUMM(N) = SUM(TEMP)*H/3 ;
               IF I   NN THEN DO ;
                  ARRAD(I) = 2*ARRAD(I) ;
                  ARRAD(I+1) = ARRIN (I+1)*4 ;
                  ARRAD(I+2) = ARRIN (I+2) ;
               END;

*/ THIS SECTION EVALUATES THE MEAN, AND THE MOMENTS ABOUT ZERO/*

SUMAR = SUM(SUMM);
        DO IJ = 1 TO LIMIT;
           ELEMENTS (IJ) = SUM(IJ)*IJ;
           END;
SIGMA = SUM(ELEMENTS);
ANSWER= SIGMA/SUMAR;
SUBMOM(1) 1 ANSWER;
        DO IZ = 2 TO 4;
              DO IQ = 1 TO LIMIT
                 ARRAY (IQ) = SUMM(IQ)*IQ++IZ;
           END; END;
           SUBMOM(IZ) = SUM(ARRAY)/SUMMAR;
           ARRAY = 0
        END;

*/THIS SECTION EVALUATES THE MOMENTS ABOUT THE MEAN, AND THE
COEFFICIENTS OF KURTOSIS AND SKEWNESS/*
MOM(1) = 0
MOM(2) = SUBMOM(2) - SUBMOM(1)**2;
MOM(3) = SUBMOM(3) - 3*SUBMOM(1)+SUBMOM(2) + 2*SUBMOM(1)**3;
MOM(4) = SUBMOM(4) - 4*SUBMOM(1)*SUBMOM(3) + 6*SUBMOM(2)*SUBMOM(1)**2 -
                     3*SUBMOM(1)**4;
```

```
KURT = MOM(4)/MOM(2)**2;

SKEW = MOM(3)/MOM(2)**1.5;

PUT SKIP (3);

PUT DATA (MOM(1),MOM(2),MOM(3),MOM(4),KURT,SKEW);

PUT SKIP(6);

    OPEN FILE(PLTDATA)TITLE('OUT') OUTPUT;

    PUT FILE (PLTDATA) EDIT (1,LIMIT)(COZ5,X(1),F(3,0));

    DO IP = 1 TO LIMIT;

    PUT FILE (PLTDATA) EDIT (IP,SUMM(IP), '  ')

    (COZ(1),F(3,0)), X(10) COL(25), F(6,3),A);

  END?

END ;

END SHAPAN
```

2. INT.

This programme smooths the output from SHAPAN into a form ready for plotting, using the appropriate system.

(SUBRG):

```
INT : PROC OPTIONS (MAIN);

OPEN FILE(01) TITLE('1') OUTPUT;
DCL (NORIG, NNEW, NA, NINT) FIXED BIN(31);
DCL (XB, INC) FLOAT(16);
DCL (PLCALL, EOIADF) ENTRY;
       NA = 8;
       GET LIST (NORIG, XB, INC, NNEW);
      NNINT = NORIG - 1

BEGIN;
DCL (A,X(NORIG), Y(NORIG), W(NORIG), D(NORIG), ANS)
       FLOAT(16);
       DO J=1 TO NORIG;
          GET LIST (X(J),Y(J));
       END;
       DO I=1 TO NNEW;
          A = XB + (I-1)* INC;
          CALL PLCALL (EOIADF, NA, ADDR(NINT), ADDR(A), ADDR(X), ADDRY(Y),
          ADDR(W), ADDR(D), ADDR(NORIG), ADDR(ANS));
          PUT FILE (01) EDIT(A,ANS)(COL(1), F(10,3), X(2), F(10,3));
       END;
END;
END;
```

REFERENCES

I.I Wertz J.E. Auzins P. Griffith J.H.E.Orton J.W. Disc. Faraday Soc. 26 66 (I958)

I.2 Thorp J.S. Vasquez R.A. Adcock C. Hutton W. J. Mat. Sci. II 89 (I976)

I.3 Wyckoff R.W.G. "Crystal Structures" Vol I Interscience (I965)

I.4 Moore W.J. "Physical Chemistry" Longman's (I970)

I.5 C.R.C. Handbook American Physical Society

I.6 Pauling L. "The Nature of The Chemical Bond" Cornel University Press (I960)

I.7 Wertz J.E. Auzins P. Phys Rev I06(3) 488 (I957)

I.8 Wertz J.E. Orton J.W. Auzins P. J.Appl. Phys. Suppl. 33 322 (I962)

2.I Valigi M. Cimino A.Z. Phys. Chem. Frankfurt 99 I3I (I976)

3.I Abragam A. Bleaney B. "E.P.R. of Transition Ions" Clarendon Press Oxford (I970)

3.2 Griffith J.S. "The theory of the Transition Metal Ion" Cambridge University Press (I96I)

3.3 Finklestein and Van Vleck J.H. J.Chem Phys 8 790 (I940)

3.4 Griffith J.S. "The Theory of the Transition Metal Ion" Cambridge University Press (I96I)

3.5 Cotton F.A. Wilkinson G. "Advanced Inorganic Chemistry" Wiley (I972)

4.I Low W. Phys Rev I05 80I (I957)

4.2 Schalaw A.L. J.Appl Phys Suppl 33 395 (I962)

4.3 Fairbank W.M. Klausinzer G.K. Phys Rev B 7 500 (I973)

4.4 Glass A.M. J. Chem Phys 46(6) 2080 (I967)

4.5 Valigi M. Cimino A.Z. Phys Chem Frankfurt 99 I3I (I976)

4.6 Sugano S. Schawlaw A.L. Varsanyi F. Phys Rev I20 2045 (I960)

4.7 Larkin J.P. Imbusch G.F. Dravnieks F. Phys Rev B 7 495 (I973)

4.8 Imbusch G.F. Schawlaw A.L. May A.D. Sugano S. Phys Rev I40 A 4830 (I965)

4.9 Castelli F. Forster L.S. Phys Rev B II 920 (I975)

5.I Low W. Phys Rev I09(2) 256 (I958)

5.2 Pappalardo R. Wood D.L. Linares R.C. J. Chem Phys 35 204I (I96I)

5.3 Mironava N.A. Ulmanis S. Ural Konf Spectrosk (Tezisy Dokl) 7th 3 69 (I97I)

5.4 Ralph J.E. Townsend M.G. J. Phys C 3 8 (I970)

5.5 Mironava N.A. Ulmanis U. Latv PSR Zinat Akad Vestis Fiz Teh Zinat Ser 4 39 (I973)

6.I Griffith J.S. "The theory of the Transition Metal Ion" Cambridge University Press (I96I)

6.2 Abragam A. Pryce M.L.H. Proc Roy Soc A205 I35 (I95I)

6.3 Jackson J.D. "Classical Electrodynamics" Wiley (I962)

6.4 Van Vleck J.H. Nuovo Cimento Suppl. 6 993 (I957)

6.5 Prof Squires (University of Durham) Private Communication

6.6 Gorter C.J. Van Vleck J.H. Phys Rev 72 II28 (I947)

7.I Reiling C.H. Hensley E.B. Phys Rev II2 II06 (I958)

7.2 Abragam A. Bleaney B. "E.P.R. of Transition Ions" Clarendon Press Oxford (I970)

7.3 Low W. Ann N.Y. Acad Sci 72 69(I958)

7.4 Fry D.J.I. Llewellyn P.M. Proc Roy Soc A266 84 (I962)

8.I Low W. Phys Rev I05(3) 80I (I957)

8.2 Wertz J.E. Auzins P. Phys Rev I06(3) 434 (I957)

8.3 Abragam A. Bleaney B. "E.P.R. of Transition Ions" Clarendon Press Oxford (I970)

8.4 "SR 56 Owner's Handbook" Texas Instruments

8.5 Maxwell L.R. McGuire T.R. Revs Modern Phys 25 279 (1953)

9.1 Low W. Phys Rev 109(2) 256 (1958)

9.2 Fry D.J.I. Llewellyn P.M. Proc Roy Soc A266 84 (1962)

9.3 Abragam A. Pryce M.L.H. Proc Roy Soc A205 135 (1951)

9.4 Orbach R. Proc Roy Soc A264 458, 485 (1961)

9.5 Woontoon G.A. Advan Electron Phys 15 163 (1961)

9.6 Brown G. Mason D.R. Thorp J.S. J. Sci Inst 42 648 (1965)

9.7 Vasquez M.A. "Magnetic Resonance in Iron Doped Magnesium Oxide" MSc. thesis. University of Durham (1975). Unpublished.

9.8 Van Vleck J.H. Phys Rev 57 426 (1940)